

SELECTIVITY AND SENSITIVITY OF ULTRATHIN MONOLAYER ELECTRODES

By

QUAN CHENG

A DISSERTATION PRESENTED TO THE GRADUATE SCHOOL
OF THE UNIVERSITY OF FLORIDA IN PARTIAL FULFILLMENT
OF THE REQUIREMENTS FOR THE DEGREE OF
DOCTOR OF PHILOSOPHY

UNIVERSITY OF FLORIDA

1995

This dissertation is dedicated to my parents and my wife

ACKNOWLEDGEMENTS

I would like to sincerely thank my graduate adviser and chairperson of my committee, Dr. Anna Brajter-Toth, for giving me the opportunity to work with her, and all her help and all support during these years. Her concern was always to help me in a manner in which I could learn the most.

I would also like to thank Dr. Winefordner, Dr. Jones, Dr. Kennedy and Dr. Holloway for their time and willingness to serve on my committee. I would like to particularly express my gratitude to Dr. Holloway and his graduate students for the technical assistance in vacuum deposition of the gold electrodes.

I would like to thank all the members of the Toth group, especially Chen-Chan Hsueh, Lisa Spurlock, and Merle Regino for their help and support. My thanks are also extended to the former members of the Toth group, especially Allen Witkowski, Mike Freund, Stephanie Myers and Maurice Thompson for their friendship and help.

I would like to offer my greatest gratitude to my parents and my parents-in-law for their constant, selfless and unconditional support.

Finally, I would like to express my greatest thanks to my wife Lan. Her love, patience, support and company make this dissertation possible.

TABLE OF CONTENTS

	<u>Page</u>
ACKNOWLEDGEMENTS	iii
LIST OF TABLES	vii
LIST OF FIGURES	viii
ABSTRACT	xiii
 CHAPTER	
1 INTRODUCTION	1
1.1 Control of Molecular Architecture on the Electrodes	1
1.2 Self-Assembled Monolayers of Thiols and Disulfides	8
1.2.1 Surface Interactions	8
1.2.2 Hydrophobic Interactions	12
1.2.3 Interactions at the Monolayer/Solution Interface	17
1.3 Theories of Mass Transport and Heterogeneous Electron Transfer	24
1.3.1 Mass Transport at Conventional Size Electrodes	27
1.3.2 Diffusion at Microelectrodes	28
1.3.3 Heterogeneous Electron Transfer	35
1.3.4 Electron Transfer Across Impermeable Membranes ..	37
1.4 Electrode Kinetics of Membrane Electrodes	39
1.4.1 Surface Potential at the Electrode/Solution Interface-Bare Electrode	39
1.4.2 Potential Distribution at a Charged Monolayer	42
1.4.3 Effect of Electrolyte on Surface Potentials of Charged Monolayers	47
1.5 Electron Mediation at a Redox Monolayer	48
1.6 Purpose of This Work	60

2 EXPERIMENTAL	62
2.1 Materials	62
2.1.1 General Reagents	62
2.1.2 Biological Probes	62
2.1.3 Synthesis of $\text{H}[\text{Ru}(\text{EDTA})(\text{H}_2\text{O})]$	67
2.1.4 Synthesis of N-(2-Aminoethyl)ferrocylacetamide....	67
2.2 Electrochemical Apparatus	68
2.3 Experimental Procedures	68
2.3.1 Preparation of Electrodes	68
2.3.2 Electrochemical Techniques	75
2.3.3 Purification of Protein Cytochrome c	83
3 SELECTIVITY AND SENSITIVITY OF THE THIOCTIC ACID MONOLAYERS	85
3.1 Capacitance Measurements and Monolayer Permeability	85
3.2 Electrochemical Reactivity of Hydrophilic Probes on the TA Monolayer Electrodes	89
3.3 Electrolyte Effect on Film Structure and Reactivity	99
3.4 Effect of Probe Structure and Hydrophobicity on Reactivity At the TA Monolayer	102
3.5 Effect of Redox Probe Size	109
3.6 Film Stability and Probe Retention	113
3.7 Effect of Substrate Quality	114
3.8 Conclusions	115
4 CHARACTERIZATION OF MONOLAYERS WITH DIFFERENT HYDROPHOBICITY	117
4.1 Investigation of Permeability of Multicomponent Monolayers by Capacitance Measurements	117
4.2 Effect of Increasing Hydrophobicity on the Response of Hydrophilic Probes	119
4.3 Reactivity of Hydrophobic Probes on the Hydrophobic Monolayers	131
4.4 Electrolyte Concentration and Composition on Response with Changes in Film Hydrophobicity	136
4.5 Stability of the Mixed Monolayer Electrodes	136
4.6 Conclusions	139

5 CHARACTERIZATION OF MONOLAYER ULTRAMICROELECTRODES	140
5.1 Background	140
5.2 Preparation and Characterization of Ordered Monolayers At Au Fiber Electrodes	143
5.3 Selectivity and Sensitivity of the Thioctic Acid Monolayer Ultramicroelectrodes	146
5.4 Effect of Electrolyte and Solution pH on Response	154
5.5 Amperometric pH Sensing with the TA UME Using $\text{Fe}(\text{CN})_6^{3-}$ as the Mediator	161
5.6 Conclusions	165
6 DIRECT ELECTROCHEMISTRY OF CYTOCHROME C ON THE MONOLAYER ELECTRODES AND <i>IN SITU</i> CHEMICAL DERIVATIZATION OF THE ULTRATHIN FILMS	167
6.1 Background of Direct Electrochemistry of Cytochrome c	168
6.2 Characterization of Cytochrome C on the TA Monolayer Electrodes	177
6.3 Electrochemical Behavior of Surface Bound Cytochrome c ...	190
6.4 <i>In situ</i> Chemical Derivatization of the TA Monolayers	195
6.5 Conclusions	201
7 SUMMARY AND FUTURE WORK	202
REFERENCES LIST	207
BIOGRAPHICAL SKETCH	218

LIST OF TABLES

<u>Table</u>	<u>Page</u>
2.1 Biological probes and their electrochemical reactions in aqueous solution	63
3.1 Results of capacitance measurements for the thioctic acid and HO(CH ₂) ₆ SH monolayer electrode	88
3.2 Cyclic voltammetric results for Fe(CN) ₆ ³⁻ and Ru(NH ₃) ₆ ³⁺ on the bare Au and thioctic acid monolayer electrodes	95
3.3 Cyclic voltammetric results of Ru(NH ₃) ₆ ³⁺ on the TA monolayer electrode at low pH	98
3.4 Cyclic voltammetric results of Ru(NH ₃) ₆ ³⁺ and Fe(CN) ₆ ³⁻ as a function of supporting electrolyte	100
3.5 Cyclic voltammetric results of DA and Q at pH 7.4	105
4.1 Results of capacitance measurements of the monolayers with multicomponents	118
4.2 Cyclic voltammetric results of Ru(NH ₃) ₆ ³⁺ and DA as a function of electrolyte concentration on the 1:1 TA/C6SH monolayer electrodes	137
5.1 Half-wave potentials and Nernstian slopes for Fe(CN) ₆ ³⁻ and Ru(NH ₃) ₆ ³⁺ in different electrolytes	152
5.2 Voltammetric results for 5 mM Fe(CN) ₆ ³⁻ and Ru(NH ₃) ₆ ³⁺ on the TA and bare Au microelectrodes	153
6.1 Cyclic voltammetric results of cytochrome c	188

LIST OF FIGURES

<u>Figure</u>	<u>Page</u>
1.1 Methods of introducing monomolecular layers on the electrode surfaces: (a) chemical reaction; (b) Langmuir-Blodgett transfer; (c) self-assembly of a monolayer	5
1.2 (a) Scanning tunneling micrograph of Au(111); (b) predicted bonding position of sulfur atoms from the alkylthiol on the Au (111) plane	11
1.3 Alkane chain arrangement in the monolayers formed from disulfide compounds: (a) symmetric disulfide; (b) asymmetric disulfide; (c) ring disulfide	14
1.4 Schematic side-view of the orientation of a single, long-chain thiol molecule adsorbed on gold	16
1.5 (a) Contact angle for water is plotted as a function of $\log K_{eq}$ for ω -substituted hexadecane thiol monolayers. The chain-terminating group (X) is shown at the top; (b) The desorption activation energies for water from ω -substituted hexadecane thiols as a function of $\log K_{eq}$	20
1.6 Structures of the self-assembled molecules: (a) thioctic acid; (b) hexanethiol	23
1.7 Cartoon representations of the pure and the mixed monolayers investigated in this study: (a) thioctic acid monolayer; (b) 1:1 thioctic acid/ $\text{CH}_3(\text{CH}_2)_5\text{SH}$ mixed monolayer; (c) 1:100 thioctic acid/ $\text{CH}_3(\text{CH}_2)_5\text{SH}$ mixed monolayer; (d) $\text{CH}_3(\text{CH}_2)_5\text{SH}$ monolayer.	26

1.8	(a) Schematic diagram of a linear diffusion layer at an electrode. The electrode radius is much larger than the thickness of the diffusion layer; (b) Schematic diagrams of diffusion layer growth at a microelectrode. Direction of diffusion changes with time to eventually become spherical	30
1.9	Stimulated current-time curve in chronoamperometry for planar and spherical diffusion (assuming $D_0 = 10^{-5} \text{ cm}^2/\text{s}$ and $r = 5 \times 10^{-4} \text{ cm}$)	34
1.10	Schematic illustration of the double layer structure at the electrode surface: (a) Helmholtz model; (b) Gouy-Chapman model; (c) Gouy-Chapman-Stern model	41
1.11	A model of the double layer structure on the TA monolayer electrode: (a) ion distribution at the interface; (b) potential distribution of the interface; (c) equivalent circuit	44
1.12	A plot of ϕ_{DL} as a function of solution electrolyte concentration. ...	50
1.13	Types of electrocatalysis on electrodes: (a) uncatalyzed reaction; (b) homogeneous catalysis; (c) heterogeneous catalysis	53
1.14	Cartoon representation of the structure of the TA monolayer in the presence of the ferrocene headgroup: (a) unfavorable residence of the hydrophobic ferrocene at the monolayer plane; (b) favorable residence of the hydrophobic ferrocene outside the monolayer plane	57
1.15	Proposed synthetic route for the <i>in situ</i> immobilization of the ferrocene headgroup onto the TA monolayer	59
2.1	Structures of cytochrome c and the heme group. The heme group (solid circles) is located in a protein pocket with the heme edge slightly exposed at the protein surface	65
2.2	A diagram of the electrode design and the electrochemical cell.	70
2.3	Cyclic voltammogram of 1 mM $\text{Fe}(\text{CN})_6^{3-}$ in 0.1 M HClO_4 (pH 1.5) on the ferrocene derivatized TA monolayer electrode. Electrode area is 0.12 cm^2 . Scan rate is 100 mV/s	77

3.1	Cyclic voltammetric response of $\text{Fe}(\text{CN})_6^{3-}$ on the TA monolayer electrode as a function of solution pH. Solution compositions: 0.1 M HClO_4 (pH 1.5), 0.1 M KCl and 10 mM tris (pH 7.4) and 0.1 M KCl and 10 mM borate (pH 9.1). Scan rate 100 mV/s. Electrode area 0.28 cm^2	91
3.2	Cyclic voltammetric response of $\text{Ru}(\text{NH}_3)_6^{3+}$ on the TA monolayer electrode as a function of solution pH. Solution compositions: 0.1 M HClO_4 (pH 1.5), 0.1 M KCl and 10 mM tris (pH 7.4) and 0.1 M KCl and 10 mM borate (pH 9.1). Scan rate 100 mV/s. Electrode area 0.28 cm^2	93
3.3	Cyclic voltammograms of 0.5 mM DA and DOPAC in 0.1 M KCl and 10 mM tris (pH 7.4) on the bare gold and the TA monolayer electrodes. Scan rate 100 mV/s. Electrode area: 0.28 cm^2 for the bare, 0.21 cm^2 for the TA monolayer electrode	104
3.4	Cyclic voltammetric response of 0.5 mM benzoquinone (Q) in 0.1 M KCl and 10 mM tris (pH 7.4) on the bare gold and the TA monolayer electrode	108
3.5	(A) Voltammetric response of 0.5 mM $\text{Ru}(\text{EDTA})(\text{H}_2\text{O})^+$ in 0.1 M HClO_4 (pH 1.5) on the bare Au and the TA monolayer electrode. (B) Voltammetric response of $\text{Ru}(\text{EDTA})(\text{H}_2\text{O})^+$ in 0.5 M $\text{NaAc}/\text{CF}_3\text{COOH}$ (pH 3.5) on the bare gold and the TA monolayer electrode. Scan rate 100 mV/s. Electrode area: 0.28 cm^2 for the bare, 0.20 cm^2 for the TA monolayer electrode	111
4.1	Cyclic voltammograms of 1 mM $\text{Ru}(\text{NH}_3)_6^{3+}$ in 0.1 M KCl and 10 mM tris (pH 7.4) on the different monolayer electrodes. Scan rate 100 mV/s	121
4.2	Cyclic voltammograms of 1 mM $\text{Fe}(\text{CN})_6^{3-}$ in 0.1 M HClO_4 (pH 1.5) on the different monolayer electrodes. Scan rate 100 mV/s	123
4.3	Cyclic voltammograms of 1 mM $\text{Fe}(\text{CN})_6^{3-}$ in 0.1 M KCl and 10 mM tris (pH 7.4) on the different monolayer electrodes. Scan rate 100 mV/s	127
4.4	A schematic illustration of double layer structure and charge distribution at the C_6SH monolayer/solution interface	130

4.5	(A) Cyclic voltammograms of 0.5 mM DA and 0.5 mM DOPAC in 0.1 M KCl and 10 mM tris (pH 7.4) on the different monolayer electrodes. Scan rate 100 mV/s. Electrode area 0.24 cm ² . (B) Cyclic voltammetric response of 0.5 mM benzoquinone (Q) in 0.1 M KCl and 10 mM tris on the different monolayer electrode. Scan rate 100 mV/s	133
5.1	Cyclic voltammograms of 5 mM Fe(CN) ₆ ³⁻ in 0.1 M KCl and 10 mM tris (pH 7.4) on (a) bare UME; (b) TA monolayer electrode formed on mechanically polished Au; (c) TA monolayer electrode formed on aqua regia etched Au. Scan rate is 25 mV/s. Electrode diameter is 12.7 μm	145
5.2	(A) Cyclic voltammograms of 5 mM Fe(CN) ₆ ³⁻ in 0.1 M HClO ₄ (pH 1.5) on bare (solid line) and TA monolayer electrodes (dash line). (B) Cyclic voltammograms of 5 mM Ru(NH ₃) ₆ ³⁺ in 0.1 M KCl and 10 mM tris (pH 7.4) on bare (solid line) and TA monolayer electrodes (dash line). Scan rate is 25 mV/s. Electrode diameter is 12.7 μm	148
5.3	(A) Plot of log ((i _L -i)/i) verses E for the reduction of 5 mM Fe(CN) ₆ ³⁻ in (a) 0.1 M HClO ₄ (pH 1.5) on the bare Au UME, (b) 0.1 M KCl and 10 mM tris (pH 7.4) on the bare Au and (c) 0.1 M KCl and 10 mM tris (pH 7.4) on the TA UME. (B) Plot of log ((i _L -i)/i) verses E for the reduction of Ru(NH ₃) ₆ ³⁺ in 0.1 M KCl and 10 mM tris (pH 7.4) on (a) bare Au UME and (b) TA UME	151
5.4	Response of 5 mM Ru(NH ₃) ₆ ³⁺ in 0.1 M KCl (pH 1.0) on the bare (solid line) and the TA monolayer microelectrodes (dash line). Scan rate is 25 mV/s	157
5.5	Response of 5 mM Ru(NH ₃) ₆ ³⁺ on bare (solid line) and the TA monolayer microelectrodes (dash line). (A) in 0.1 M phosphate (pH 7.4). (B) in 0.1 M NaF and 10 mM tris (pH 7.4). (C) in 0.1 M NaF (pH 9.6)	160
5.6	(A) Titration curve of 0.1 M HClO ₄ by 2 M KOH. ○ results obtained by potentiometric monitoring. ● results by amperometric method using 5 mM Fe(CN) ₆ ³⁻ as mediator. (B) First derivative of amperometric titration curve.	164

6.1	The oxidative phosphorylation electron transport chain	170
6.2	A schematic of the interactions of cytochrome c on the Au electrode modified by adsorption of 4,4'-bipyridyl. Note the hydrogen bonding between the N of the 4,4'-bipyridyl and the NH_3^+ amino acid residue on the protein surface	174
6.3	(A) Cyclic voltammetric response of 46 μM cytochrome c in 35 mM phosphate at pH 7.4 on the a freshly prepared TA monolayer electrode. (B) Cyclic voltammogram of 46 μM cytochrome c in 35 mM phosphate at pH 7.4 on a TA monolayer electrode redipped in the 0.1 % TA ethanol solution for 10 min. See text for detail. Scan rate is 25 mV/s. The electrode area is 0.27 cm^2 . (C) A plot of $\log i_p$ vs $\log v$ in 46 μM cytochrome c in 35 mM phosphate at pH 7.4. Scan rate range: 10-100 mV/s. The slope of the line is 0.66	179
6.4	(A) Cyclic voltammetric response of adsorbed cytochrome c on the TA monolayer electrode in 10 mM phosphate (pH 7.4). (B) Background subtracted CV for (A)	183
6.5	Voltammetric response of 46 μM cytochrome c in 35 mM phosphate at pH 7.4 on a bare Au electrode vacuum deposited on silicon wafers. Scan rate is 25 mV/s. The electrode area is 0.21 cm^2 . Solid line (-): response for the first run. Dash line (- -): for the second run (5 min later). Dotted line (...): for the third run (10 min later). During the three runs, the electrode stayed in the cytochrome c solution	187
6.6	Cyclic voltammetric response of adsorbed cytochrome c on the TA monolayer electrode in 0.1 M phosphate (pH 7.4). Scan rate is 25 mV/s	194
6.7	(A) Cyclic voltammogram of 0.5 mM N-(2-aminoethyl) ferrocylacetamide in 0.1 M phosphate at pH 7.4 on the TA monolayer electrode. Scan rate is 100 mV/s. (B) A plot of $\log i_p$ vs. $\log v$ in the scan rate range of 75 - 500 mV/s for 0.5 mM N-(2-aminoethyl) ferrocylacetamide on the TA monolayer electrode. (C) Cyclic voltammogram of the covalently bound ferrocene derivatized TA monolayer electrode in 0.1 M HClO_4 at pH 1.5	199

Abstract of Dissertation Presented to the Graduate School
of the University of Florida in Partial Fulfillment of the
Requirements for the Degree of Doctor of Philosophy

SELECTIVITY AND SENSITIVITY OF ULTRATHIN MONOLAYER ELECTRODES

By

QUAN CHENG

May 1995

Chairperson: Dr. Anna Brajter-Toth

Major Department: Chemistry

The objective of this work is to build a molecular architecture on the electrode surface with a well-defined morphology and desirable electrochemical characteristics. The goal is accomplished by means of self-assembly of thioctic acid, a sulfur-terminated organic molecule with a short alkyl chain and a hydrophilic carboxylic headgroup, on a gold electrode.

Characterization of the monolayer structure and the electrochemical response of the monolayer electrodes is performed by means of capacitance measurements and voltammetry. Investigation of the capacitance of the self-assembled monolayers provides insight into the macroscopic permeability of the films and reveals that penetration of solvent/ions into the thioctic acid monolayer film occurs extensively.

Voltammetric results demonstrate that permselectivity of the monolayer electrode can be obtained as a result of the induced electrostatic interactions between the monolayer interface and the electroactive species. Measurement of the voltammetric response of the redox probes at the monolayers as a function of the electrolyte concentration and

composition is used to qualitatively analyze the effect of electrolyte on response. A model describing the role of the interfacial charge in the electrochemical response of the monolayers as a function of the solution composition and surface smoothness is proposed.

A strategy is developed to further explore the applications of the monolayer electrodes to control the electrochemical response of the biological molecules such as catecholamines. The ability to control the surface hydrophobicity of the monolayer electrodes through coadsorption of thioctic acid and hexanethiol, to display different electrochemical properties towards biological molecules is tested. The optimum conditions for detection of the biological molecules on the monolayer electrodes are discussed.

In order to pursue selective analysis in microenvironments, the thioctic acid monolayer formed on the ultramicroelectrodes (UME) is investigated, demonstrating high permselectivity and high sensitivity of the monolayer modified UMEs. Because of the more effective mass transport to the UMEs, effects of electrolyte on the monolayer response can be characterized facilely. Amperometric pH sensing on the thioctic acid UMEs using a redox mediator is discussed

Finally, the thioctic acid monolayer microelectrode is applied to investigate direct electrochemistry of a redox protein, cytochrome c. A sketch for developing a biosensor via mediation effects using the monolayer assembly is proposed.

CHAPTER 1 INTRODUCTION

1.1 Control of Molecular Architecture on Electrodes

Modern electrochemistry has extensively involved deliberate chemical derivatization of the electrode-solution interface.¹ One postulate is that if the local chemical environment at the electrode surface can be controlled, the sensitivity and the selectivity of electrode reactions can be controlled, ultimately providing advantages in electroanalysis.²

The rational approach to the control/investigation of the chemical nature of the interfacial region includes two strategies: (a) design of sensitive measurements to provide a better structural and dynamic understanding of the known kinds of interfaces and thereby of their electrochemical reactivity; and (b) known chemical or electrochemical reactivities are used to fabricate a new interface region possessing a predictable structure and/or dynamic properties.³ No matter what direction is pursued, the ultimate goal is to gain understanding of how to control the electrochemical reaction kinetics, the reaction pathways, the selectivity of the reactions conducted in the presence of multiple potential reactants, and the sensitivity of the electrochemical response as applied to chemical sensors.⁴

Since the mid-1970s, considerable research has concentrated on how to attach molecular species to electrodes.⁵⁻⁸ These electrodes are usually referred to as chemically

modified electrodes (CME). The idea is to transfer the known chemical or electron-transfer reactivity of the attached molecular species to the electrode/electrolyte interface. However, although the chemical composition of the early modifying layers was often known, the layer structures were not clear and coherently organized.⁹ For instance, redox and other chemical characteristics of the surface-attached electroactive reagents such as porphyrins,¹⁰ quinones¹¹ and metal complexes¹² were generally preserved. However, limitations existed in the stability, and more particularly in the ability to define and control the structural and the dynamic aspects of the immediate microenvironment of the immobilized reagents. Later advances in this field have involved use of various polymers, conductive and nonconductive, on which electrochemical reactivity is achieved by selective preconcentration or transport of the substrates through the film based on membrane partitioning or permeability effects.¹³⁻¹⁶

In order to perform increasingly complicated and demanding tasks using chemically modified electrodes, complex molecular structures would have to be constructed with a high degree of control over the design and structure of the systems. This need has been recognized and tackled to some extent through the use of polymer films on electrodes, where it has been demonstrated that by constructing polymeric bilayers in a rational manner the electrode system could be made to display some unique properties.¹⁷⁻¹⁹

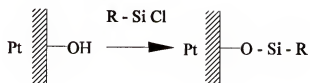
Generally speaking, the polymer-based chemically modified electrodes can be easily prepared. However, polymers as modifiers have intrinsic drawbacks. The nature of the polymerization process usually results in a random orientation of polymers without

well defined morphology.²⁰ Therefore, the effect of film structure on electrode response is often difficult to determine. For instance, the thickness of a polymeric Nafion film, which is an ion-exchange membrane used for achieving anion exclusion, is very difficult to control.²¹⁻²³ Since diffusion coefficients of probes inside Nafion membranes have been found to be 2-3 orders of magnitude lower than that in the bulk solution,²⁴ variations in film thickness have an impact on the current magnitude, and possibly on the apparent kinetics on the polymer modified surfaces.²⁵ Though control of some of the polymer properties such as membrane thickness can be achieved by controlled electro-polymerization of conductive polymers such as polypyrrole,²⁶ the three-dimensional molecular orientation of the polymer usually remains unclear. It is thus highly desirable if both structure and orientation can be introduced into the electrode coating.

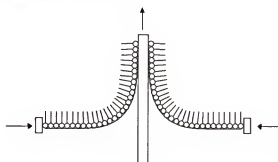
Figure 1.1 summarizes some of the methods for fabricating monomolecular layers on electrode surfaces. Chemical reactions using surface functionalities as anchoring groups were among the first attempted for attachment of monomolecular layers on electrode surfaces (Fig. 1.1A).⁶ This approach offered substantial synthetic diversity, and various substances have been immobilized at metal oxide and carbon electrodes. Pt, which readily forms a layer or two of platinum oxide terminated by Pt-OH, is reactive with organosilane reagents.²⁷ Carbon electrodes, which are rich in different functionalities such as carbonyl and carboxylic groups, may react readily, with help of catalysts, with nucleophiles such as alcohol and amine to form covalent linkages.²⁸⁻³² However, chemical reactions at the surface are usually accompanied by complicated interactions and dramatic changes of the surface properties, and the attached monolayers often fail to show any characteristics of an ordered film.³³

Figure 1.1 Methods of introducing monomolecular layers on the electrode surfaces: ^{1,34,54} (a) chemical reaction; (b) Langmuir-Blodgett transfer; (c) self-assembly of a monolayer

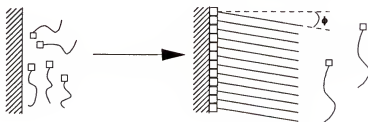
(a) Chemical Reactions



(b) Langmuir-Blodgett



(c) Self-Assembly of Alkylthiol Monolayers



Molecular assemblies can also be introduced to electrode surfaces through Langmuir-Blodgett (L-B) transfer of amphiphiles (Fig. 1.1B).³⁴⁻³⁶ Amphiphiles are compounds which possess both hydrophilic and hydrophobic terminals. A classical example of an amphiphile is stearic acid ($C_{17}H_{35}COOH$), where the long hydrocarbon tail ($C_{17}H_{35}$) is hydrophobic, and the carboxylic acid headgroup ($-COOH$) is hydrophilic. Therefore, when such compounds are spread at the water surface, the hydrophilic end is preferentially immersed in the water while the hydrophobic end preferentially resides in the air. The monolayers of amphiphiles can be compressed at the water-air interface. The strong, attractive van der Waals forces between the compressed hydrophobic segments lead to molecular orientation and result in well-organized monomolecular assemblies. Such monolayers can be introduced onto the electrode surfaces by mechanically lifting an electrode substrate through the monolayer at the air/water interface.³⁴

The Langmuir-Blodgett method was the first technique to provide chemists with a practical capability to construct ordered molecular assemblies at electrodes.³⁴ Various amphiphiles, including those derivatized with an electroactive redox center at one terminal, have been introduced and characterized at electrode surfaces.³⁵ Mixed multicomponent L-B films showing "gating" electrochemical characteristics have been reported.³⁶ However, L-B films suffer a great drawback: the compressed monolayers often relax following exposure to solution, leading to an inevitable destruction of the monolayer and a complete loss of its expected impermeability.³⁷

Recently, self-assembly of monolayers at metal surfaces has proved to be a very effective method for introducing well-defined and controllable monolayer architecture

onto electrodes.³⁸⁻⁵² Self-assembled monolayers rely on a strong, specific interaction between an adsorbate and a substrate to drive the spontaneous formation of a monolayer film (Fig. 1.1C). To prepare a self-assembled monolayer the substrate is simply immersed in a dilute solution of the adsorbate at room temperature for an interval varying from a few minutes to several days, depending on the system. Miller and coworkers⁴² have concluded that the ability of an amphiphile to form a compact, self-assembled monolayer, and its subsequent stability at the surface, depend on three principal interactions: the strength of binding of the headgroup with the surface, the attractive forces between the adsorbed amphiphiles within the monolayer, and the interaction of the amphiphiles' terminal function with the surrounding solution environment. Therefore, in order to produce as ideal a monolayer as possible one should try to maximize each of these interactions. Many atoms show strong interactions at metal surfaces, such as nitrogen on platinum, sulfur on gold and silver.⁵³ Among these, sulfur, particularly in the form of a thiol, exhibits very strong adsorption on the Au surface. Monolayers of thiols on Au are thermodynamically stable and mechanically robust.⁵⁴ They can be removed from the solutions from which they have been adsorbed and immersed in aqueous acid or base solutions without apparent adverse effects. The range of organic species that can be incorporated into these monolayers is large: few ligands compete effectively with a thiol in coordinating to gold, and the chemical properties of the thiol group, similar to those of alcohol, are sufficiently inert to allow a thiol to be compatible with most other functional groups such as alcohol, amine, acid and acid derivatives. It has been proposed that a variety of chemical reactions can be performed on the monolayer to interrogate the

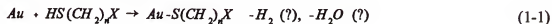
structure⁵⁴ and to introduce redox centers.⁴⁹ Monolayers with these functional groups are generally assembled from the molecules with these functional groups obtained from synthesis,^{48,49} direct chemical derivatization of the monolayer surface via *in situ* surface reactions needs to be further justified. Nevertheless, self-assembled monolayers of thiols and disulfides adsorbed on gold are the best characterized monolayer assemblies.⁵⁵

1.2 Self-Assembled Monolayers of Thiols and Disulfides

Self-assembled monolayers (SAM) of organic thiols and disulfides on gold were first introduced by Nuzzo and Allara in 1983.³⁸ Formation of a self-assembled molecular monolayer on a surface is generally a combination of two processes. It includes the binding of a chemical functionality on the reagent to the surface, and a microstructural organization of the assembled monolayer that is driven by the hydrophobic effect and the van der Waals attraction between the low polarity (hydrophobic) segments of the reagent.⁵⁶

1.2.1 Surface Interactions

Some of the best characterized SAMs are those formed on gold surfaces by the adsorption of alkanethiols. The firm attachment of the molecules to the gold surface is believed to occur through the formation of a gold-thiolate bond (eq. 1-1).^{41,56} This is an extremely strong surface bond (homolytic bond strength of ~44 kcal/mol)^{56,57} and, therefore, the resulting monolayers are quite stable.



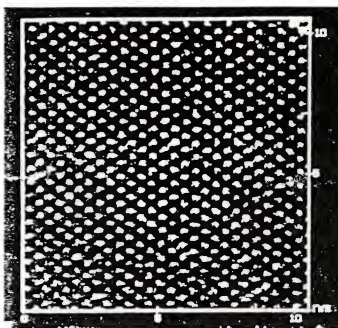
However, the formation of a gold-thiolate from a thiol requires the loss of a hydrogen, but whether this hydrogen is lost as a H_2 or is lost as a water molecule by the reaction with traces of oxidants in the system is not known. As a result, the mechanism for the formation of the thiolate has not been established.

The gold substrate is typically a 100-2000 nm thick film evaporated in vacuum onto smooth substrates such as a single crystal silicon wafer or mica. The resulting gold surfaces are polycrystalline, and the polycrystallites are oriented in a way that presents predominantly the Au (111) crystal face.⁵⁷ Figure 1.2 (a) shows a STM image of an Au (111) surface. This surface is ideal for self-assembly of alkythiols since it has the lowest surface free energy.⁵⁷ As a result, the energy barrier for adsorption is low. Unlike most metals, gold does not form an oxide under ambient conditions.⁵⁷ With gold as a substrate, SAMs form on a polycrystalline metal rather than on an amorphous overlayer of oxide.⁵⁵

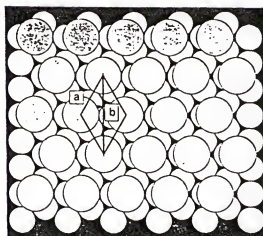
Figure 1.2 (b) illustrates the bonding position of the sulfur atoms of the alkythiols. On the Au (111) surface, the sulfur atoms occupy the threefold hollow sites and form a hexagonal lattice. The lattice of the sulfur atoms is displaced 30° relative to the gold (111) hexagon, and the intramolecular distances between the two alkythiol molecules are $\sqrt{3}$ times larger than the interatomic distance of gold.⁵⁵⁻⁵⁸ The spacing between the adjacent sulfur atoms in this structure (5 Å) is nearly three times that of the van der Waals diameter of a sulfur atom (1.85 Å); thus sulfur-sulfur interactions are believed to be minimal. This distance is also greater than the distance of the closest approach of the alkyl chains (4.24 Å); therefore, the chains tilt to minimize the distance between them in order to maximize their van der Waals interactions. This lattice formed by the adsorption of alkythiols onto gold is referred to as $(\sqrt{3} \times \sqrt{3})R30^\circ$.⁵⁷

Figure 1.2 (a) Scanning tunneling micrograph of Au (111); (b) predicted bonding position of sulfur atoms from the alkylthiol on the Au (111) plane ⁵⁶

(a)



(b)



$$a = 5.0 \text{ \AA}$$

$$b = 8.7 \text{ \AA}$$

○ = Au atom

○ = Alkanethiolate adsorbate

Disulfide compounds are believed to form Au-thiolate bond when adsorbing on a gold surface, as thiols are,⁵⁹⁻⁶¹ though the detailed mechanism of the reaction is not clear at this moment. During the course of the formation of the monolayer, disulfides adsorb on the gold surface with a cleavage of their sulfur-sulfur bond and form the gold thiolate bond. Figure 1.3 shows the schematic illustration of the monolayers formed from different kinds of disulfides. If the disulfide is symmetric, the formed monolayer is similar to that formed from an alkylthiol. If the disulfide is asymmetric, the two thiolates formed from a single disulfide behave as independent entities in their subsequent reactions.

1.2.2 Hydrophobic Interactions

X-ray and spectroscopic methods have indicated that the polymethylene chains in the self-assembled monolayers of alkylthiols are fully extended, tilted with respect to the surface normal, and in all-trans configuration.^{39, 55-57} Figure 1.4 illustrates a single chain model of a thiol on gold. It predicts that there is an average tilt of 27° of alkylthiol molecules from surface normal. Nuzzo and coworkers have found that the existence of small headgroup such as OH, COOH, CONH₂, etc. does not change the tilt angle significantly for the long alkyl chain monolayers.⁶²

Structural information of the alkylthiol monolayers such as bond length, tilt angle and molecular configuration, as mentioned above, makes it possible to predict the film thickness of the monolayers. Typically for alkylthiols, each methylene group approximately occupies ca. 1.3 Å in length.⁴⁷ This has been verified by the results from the ellipsometry experiments.^{47, 48}

Figure 1.3 Alkane chain arrangement in the monolayers formed from disulfide compounds: (a) symmetric disulfide; (b) asymmetric disulfide; (c) ring disulfide.

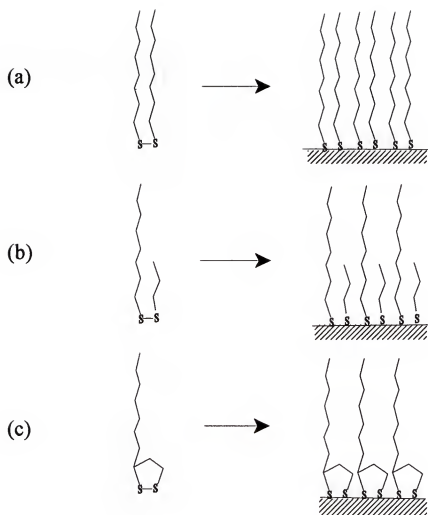
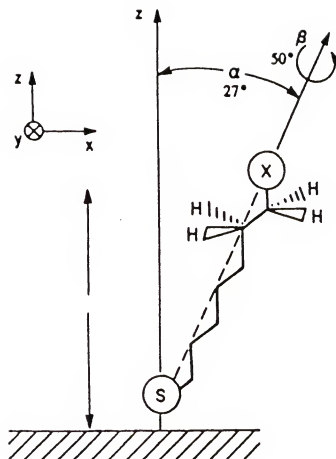


Figure 1.4 Schematic side-view of the orientation of a single, long-chain thiol molecule adsorbed on gold. ⁵⁷



1.2.3 Interactions at the Monolayer/Solution Interface

From the point of view of surface chemistry, the structure and the orientation of the chain-terminating functionality is very important. This is the portion of the adsorbate molecule that dominates the interactions occurring between the monolayer and a contacting phase, and results in various surface properties such as functionalizing reactions and molecular recognition.⁶³ One of the most fundamental characteristics of the surface closely related to the film/solution interface is the film wettability.⁴³⁻⁴⁶

Wettability is a representative physical property of a surface that has been studied extensively.⁶⁴⁻⁶⁶ The macroscopic wetting properties of materials can be quantified by contact angle measurements. Contact angle, θ , is related to surface interactions through Young's equation:³⁴

$$\gamma_{sv} - \gamma_{sl} = \gamma_{lv} \cos \theta \quad (1-2)$$

where γ_{sv} , γ_{sl} and γ_{lv} are interfacial energy of solid-vapor, solid-liquid and liquid-vapor, respectively. If $\theta=0$, complete wetting occurs; if θ is finite, the surface is partially wet. Another quantitative measure of the hydrophilicity of the surface was introduced by Wolfenden,⁶⁷ who defined the molecular partition coefficient K_{eq} , as the ratio of the concentration of a particular compound in the gas phase over that in the aqueous solution.

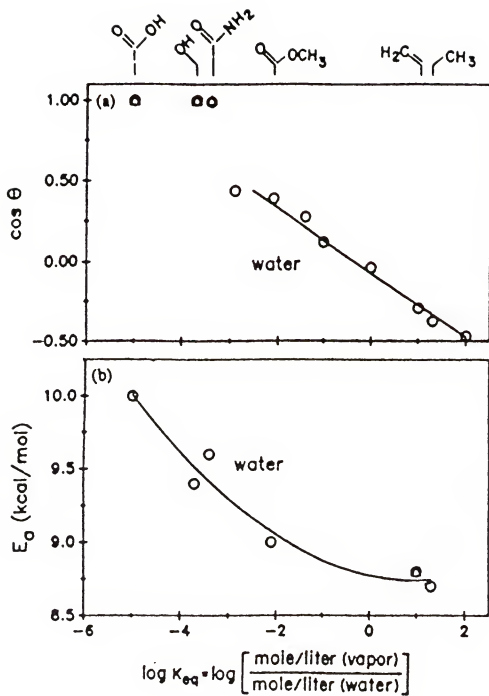
$$K_{eq} = \frac{[\text{mole / liter (vapor)}]}{[\text{mole / liter (water)}]} \quad (1-3)$$

where [mole/liter (vapor)] is the concentration of the compound in the gas phase and [mole/liter (water)] is the solution concentration of the compound. By comparing the gas

phase concentrations of a series of organic compounds with different functional groups, such as ethanol, ethylamine, etc. to their aqueous solution concentrations, the hydrophilic character of the organic functional groups can be obtained. For instance, the K_{eq} of the compound with carboxylic functional group is 10^{-5} , indicating that removal of this compound from water to the gas phase is difficult, pointing to a strong interaction of the compound with the water surroundings or the high hydrophilicity of the carboxylic groups. On the other hand, a compound with the CH_3 group has K_{eq} around 10. The CH_3 group can thus be regarded as very hydrophobic. Figure 1.5 plots the cosine of the contact angle for water, and the measured desorption energy E_a , versus $\log K_{eq}$ for the self-assembled monolayers with various terminal functional groups.⁵⁷ Clearly, contact angle and desorption energy are both highly terminal dependent. Changing the monolayer headgroups can allow K_{eq} of the monolayers to be varied by more than seven orders of magnitude. Figure 1.5 (a) shows that the measured contact angle θ is zero for the monolayer with carboxylic terminals, indicating a complete wetting on this interface. Figure 1.5 (b) indicates that the energy for desorption of water from a variety of ω -substituted hexadecane thiols is the highest for the carboxylic headgroup, also pointing to a high degree of hydration of the headgroups at this monolayer. The results clearly show the excellent wettability of the monolayers with the carboxylic terminal groups, pointing to the importance of the carboxylic terminals for the construction of SAMs aimed to probe reactivity in aqueous solutions.

The monolayers we have developed in this project are fabricated from the thioctic acid (1,2-dithiolane-3-pentaoic acid, abbreviated as TA). The schematic illustration of

Figure 1.5 (a) Contact angle for water is plotted as a function of $\log K_{eq}$ for ω -substituted hexadecane thiol monolayers. The chain-terminating group (X) is shown at the top; (b) The desorption activation energies for water from ω -substituted hexadecane thiols as a function of $\log K_{eq}$.⁵⁷

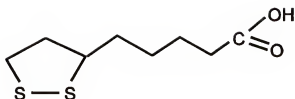


thioctic acid is given in Figure 1.6. Thioctic acid is a growth factor for many bacteria and protozoa.⁶⁸ It occurs widely in plants and animals, and acts as a coenzyme in many enzyme-catalyzed reactions, particularly in oxidative decarboxylations.⁶⁸ Structurally, it contains a disulfide bond, which is proposed to cleave to form two gold-thiolate bonds when the TA adsorbs on the gold surface, as with other disulfides.⁵⁹⁻⁶¹ This should provide very stable attachment of the molecules on the Au electrode surface. The alkyl chain of thioctic acid is short (C5). As the hydrophobic interactions of the low polarity segments in the monolayers are proportional to the chain length,⁴⁷ the interactions between the methylene groups in the thioctic acid monolayer are not as strong as in the long alkyl chain monolayers. In addition, thioctic acid is a ring compound with an asymmetric disulfide. From the structural point of view, it "misses" the second alkyl chain in its structure. These features, including less strong hydrophobic interactions and a "missing" chain in the structure, render thioctic acid to form a less densely packed film when adsorbed on the gold surface. In fact, thioctic acid monolayer has been found to be permeable to ions.^{69,70}

Biological materials, including proteins, are difficult to detect on the electrode surface.⁷⁰⁻⁷² Due to the hydrophobic moieties in their structures such as aromatic rings, they often exhibit quite unfavorable properties when contacted with metal electrodes.⁷⁰⁻⁷² These properties, in fact, largely determine the response of these molecules on the surface. For instance, large redox proteins, e.g. cytochrome c, may irreversibly adsorb on the electrode surface and cause the electrode fouling, which prohibits reversible electron transfer.⁷³⁻⁷⁶ In order to study the response of these molecules, a surface with tunable hydrophobicity is highly necessary. Self-assembled monolayers on gold electrodes can

Figure 1.6 Structures of the self-assembled molecules: (a) thioctic acid;
(b) hexanethiol

(a)

*Thioctic Acid*

IUPAC name: 1,2-dithiolane-3-pentanoic acid
 $\text{pK}_a = 5.0$

(b)

*Hexanethiol*

provide a convenient route for fabricating surfaces with a different degree of hydrophobicity. By coassembly of more than one functional group into the monolayer, a surface with a variable hydrophobicity can be obtained. In this work, such surfaces are obtained through the coassembly of thioctic acid with *n*-hexanethiol (C_6SH , Figure 1.6B). Figure 1.7 illustrates the mixed monolayers with different hydrophobicity studied in this project.

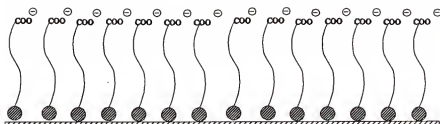
Whitesides and coworkers have studied the wettability of mixed monolayers with the methyl and the carboxylic headgroups by contact angle experiments.^{67,77,78} It has been found that the surface hydrophobicity is a function of the ratio of the two molecules. It was also concluded that the two constituents are not phase separated.^{67,78} Although a detailed understanding of the water-surface interactions at a molecular level and the dependence of the surface composition of the mixed monolayers on the solution composition is not yet available, coadsorption of molecules with different headgroups provides some empirical choices for the studies of different hydrophobic interactions. The choice of *n*-hexanethiol in our study, which has similar chain length to TA, is aimed to minimize the monolayer surface roughness, which may strongly change the double layer structure and the surface charge distribution of the monolayer at the interface.

1.3 Theories of Mass Transport and Heterogeneous Electron Transfer

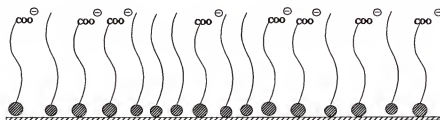
Electrochemical processes are complex because they involve many different phenomena simultaneously. Consider an electrochemical reaction:

Figure 1.7 Cartoon representations of the pure and the mixed monolayers investigated in this study: (a) thioctic acid monolayer; (b) 1:1 thioctic acid/ $\text{CH}_3(\text{CH}_2)_5\text{SH}$ mixed monolayer; (c) 1:100 thioctic acid/ $\text{CH}_3(\text{CH}_2)_5\text{SH}$ mixed monolayer; (d) $\text{CH}_3(\text{CH}_2)_5\text{SH}$ monolayer.

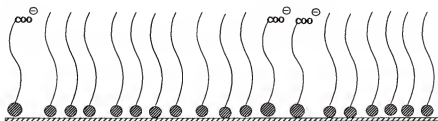
(a)



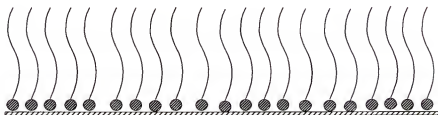
(b)



(c)



(d)





where Ox and Red are the oxidized and the reduced forms of the species involved in the reaction present in solution. In order to be electrochemically oxidized or reduced, the electroactive species must first come to the interface from the solution through a mass transport process. Upon arrival at the electrode surface, the electroactive species must experience a solvent exchange during which the reacting centers are geometrically positioned for electron transfer. Then electron transfer takes place, and finally the product(s) of the reaction move away from the electrode. Obviously, the electrochemical processes are heterogeneous and both the electron transfer and the transport of the electroactive material are the inherent parts of the overall reaction.

1.3.1 Mass Transport at Conventional Size Electrodes

Mass transport arises either from the differences in the electrical or the chemical potential at two locations, or from the movement of a volume element of solution. Mass transport consists of three modes: diffusion, migration and convection. Under general experimental conditions used in this study, convection and migration are the unwanted mass transport forms and can be avoided.

Diffusive profile of mass transport depends on the electrode geometry and the time of the experiment.⁷⁹ In order to better understand the diffusion process, we introduce the concept of a diffusion layer thickness, $\delta(t)$, a distance from the electrode surface over which there is a concentration gradient. Under the diffusion limited conditions, $\delta(t)$, as a function of time t , is described by

$$\delta(t) = (\pi D_o t)^{1/2} \quad (1-5)$$

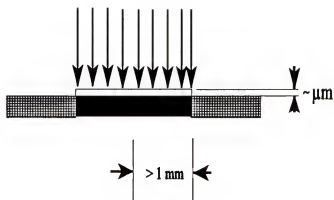
where D_o ($\text{cm}^2 \cdot \text{s}^{-1}$) is the diffusion coefficient of the species. At typical experimental conditions, time t is on the order of subseconds. The values of diffusion coefficients of small electroactive species in aqueous solution are typically on the order of $1 \times 10^{-5} \text{ cm}^2 \cdot \text{s}^{-1}$, which results in a typical diffusion layer thickness of ca. 50 μm . On a conventional size disk electrode (radius $r > 1 \text{ mm}$), the diffusion layer thickness is much smaller than the electrode radius. In mathematical terms, the diffusion process under such conditions corresponds to mass transfer in a one-dimensional diffusion field. This type of diffusion is termed as a semi-infinite linear diffusion.⁷⁹ Figure 1.8 (a) illustrates the concentration profiles, i.e. the diffusion layer profiles for the semi-infinite linear diffusion.

1.3.2 Diffusion at Microelectrodes

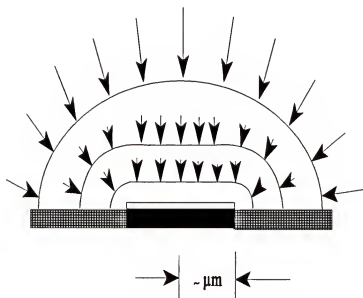
Equation 1-5 predicts that the diffusion layer thickness $\delta(t)$ increases with time. In addition to the mass transport perpendicular to the electrode, mass transport also develops parallel to the electrode.⁸⁰ At a sufficiently long time, the contribution from the parallel direction (the edge effect) becomes increasingly noticeable and the diffusion layer can be approximated by spherical diffusion where the mass transport takes place radially. The time scale for a diffusion layer to grow from a thickness much smaller than the radius of the disk electrode to significantly larger than the radius of the disk electrode is dependent on the electrode dimension (radius) and the diffusion coefficient of the electroactive species. At a subsecond time scales, the conditions for the linear (planar) diffusion are fulfilled on the conventional size disk electrode (radius $> 1 \text{ mm}$). As the electrode becomes

Figure 1.8 (a) Schematic diagram of a linear diffusion layer at an electrode. The electrode radius is much larger than the thickness of the diffusion layer; (b) Schematic diagram of diffusion layer growth at a microelectrode. Direction of diffusion changes with time to eventually become spherical.

(a)



(b)



smaller and smaller, the radius of the electrode can be comparable to the diffusion layer thickness at typical subsecond time scales and the radial diffusion occurs. The electrode radius for a fully developed hemispherical diffusion are typically on the order of micrometers at subsecond time scales. The electrodes of these dimensions are usually referred to as ultramicroelectrodes (UME).

Figure 1.8 (b) shows that as the electrode radius decreases, the semi-infinite linear diffusion is gradually transformed into semi-infinite hemispherical diffusion.⁸¹ As a consequence, many more electroactive molecules reach the electrode surface per unit time than in the case of pure linear diffusion.

In the following discussion, we will focus on response of the electroactive species for the case of chronoamperometry. In this simple electrochemical method, the electrode potential is stepped from a region where the redox reaction of the electroactive species does not occur to a value where its current is limited only by the diffusion of the electroactive species to the electrode surface. The current on a disk microelectrode is described by⁸¹

$$i = \frac{nFAD^{1/2}c^*}{\pi^{1/2}t^{1/2}} \left(1 + 4\pi^{-1/2} \left(\frac{Dt}{r^2}\right)^{1/2}\right) \quad (1-6)$$

where n is the number of electrons, F is the Faraday constant (96485 C/mole), A is the electrode area (cm^2), D and c^* are the diffusion coefficient (cm^2/s) and the bulk concentration of the electroactive species (mole/cm^3), t is the experimental time (s) and r is the electrode radius (cm). As long as linear diffusion dominates the mass transport and the

measurement time is short, the second term on the right hand side of eq. 1-6 can be neglected which results in a Cottrell equation that describes the planar diffusion current:⁷⁹

$$i = \frac{nFAD^{1/2}c^*}{\pi^{1/2}t^{1/2}} \quad (1-7)$$

By contrast, if the measurement time is long, the first term on the right-hand side becomes negligible and a steady state current is obtained:⁸¹

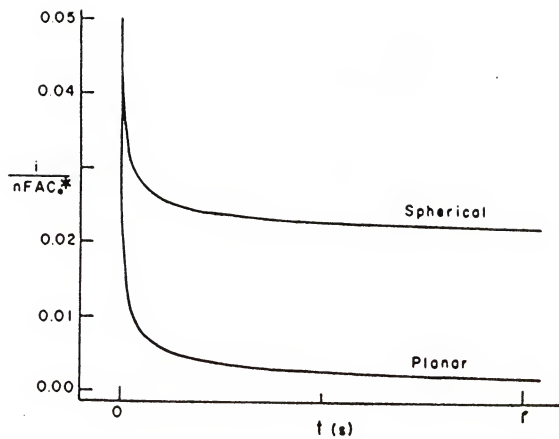
$$i = 4nFADrc^* \quad (1-8)$$

A practical comparison of the mass transport efficiency between the spherical diffusion and the linear diffusion can be conveniently made by evaluating the current under the two diffusion modes (Figure 1.9).⁸⁰ This can be achieved by division of eq. 1-6 by the current under the conditions of planar diffusion, i.e., the Cottrell equation (eq. 1-7). If the areas are *assumed* equal, we obtain

$$\frac{i_{\text{spherical}}}{i_{\text{planar}}} = 1 + \left(\frac{16Dt}{\pi r^2}\right)^{1/2} \quad (1-9)$$

Despite a small absolute value, the current on an electrode of 1 μm diameter under radial diffusion mode is ca. 130 times greater than under linear diffusion mode (using $t = 1$ s and $D = 1 \times 10^{-5}$ cm^2/s). It is therefore clear that radial diffusion is inherently more efficient in terms of mass transport than linear diffusion. This conclusion can also be obtained by examining the surface area of the interface between the diffusion layer and the bulk solution during diffusion. In linear diffusion, the area of the planar interface is essentially

Figure 1.9 Stimulated current-time curve in chronoamperometry for planar and spherical diffusion (assuming $D_0 = 10^{-5} \text{ cm}^2/\text{s}$ and $r = 5 \times 10^{-4} \text{ cm}$).⁸⁰



constant with time, while in radial diffusion the surface area increases as a function of time.⁸²

Due to the high mass transport rate, UMEs can be used to study kinetics of fast electrochemical reactions which are otherwise under diffusion control at the macroelectrodes. For the same reason UMEs can also be very useful for characterizing the properties of thin films where the electrode kinetics of the electrochemical probes are sensitive to the changes at the solution/monolayer interface. Detailed discussion of the last issue will be given in Chapter 5.

1.3.3 Heterogenous Electron Transfer

For simplicity, we assume that the electrode process described by eq. 1-4 is of the first order, the rate of the electrode reaction, expressed in moles of the substance transformed at the electrode surface per unit time and per unit area is

$$-\frac{dN_{Ox}}{dt} = \frac{dN_{Red}}{dt} = k_f C_{Ox}(0, t) - k_b C_{Red}(0, t) \quad (1-10)$$

where $C_{Ox}(0, t)$ (mole/cm³) is the surface concentration of the species in the oxidized state, $C_{Red}(0, t)$ (mole/cm³) is the surface concentration of the reduced species, and k_f and k_b are the heterogeneous rate constants for the forward and the back processes, respectively. These k 's characterize the kinetics of the heterogeneous process and are expressed in cm²sec⁻¹. In general, the standard heterogeneous rate constant (no excess potential), k^0 , can be expressed by⁸³

$$k^{\circ} = K_e v_s \kappa \exp\left(-\frac{\Delta G^{\ddagger}}{RT}\right) \quad (1-11)$$

where K_e is the pre-equilibrium constant for the reactant to form the precursor state before electron transfer (cm), v_s is nuclear frequency factor reflecting the rate at which reacting species in the transition state is transformed into product (s^{-1}), κ is the transition probability, R is the gas constant ($8.314 \text{ J mol}^{-1} \text{ K}^{-1}$), T is the temperature (K), and ΔG^{\ddagger} (kJ mol^{-1}) is the activation free energy for the overall reaction (eq. 1-4), which is a function of the reaction's driving force and the solvent reorganization energy, which measures the energy required for changing the solvent or ligand atmospheres from the reactants to the products. For electrode reactions, the potential difference is controllable in a precise way and the dependence of k_f and k_b on the externally applied potential, E , can be predicted. Using the Butler-Volmer model ⁷⁹

$$k_f = k^{\circ} e^{-\frac{\alpha n F}{RT}(E-E^{\circ'})} \quad (1-12)$$

$$k_b = k^{\circ} e^{\frac{(1-\alpha)nF}{RT}(E-E^{\circ'})} \quad (1-13)$$

where k° is the standard heterogeneous rate constant (cm s^{-1}), which is the value of k_f or k_b at $E^{\circ'}$, α is the transfer coefficient (symmetry factor, representing the distribution of electrons between the activated complex and the electrode), n is the number of electrons involved in the reaction, F is the Faraday constant (96485 C/mole), E is the electrode

potential (V) and E^0 is the formal potential of the redox couple (V). In a heterogeneous electrode reaction (eq. 1-4) the rate of the reaction is directly reflected by the rate of electrons passing through the interface, i.e. the observed current. Combining eqs 1-10, 1-12 and 1-13 and realizing that $i = nFAv$ where v is the rate of the electrode reaction expressed by eq 1-10, we obtain

$$i = nFAk^0 \left[C_{Ox} e^{-\frac{\alpha nF}{RT}(E-E^0)} - C_{Red} e^{\frac{(1-\alpha)nF}{RT}(E-E^0)} \right] \quad (1-14)$$

Equation 1-14 reveals that there are two major components that determine the current response of a redox reaction. When the rate of the reaction is sufficiently fast, the mass transport can be the limiting process, and vice versa.⁷⁹

1.3.4 Electron Transfer Across Impermeable Membranes

Long-distance, interfacial electron transfer plays a crucial role in numerous chemical and biological processes.^{84,85} Such fundamental questions as the dependence of the electron transfer rate on the reaction free energy, the electron transfer distance, and the molecular structure at the interface have yet to be fully answered.⁵⁷ SAMs of the long alkyl chain thiols were originally designed as a barrier to mass or electron transport between the electrode and the electrolyte solution, and are an ideal interface for studying the heterogeneous electron transfer.⁵⁶ For instance, changes in the number of the carbon atoms in the polymethylene tether can be used to control the electron transfer distance in a controlled manner.⁵⁷ In addition, SAMs can also shut off some unwanted electrode processes such as the formation of oxides on metal surfaces which may interfere with

measurements. Early efforts in monolayer construction have been focussed extensively on how to construct pinhole-free films on which electron transfer is solely carried out by tunneling. In the case of electron tunneling, the rate constant of electron transfer, k_{ET} , is described by Marcus theory:⁸⁶

$$k_{ET} = \kappa v_s \exp \left(- \frac{(\Delta G^\circ + \lambda)^2}{4RT\lambda} \right) \quad (1-15a)$$

$$\kappa v_s = 10^{13} \exp(-\beta(d-3)) \quad (1-15b)$$

Compared to the standard heterogeneous rate constant k° ($\text{cm}^2 \text{s}^{-1}$) expressed in eq. 1-11, it is clear that k° is the product of k_{ET} (s^{-1}), the unimolecular rate constant for the elementary electron-transfer step, and the pre-equilibrium constant for forming the precursor state, K_e (cm). The κv_s term in eq. 1-11 is more specifically expressed in Marcus theory using $v_s = 10^{13}$ and κ as a function of d , the distance between the electron donor and the receptor (\AA) (eq. 1-15b). β (\AA^{-1}) is the electron tunneling constant for a given medium, $-\Delta G^\circ$ (kJ mol^{-1}) is the driving energy and λ (kJ mol^{-1}) is the Marcus (solvent) reorganization energy. The last two energy terms are related to activation free energy ΔG^\ddagger in eq. 1-11 by $\Delta G^\ddagger = (\Delta G^\circ + \lambda)^2/4\lambda$. From eq. 1-15, it is clear that the electron transfer rate decreases exponentially with the distance between the electron donor and the receptor.

1.4 Electrode Kinetics on Membrane Electrodes

1.4.1 Surface Potential at the Electrode/Solution Interface--Bare Electrode

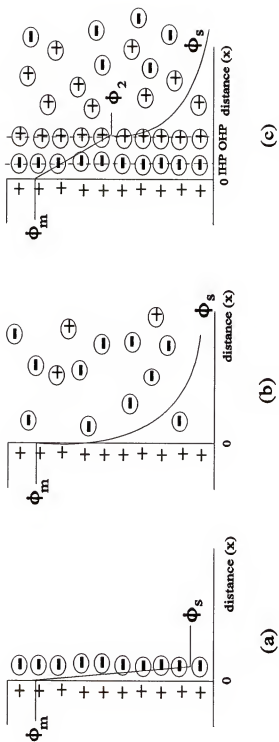
When a potential is applied to the electrode, an electrical double layer develops at the interfacial electrode/solution region. Helmholtz was the first to address the nature of the charge distribution at the interfaces and proposed that there would be two sheets of charge, having opposite polarity, separated by a distance on the order of a molecule. Figure 1.10 (a) illustrates the Helmholtz model of the electrical double layer which shows that the electrical potential changes sharply from its value in the solid (ϕ_m) to that at the center of the ionic layer (ϕ_0).

Gouy and Chapman took the Boltzmann distribution of the ions in a varying potential field at interfaces into consideration and worked out, independently, a treatment for the distribution of ions in the neighborhood of a charged solid. The surface potential across the electrode/solution interfacial region is thus expressed by⁷⁹

$$\psi = \frac{4kT}{ze} \exp(-\kappa x) \quad (1-16)$$

where k is the Boltzmann constant ($1.38 \times 10^{-23} \text{ J K}^{-1}$), z is species charge, e is electron charge ($1.60 \times 10^{-19} \text{ C}$) and κ (cm) is the Debye reciprocal length parameter, which is associated with the size of the ion atmosphere. At $x = 1/\kappa$ the potential has reached the $1/e$ fraction of its value at the surface and, therefore, this plane is taken as the effective thickness of the diffuse double layer. As shown schematically in Figure 1.10 (b), the Gouy-Chapman treatment leads to an ionic-atmosphere type of distribution, with the potential falling more gradually through the diffusion layer.

Figure 1.10 Schematic illustration of the double layer structure at the electrode surface: (a) Helmholtz model; (b) Gouy-Chapman model; (c) Gouy-Chapman-Stern model.



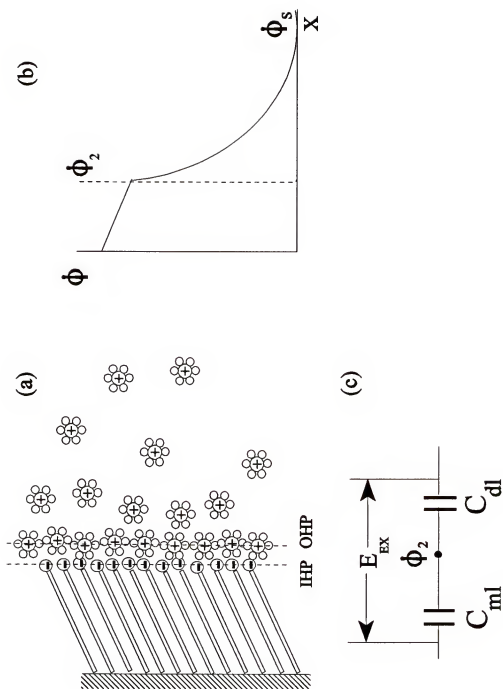
A more satisfactory double layer model was proposed by Stern which combines the Helmholtz and Gouy-Chapman ideas.^{79,87} Stern recognized that a satisfactory treatment must take into account the finite size of the ions involved, and the specific chemisorptive interactions between the ions and the surface. His model is presented schematically in Figure 1.10C. The surface is shown bearing a positive charge relative to the solution, and there is a layer of negative ions held at the surface by chemisorptive and electrostatic attraction. The region from the surface to the center of this layer of ions may be referred to as the Helmholtz compact layer. There is a sharp potential drop from ϕ_m to ϕ_2 . Outside the Helmholtz compact layer there is a Gouy-Chapman or the diffuse Helmholtz layer, over which the potential drops more gently from ϕ_2 to ϕ_s , the potential of the bulk of the solution.

The structure of the electrical double layer present at an electrode/electrolyte interface can affect the rates of heterogeneous electron transfer. For electrode with non-zero charge, a portion of the applied potential is dropped outside the plane of the closest approach of the nonspecifically adsorbed redox species within the diffuse layer.⁸⁸ This potential also distorts the concentrations of ionic species within the double layer from their bulk values.⁸⁹

1.4.2 Potential Distribution at a Charged Monolayer

When a monolayer is assembled on the electrode, the surface double layer structure is greatly altered. We propose a modified Stern model to describe the double layer structure on the electrode with a monolayer present (Figure 1.11),⁷⁰ where the fundamental modification of the model is to use the self-assembled monolayer to replace

Figure 1.11 A model of the double layer structure on the TA monolayer electrode: (a) ion distribution at the interface; (b) potential distribution of the interface; (c) equivalent circuit.



the concept of the compact layer in the Gouy-Chapman-Stern model (Figure 1.10 (c)).

The double layer structure is then approximated by a simple two-capacitor system consisting of an ideal compact monolayer as the inner layer capacitor and the diffuse double layer capacitor, connected in series. The overall capacitance, C_{total} , is⁷⁰

$$\frac{1}{C_{total}} = \frac{1}{C_{dl}} + \frac{1}{C_{ml}} \quad (1-17)$$

where C_{dl} is the double layer and C_{ml} is the monolayer capacitance in $\mu\text{F}/\text{cm}^2$. Each term in eq. 1-17 can be calculated individually. C_{ml} may be obtained using the Helmholtz capacitor model:

$$C_{ml} = \epsilon_o \epsilon A / d \quad (1-18)$$

where ϵ is the dielectric constant of the monolayer, ϵ_o is the permittivity of free space ($8.85 \times 10^{-14} \text{ F/cm}$), A is the electrode area (cm^2) and d is the monolayer thickness (cm). C_{dl} , on the other hand, can be calculated from Gouy-Chapman theory.⁷⁹ For dilute aqueous solutions at 25° , C_{dl} is

$$C_{dl} = 228 zc^{1/2} \cosh(19.5z\phi_2) \quad (1-19)$$

where z is the electrolyte charge, c^* is electrolyte concentration (M) and ϕ_2 is monolayer surface potential in mV. The value of ϕ_2 is usually very small for a surface coated with an uncharged layer, since a large portion of the potential drops across the film so that the double layer at the solution/film interface is only weakly developed compared to that on a bare electrode. However, when the surface coating becomes charged, the potential

difference between the film surface and the bulk is no longer small due to the fixed charge on the monolayer and the associated movement of counterions that build a Donnan potential at the interface. Under such conditions, the value of ϕ_2 has a significant impact on both the equilibrium between the externally applied potential and the degree of the electrochemical oxidation or reduction processes, as well as on the rate constants of the electroactive species, i.e. electrode kinetics. For instance, if ϕ_2 is non-zero, a fraction of the applied potential will be unavailable to drive the electron transfer, and the rate constants must be adjusted accordingly.⁹⁰

The ϕ_2 on the monolayer surface is a function of the experimental parameters such as external applied potential (E_{ex}), and the monolayer and solution properties.⁹⁰ Using the equivalent circuit shown in Figure 1.11 (c), ϕ_2 is described by

$$\phi_2 = E_{ex} \frac{C_{ml}}{C_{ml} + C_{dl}} \quad (1-20)$$

The rate constants for the electrochemical reactions on the monolayer electrode, k_{ml} (cm/s), are thus influenced by the non-zero values of ϕ_2 through^{91,92}

$$k_{ml} = k_o \exp [-z\phi_2/kT] \quad (1-21)$$

where z is the probe charge, k_o (cm.s⁻¹) is the standard heterogeneous rate constant, k is the Boltzmann's constant and T (K) is the absolute temperature. It is worth noting that on thin monolayers with hydrophilic headgroups both C_{ml} and C_{dl} are greatly influenced by the solution properties.

1.4.3 Effect of Electrolyte on Surface Potentials of Charged Monolayers

When a charged monolayer is immersed in a dilute electrolyte solution, the concentration of the counterions adjacent the charged plane is typically higher than that in the bulk solution. For example, at the TA monolayer/solution interface, the concentration of cations, counterions to carboxylate after dissociation, will be much higher than in the bulk (Figure 1.11A). Thus, under the influence of the concentration gradient, cations tend to diffuse into the solution while anions diffuse to the film surface. A Donnan potential develops at the interface, which results in a negative monolayer surface potential with respect to the adjacent electrolyte. An equilibrium is established in which the tendency of the ions to level out the existing concentration difference is balanced by the action of the electric field. Compared to the double layer structure on the bare electrode described by Gouy-Chapman-Stern model, as illustrated in Figure 1.10C, the layer of the carboxylic headgroups can be regarded as the inner Helmholtz plane (IHP) distance, while the layer of counterions is taken as the outer Helmholtz plane (OHP) distance (Figure 1.11C). The potential drop across the double layer ϕ_{DL} , defined as $\phi_2 - \phi_s$, can be estimated on the basis of the Gouy-Chapman theory.^{93,94}

$$\phi_{DL} = \frac{kT}{e} \sinh^{-1} \left[2 \frac{134}{AC^{1/2}} \right] \quad (1-22)$$

where k is the Boltzmann constant ($1.38 \times 10^{-23} \text{ J K}^{-1}$), e is electron charge ($1.60 \times 10^{-19} \text{ C}$), A is the surface area of the adsorbed molecule (\AA^2), which is the carboxylic group in this case, and C is the concentration (M) of the 1:1-type electrolyte.

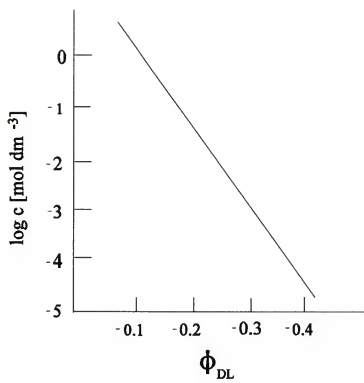
Equation 1-22 allows us to evaluate the dependence of the potential drop across the diffuse layer on the electrolyte concentration. Values of ϕ_{DL} calculated with eq. 1-22 using the surface area of the carboxylic group $A = 20 \text{ \AA}^2$ and $T = 298 \text{ K}$ are plotted in Figure 1.12. From Figure 1.12, the higher the electrolyte concentration, the smaller the potential drop across the diffuse layer, indicating that the thickness over which the surface potential has an electrical impact on the species in solution is smaller compared to that at low electrolyte concentration. As a result, the closest approach distance of the electroactive species on the monolayer becomes smaller at high electrolyte concentration, and the kinetics of the species are fast accordingly.

For the thioctic acid monolayers, penetration of ions into the monolayer may occur at high ionic concentration, resulting in high measured capacitance of the monolayer. Therefore, the film becomes apparently more "conductive", and the potential drop over the monolayer is lower compared to that in electrolytes of lower concentration.⁷⁰ This may further contribute to the fast kinetics of the electroactive species at high electrolyte concentration.

1.5 Electron Mediation at a Redox Monolayer

Electrocatalysis of electrode reactions is important since it is often observed that the electrode kinetics of an analyte at a naked electrode surface are slow. As a result, the oxidation or reduction occurs at a potential that is much more positive or negative, respectively, than the expected thermodynamic potential.⁹⁵ The problem of the overpotential limits applications of electrochemical measurements in the biological fluids

Figure 1.12 A plot of ϕ_{DL} as a function of solution electrolyte concentration.



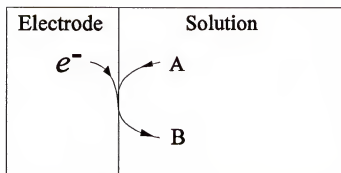
where the presence of electroactive species such as ascorbic acid or uric acid and even oxygen interferes with the measurements.⁹⁶⁻⁹⁸ The practical strategy of tackling this problem is to decrease the overpotential by accelerating the desired reaction with an immobilized mediator catalyst.⁹⁹⁻¹⁰⁰

The principle of such strategy is illustrated in Figure 1.13. In the uncatalyzed reaction, substrate (A) diffuses toward the electrode surface, where it is reduced or oxidized into the product (B). In the homogeneously catalyzed processes, the catalyst is introduced into the solution, together with the substrate (A), in its unreactive form P. P is the oxidized half of the catalyst couple, if the overall reaction is a reduction, and is its reduced half, if the overall reaction is an oxidation. In the case of a reduction, the catalyst couple P/Q is selected so as to have its standard potential positive to the reduction potential of the substrate, and vice versa in the case of an oxidation reaction. The reaction is carried out at a potential where the active form of the catalyst couple Q is generated. Since the substrate is not directly reduced (or oxidized) at the electrode at this potential, it reacts with the active form of the catalyst instead of reacting with the electrode.

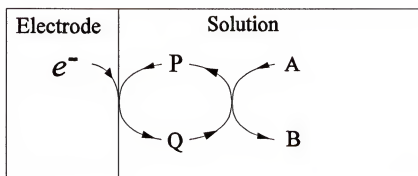
The principle of electrocatalysis at monolayers is similar except that the redox couple is now confined within the monolayer surface instead of being dispersed in the solution. The advantage of a supported system over a homogeneous system in sensor applications stems from the physical separation of the catalyst from the substrate.¹⁰¹ It is also important to point out that the catalytic response of the coating is not only a function of the intrinsic reactivity of the catalyst but also of the properties of the supporting materials such as film permeability and electron transfer rate on it.¹⁰²

Figure 1.13 Types of electrocatalysis on electrodes: (a) uncatalyzed reaction; b) homogeneous catalysis; (c) heterogeneous catalysis.¹⁰⁴

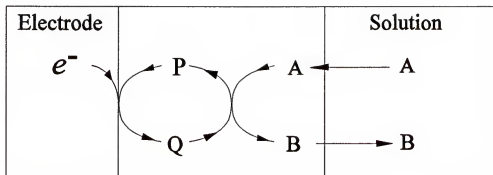
(a)



(b)



(c)



Ferrocene (Fc) and its derivatives are excellent mediator compounds for constructing electrochemical sensors for the analysis of biologically important compounds. Ferrocene is a transition metal π -arene complex which consists of an iron atom sandwiched between two cyclopentadienyl rings. It is chemically inert and has a mild thermodynamic formal potential ($E^0 = 0.165$ V vs. SCE). More importantly, it has an extraordinarily fast mediation rate constant with many enzymes ($k_{\text{med}} \sim 10^6 \text{ M}^{-1} \cdot \text{s}^{-1}$).¹⁰³ The ferrocene group has been applied in the development of sensors for the determination of glucose,¹⁰⁴⁻¹⁰⁸ cholesterol,¹⁰⁹ glycolate,¹¹⁰ lactate,¹¹¹ pyruvate,¹¹² and NADH,¹¹³⁻¹¹⁴. The methods of introducing Fc to the detection system varied from adding free Fc to solution,¹⁰⁴ attaching Fc to a carbon electrode by a chemical reaction involving formation of covalent bond,¹¹⁵ entrapment of Fc in poly(acrylic acid) layer,¹¹⁶ to covalently binding Fc through amide linkage to enzymes embedded in the redox epoxy.¹¹⁷⁻¹²⁰ Recently, Majda and coworkers used Langmuir-Blodgett films to immobilize a Fc surfactant on a porous alumina electrode and a lateral mediation effect of ferrocene to glucose oxidase, resulting in amperometric detection of glucose, was observed.¹²¹

Covalent immobilization of fast redox center Fc onto the TA monolayers was attempted in this work. The aim was to improve the response sensitivity of large biological molecules on the TA monolayer electrode by introducing Fc onto the monolayer to function as "electrical relays" between the electrode and the substrate. Therefore, facilitated electron transfer was expected between the electrode and the redox centers of the enzymes as a result of the expected reduced electron transfer distance (eq. 1-15).

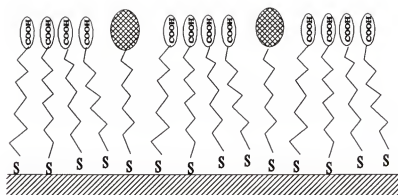
In the immobilization of fast redox centers onto the TA monolayer, structural and chemical properties of the redox center, as well as the compatibility of the redox center

with the monolayer had to be considered. The residence of a bulky, hydrophobic center, e.g. ferrocene, on the TA monolayer is not favored because of the hydrophilic carboxylic acid headgroup environment. As illustrated in Figure 1.14 (a), the presence of ferrocene can interrupt the hydrophilic interactions and the monolayer structure. Due to differences in hydrophilicity, the ferrocene may repel the hydrophilic carboxylic headgroups, resulting in local aggregation of the TA molecules and thus perturbing the film structure, and ultimately the structure and the selectivity of the TA monolayers may be lost. To prevent this from happening, a strategy was proposed to add a short, ca. 5-6 Å, hydrocarbon chain to "lift" the hydrophobic moiety above the TA monolayer plane, as illustrated in Figure 1.14 (b). Therefore, the unfavorable interactions between the hydrophobic redox center and the carboxylic groups may be minimized.

Figure 1.15 shows the proposed chemical reaction route for immobilizing ferrocene on the TA monolayers. In order to preserve the monolayer structure, DEC (1,3-(dimethylamino)propyl-3-ethylcarbodiimide hydrochloride) was used as the coupling reagent so that the immobilization reaction can be carried out in aqueous solution and at room temperature. DEC is an excellent water-soluble reagent to couple amines with carboxylic acid by forming amide linkage, and has found extensive applications in peptide synthesis and protein modification.¹²² It promotes amide formation by reacting with the carbonyl group of an acid and activating it towards nucleophilic substitution.¹²³ As illustrated in Figure 1.15, a ferrocene derivative with an amine terminal would be synthesized as the immobilization precursor. After the TA monolayer is activated by DEC, the amine end of the precursor is expected to attack the activated carboxylic headgroup on

Figure 1.14 Cartoon representation of the structure of the TA monolayer in the presence of the ferrocene headgroup: (a) unfavorable residence of the hydrophobic ferrocene at the monolayer plane; (b) favorable residence of the hydrophobic ferrocene outside the monolayer plane.

(a)



(b)

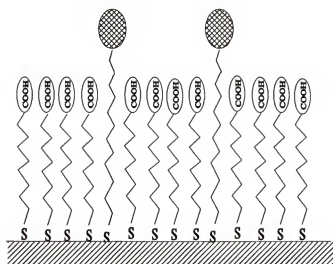


Figure 1.15 Proposed synthetic route for the *in situ* immobilization of the ferrocene headgroup onto the TA monolayer.

the TA monolayer, and connect the ferrocene molecule to the monolayer through an amide linkage.

1.6 Purpose of This Work

The objective of this work is to develop a strategy for building molecular architecture on an electrode surface with well-defined molecular structure, providing control over the local chemical environment as to ultimately endow the electrode surface with advantages in electroanalysis of the biological molecules. This is attempted by constructing self-assembled monolayers (SAM) with a nanometer level structural resolution on the gold electrodes.

The SAMs aimed to control the interfacial reactivity of the electrode were prepared through the self-assembly of thioctic acid (1,2-dithiolane-3-pentanoic acid, abbreviated as TA). The SAMs of thioctic acid were expected to combine the advantages of "traditional" long alkyl thiol monolayers as stable, organized molecular structures, with the chemical properties of the carboxylic headgroups such as pH-dependent association/dissociation and the inherent hydrophilicity. In Chapter 3, capacitance measurements are first introduced to reveal the structural information and the permeability of the TA monolayers. Next, cyclic voltammetry combined with fast redox probes is utilized as a major tool to explore the electrochemical sensitivity and selectivity of the monolayers. The focus will be placed on revealing the factors that control the interfacial charge distribution on the monolayer, and the consequence of the charge distribution on electrochemical characteristics at the monolayer. The electrochemical probing is conducted as a function of the solution and the probe properties to establish the

correlation between the film structure and the resulting electrochemical response at the monolayer. A model for the TA monolayer/solution interface is proposed based on the observed experimental results. Finally, the effect of substrate smoothness on film quality and selectivity, and the stability of the TA films is investigated.

In Chapter 4, the electrochemical properties of the monolayer electrode are investigated as a function of the surface hydrophobicity, in an attempt to reveal the correlation between the electrochemical response of the biological probes and the surface hydrophobicity.

The characterization of the thioctic acid monolayers on ultramicroelectrode (UME) is described in Chapter 5. UMEs can be utilized as a tool to explore the fine changes in the monolayer structure and their effect on the electrochemical response due to the highly effective mass transport to the electrode. Applications using the TA UME in conjunction with the redox probes for amperometric pH sensing are explored.

The objective of Chapter 6 is to explore protein interactions on the TA monolayers in order to evaluate the perspective of the monolayers for developing biosensors. The focus will be placed on the ability of the TA monolayers to provide an appropriate interface for protein interactions, and on the role of protein/monolayer interactions on the electrode response. On the basis of the understanding of the TA monolayer/protein interactions, a strategy for promoting electron transfer at the monolayer electrode is proposed by covalently immobilizing fast redox centers on the TA monolayer to achieve mediation effects. Finally, the results of this work are summarized and future research plans are discussed in Chapter 7.

CHAPTER 2 EXPERIMENTAL

2.1 Materials

2.1.1 General Reagents

Thioctic acid (TA) was purchased from Aldrich. Hexaammineruthenium (III) trichloride ($\text{Ru}(\text{NH}_3)_6\text{Cl}_3$) was obtained from Alfa Products. Potassium ferricyanide ($\text{K}_3\text{Fe}(\text{CN})_6$), potassium chloride, potassium phosphate monobasic, dibasic, sodium fluoride, hydrogen peroxide (30%) and sulfuric acid were obtained from Fisher Scientific. Sodium phosphate monobasic and dibasic were obtained from Mallinckrodt. Potassium fluoride was from Kodak Chemical. Absolute ethanol (200 proof) was obtained from Florida Distillers Company. Tris (acid and base forms) were obtained from Sigma. All chemicals were reagent grade and were used as received.

Aqueous solutions were freshly prepared from doubly distilled, deionized water. Prior to use, solutions were purged with nitrogen (N_2) for at least 5 minutes. All measurements were made at room temperature (25°C).

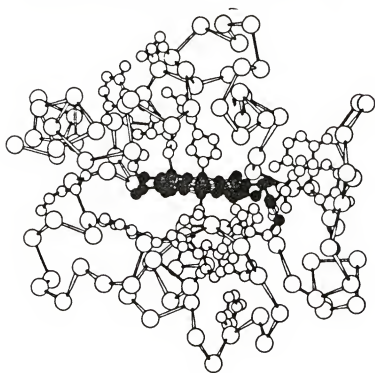
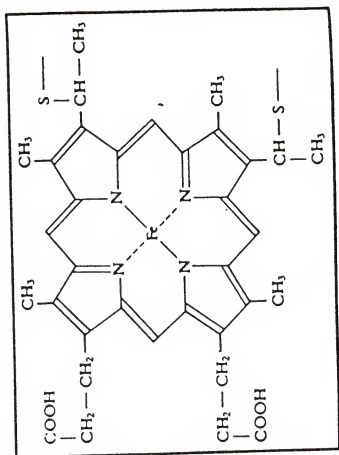
2.1.2 Biological Probes

3-Hydroxytyramine (dopamine, DA), 3,4-dihydroxypheylacetic acid (DOPAC) and benzoquinone (Q) were chosen as probes with biological significance to investigate the electrochemical characteristics at the monolayer electrodes. Table 1 shows the structures and the electrochemical properties of the three probes at pH 7.0. DA is an important neurotransmitter in central nervous system (CNS) and DOPAC is the metabolite of DA,¹²⁴

Table 2.1 Probes and Their Electrochemical Reactions in Aqueous Solutions

Structure	Name	pK _s	Charge at pH 7	Electrochemical reactions
$\text{NH}_3^+-\text{CH}_2-\text{CH}_2-\text{C}_6\text{H}_3(\text{OH})_2$	DA	8.92	+1	$\text{NH}_3^+-\text{CH}_2-\text{CH}_2-\text{C}_6\text{H}_3(\text{OH})_2 \xrightarrow{-2e, -2\text{H}^+} \text{NH}_3^+-\text{CH}_2-\text{CH}_2-\text{C}_6\text{H}_2(\text{OH})(\text{O})$
$\text{O}=\text{C}(\text{O}^-)-\text{CH}_2-\text{CH}_2-\text{C}_6\text{H}_3(\text{OH})_2$	DOPAC	4.22	-1	$\text{O}=\text{C}(\text{O}^-)-\text{CH}_2-\text{CH}_2-\text{C}_6\text{H}_3(\text{OH})_2 \xrightarrow{-2e, -2\text{H}^+} \text{O}=\text{C}(\text{O}^-)-\text{CH}_2-\text{CH}_2-\text{C}_6\text{H}_2(\text{OH})(\text{O})$
$\text{O}=\text{C}_6\text{H}_4=\text{O}$	Q	-	0	$\text{O}=\text{C}_6\text{H}_4=\text{O} \xrightarrow{2e, 2\text{H}^+} \text{HO}-\text{C}_6\text{H}_4-\text{OH}$

Figure 2.1 Structures of cytochrome c and the heme group.¹²⁷ The heme group (solid circles) is located in a protein pocket with the heme edge slightly exposed at the protein surface.



while Q plays an important role in the biological electron transfer chain in mitochondrial respiration.¹²⁵ DA and DOPAC have structural similarity except that DA has an amine terminal while DOPAC has a carboxylic terminal. (Table 2.1) Q is chosen primarily because of its aromatic ring that resembles that in the catecholamine DA. The pK_a 's of DOPAC are 4.22, 9.58 and 12.15 and for DA it is 8.92.¹²⁶ Therefore, at pH 7.0, DA is positively charged, DOPAC is negatively charged and Q is neutral.

Horse heart cytochrome c is a redox-active protein found in cell mitochondria.¹²⁷ It is involved in the electron transfer reactions in mitochondrial respiration cycle as the electron carrier.¹²⁷ Cytochrome c may be the most characterized redox protein due to its important role in the biological electron transfer. Figure 2.1 shows the structure of cytochrome c. The iron containing prosthetic heme group resides in a protein pocket, with a heme edge slightly exposed at the protein surface. Upon receiving an electron from cytochrome c_1 , as in the oxidative phosphorylation electron transfer chain, native cytochrome c in the oxidized state (Fe^{III}) can be reduced to heme- Fe^{II} .¹²⁷ The formal potential, E^o , for the solution free cytochrome c is reported to be 0.01 V vs SCE in phosphate.¹²⁷

Cytochrome c is the best candidate for the investigation of the protein/interface interactions, owing to the vast volume of the existing literature about the properties of this protein.¹²⁸ It has a molecular weight of 12,000 daltons with the dimensions of 25x25x35 Å.¹²⁸ The protein surface is positively charged (+9) at neutral pH due to the presence of lysine groups around the heme edge.¹²⁸

DA, DOPAC and horse heart cytochrome c were purchased from Sigma. Benzoquinone was from Fisher Scientific.

2.1.3 Synthesis of $H[Ru(EDTA)(H_2O)]^{129}$

Potassium chlorideruthenite ($K_2RuCl_5(H_2O)$) was obtained from Johnson Matthey. Sodium ethylenediaminetetraacetate (Na_2EDTA) was from Fisher Scientific and trifluoroacetic acid (CF_3COOH) was purchased from Aldrich.

One gram $K_2RuCl_5(H_2O)$ (2.67 mmol) was dissolved in a 150-ml beaker with 50 ml, pH 2 solution prepared by CF_3COOH and heated to near boiling for 30 min. One gram Na_2EDTA was dissolved in 50 ml water and the EDTA solution was added to ruthenium solution and boiled for 45 min. The solution was evaporated slowly until light yellow precipitate appeared. Fifty milliliters ethanol was added and the solution was cooled to room temperature. The solution was filtered and the product was rinsed with ethanol and air dried. The product was recrystallized with hot 0.1 M CF_3COOH . The obtained product was confirmed with UV (347 nm, 278 nm) and electrochemical methods.

2.1.4 Synthesis of N-(2-Aminoethyl)ferrocylacetamide

Ferrocylacetic acid and phosphorous trichloride were obtained from Aldrich. Tetrahydrofuran (THF) and ethylenediamine were from Fisher Scientific. Ethylenediamine was distilled before use.

Fifty milligrams ferrocylacetic acid (2.05×10^{-4} moles) was added and dissolved in excess PCl_3 (10 ml), and the solution was refluxed for 2 hours. Excess PCl_3 was removed by raising the temperature. The dark brown residue was dissolved in ca. 3 ml THF and added drop by drop to 5 ml ethylenediamine under vigorous stirring. The solution was left for an hour to allow the reaction to complete. The excess ethylenediamine was removed

under reduced pressure. The raw product was dissolved in 75 % ethanol/water and placed in refrigerator at 4 °C. The product was precipitated out as a brown powder. The product was verified by electrochemical methods in aqueous solutions.

2.2 Electrochemical Apparatus

Electrochemical measurements were carried out with a Bioanalytical Systems electrochemical analyzer, BAS-100. The data were downloaded to an IBM compatible PC for storage and analysis. A conventional three-electrode setup was employed, with the monolayer electrode as the working electrode, a platinum wire electrode as the auxiliary electrode and a saturated calomel electrode (SCE) as the reference electrode. All potentials are reported at room temperature versus SCE unless otherwise specified.

For electrochemical measurements conducted on an ultramicroelectrode, a BAS-100 electrochemical analyzer equipped with a home made preamplifier was used.^{26,130} Since the absolute current is very small, a two-electrode setup was employed, with the ultramicroelectrode as the working electrode, and the SCE in saturated KCl as both the auxiliary and the reference electrode.

2.3 Experimental Procedures

2.3.1 Preparation of Electrodes

2.3.1.1 Preparation of atomically smooth gold substrate

The gold substrates were prepared by thermal evaporation of a ca. 3000 Å thick layer of high purity Au (99.99%) onto the electronic grade single-crystal silicon wafers.

Prior to evaporation, silicon wafers were cleaned in hot piranha solution (1:4 30 % $\text{H}_2\text{O}_2\text{:H}_2\text{SO}_4$) for an hour. (CAUTION: piranha solution is a strong oxidizing agent and can react explosively with organic materials.) The wafers were then rinsed extensively with twice-distilled deionized water and dried in an Ar stream. The base operating pressure of the evaporator during evaporation is ca. 1×10^{-6} Torr. The evaporation rate, which was measured with a quartz thickness monitor, was ca. 10 nm/min. After preparation, the gold substrates were stored in a glass jar filled with Ar.

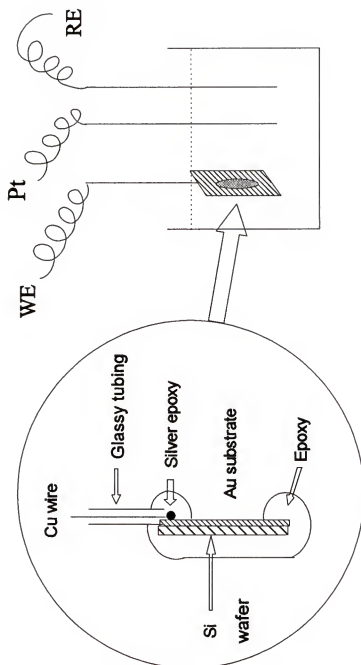
Nuzzo and coworkers pointed out that the gold substrates prepared with the above procedure were polycrystalline gold films exhibiting a dominant (111) texture.⁵⁷ The gold substrates obtained for this study had a homogeneous physical appearance and were uniformly and sharply reflective to the eye.

In order to investigate the effect of substrate quality on the electrochemical response at the monolayers, gold films evaporated onto the conventional microscope glass slides (Fisher Scientific) were prepared. The procedure for cleaning, evaporation, and storage of these substrates was the same as used for the silicon wafers. The physical appearance of the gold films on the glass slides had no difference to the eye from that of the films on the silicon wafers.

2.3.1.2 Fabrication of Au electrodes

The gold electrodes used for monolayer assembly were prepared from the vacuum deposited Au films on the silicon wafers. Figure 2.2 is an illustrative diagram of an Au electrode used in this study. The silicon wafer was cut with a glass cutter into 1.5 cm x 1.5 cm pieces. During this process, an Ar stream was used to blow the dust away to protect

Figure 2.2 A diagram of the electrode design and the electrochemical cell.



the gold surface from being damaged by the silicon dust. A copper wire was connected to the gold substrate surface via silver epoxy (Type 410E, Epoxy Technology, MA). It takes 2 or 3 days for the silver epoxy to completely cure at the room temperature. The copper wire was inserted into a soft glassy tubing which had been cut to be ca. 10 cm long. The silver epoxy joint as well as the back of the electrode was sealed with an inert epoxy (Epoxy-patch, The Dexter Corporation, Hysol Division, CA), leaving a defined area exposed to the solution. The electrode was then baked in an oven at 50°C for 24 hours to complete the curing of epoxy. The electrode area was determined by chronocoulometry with 1 mM $\text{Ru}(\text{NH}_3)_6^{3+}$ in 0.1 M phosphate at pH 7. 4 (diffusion coefficient of $\text{Ru}(\text{NH}_3)_6^{3+}$, $D_0 = 5.5 \times 10^{-6} \text{ cm}^2/\text{s}$).¹³¹ The potential window for the electrode area determination was from -50 mV to -350 mV vs SCE with a pulse width of 250 ms.

2.3.1.3 Ultramicroelectrodes

The microdisk ultramicroelectrodes were fabricated from gold fibers. A gold fiber ($d=12.7 \text{ }\mu\text{m}$, 99.9%, obtained from Johnson Matthey, MA) was mounted on a copper wire with silver epoxy (Type 410E, Epoxy Technology, MA). The gold wire as well as the connecting joint were sealed in a glass capillary with inert epoxy (Epoxy-patch, The Dexter Corporation, Hysol Division, CA). The electrode was then baked in an oven at 50°C for 24 hours to complete the curing of epoxy. Before use, the electrode was first polished on 600 grit polishing paper (Mark V Laboratory, East Granby, CT) and then on a polishing cloth using 0.1 μm gamma alumina slurry (Fisher Scientific). After polishing the electrode was sonicated in distilled water for 5 min.

2.3.1.4 Preparation of self-assembled monolayer films

The self-assembled monolayer electrodes were prepared by immersing the electrodes into the 0.1 % ethanol solution of thioctic acid for not less than 12 hours. It has been reported that variation of solution concentration of the thiols and sulfides in the range from 0.05 % to 0.5 % would not significantly affect the monolayer quality.^{42-48,57} Prior to immersing the electrode into the solution, the gold surface of the electrode was cleaned with piranha solution (Do not let piranha solution stay on the electrode surface longer than 10 seconds, otherwise it may carbonize the epoxy), and rinsed with a large volume of water and ethanol. The monolayers prepared from brief exposure (1 hour) of the Au electrode to the TA solution tended to be of slightly poorer quality. Electrodes were removed from the solution and rinsed with ethanol, and then with water prior to use.

Electrodes coated with the mixed self-assembled monolayers were prepared similarly. The coating solutions were 1:1 thioctic acid:*n*-hexanethiol, 1:100 thioctic acid:*n*-hexanethiol, and pure *n*-hexanethiol, all were 0.1 % solutions in absolute ethanol. The ratios here were simply the composition of the solutions. They do not necessarily reflect the real composition of the films on the electrodes.

The monolayer modified ultramicroelectrodes were prepared in a slightly different way due to the polycrystalline surface features of the gold fiber. An etching procedure was introduced to smooth the surface. Before the modification with TA, the polished gold wire was dipped in dilute aqua regia ($\text{HCl}:\text{HNO}_3:\text{H}_2\text{O}$ 3:1:16) for 5 min, washed thoroughly and sonicated for 5 min in deionized water. The electrode was then immersed in 0.2 % TA/ethanol solution for 30 min. Further studies revealed that by immersing UME in the

TA solution for 30 min, the monolayers resulted had the same quality as the monolayer formed by immersing the UME in the TA solution for 5 hours. Longer exposure (12 hours) was avoided since it produced electrodes with erratic responses, presumably due to the partial dissolution of the epoxy around the disk area which may have affected the monolayer structure. The electrodes were rinsed extensively with deionized water before measurements.

The TA UMEs made by the above procedure generally show a characteristic sigmoidal electrochemical response at the subsecond time scales. However, after several scans in acidic solutions of $\text{Fe}(\text{CN})_6^{3-}$ peak shaped response was observed. When the electrode was subsequently transferred to $\text{Fe}(\text{CN})_6^{3-}$ free, 0.1 M KCl solution (pH 7.4), $\text{Fe}(\text{CN})_6^{3-}$ response was observed which gradually disappeared. $\text{Fe}(\text{CN})_6^{3-}$ adsorption may be responsible for the observed behavior. Since $\text{Fe}(\text{CN})_6^{3-}$ response did not disappear when the electrode was transferred to $\text{Fe}(\text{CN})_6^{3-}$ free, acidic 0.1 M HClO_4 solution (pH 1.5), low pH must play an important role in the apparent adsorption of $\text{Fe}(\text{CN})_6^{3-}$. It is presumed that at low pH strong interactions between $\text{Fe}(\text{CN})_6^{3-}$ and the electrode surface (possibly involving the adjacent epoxy, which can be protonated at low pH) may occur, while at the higher pH the interactions do not take place. In the electrochemical measurements of $\text{Fe}(\text{CN})_6^{3-}$ at the low pH, long exposure of the electrode to the solution was avoided; before each measurement the surface was polished in order to obtain reproducible results..

2.3.1.5 Preparation of ferrocene derivatized monolayer films

The chemical reaction route used to immobilize ferrocene moiety on the TA monolayers is shown in Figure 1.15. DEC (1,3-(dimethylamino)propyl-3-ethylcarbodiimide

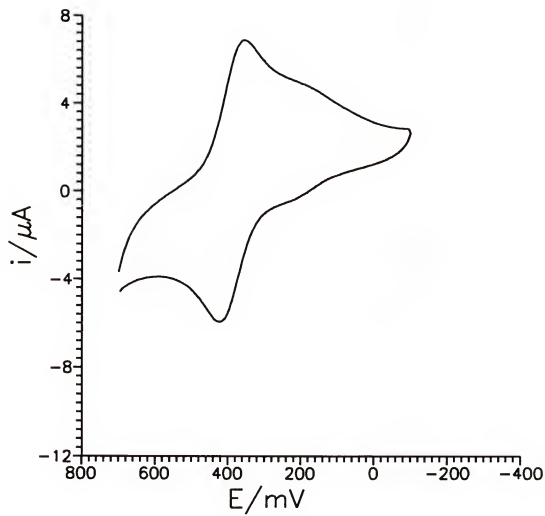
hydrochloride) was used as the coupling reagent to link N-(2-aminoethyl)-ferrocylacetamide to the TA monolayer, and the reaction was carried out at the room temperature. In the experiment, the TA monolayer was first prepared by immersing Au electrode in the 0.1 % TA ethanol solution overnight, as described previously. The electrode was then rinsed extensively with water, immersed into a 0.15 M Na-HEPES solution (pH 7.4) containing 5 mM DEC and 5 mM N-(2-aminoethyl)ferrocylacetamide and incubated overnight. The electrode was then rinsed with a large volume of water prior to use. The monolayer electrode was tested by using 1 mM $\text{Fe}(\text{CN})_6^{3-}$ in 0.1 M HClO_4 (pH 1.5) to determine if the monolayer electrode had been fouled after surface reactions. Figure 2.3 shows the CV result. Clearly, the electrochemical reactivity of the TA monolayer electrode was preserved after surface immobilization reactions. The shoulder peaks observed at ca. 0.20 V in Figure 2.3 indicate the presence of Fc compound on the monolayer.

2.3.2 Electrochemical Techniques

2.3.2.1 Cyclic voltammetry at conventional size electrodes

Cyclic voltammetry (CV) was employed in this study to obtain the kinetic information of the electroactive species on the monolayer electrodes. At conventional size Au electrodes on which response is controlled by semi-infinite planar diffusion at the subsecond time scales, peak shape current-potential curve is obtained as a result of the depletion of the redox concentration at the electrode due to electrolysis.⁷⁹ Therefore, the measured parameters of interest include the cathodic peak current $i_{p,c}$, the anodic peak current $i_{p,a}$, and the separation of the cathodic and anodic peak potential, ΔE_p . For

Figure 2.3 Cyclic voltammogram of 1 mM $\text{Fe}(\text{CN})_6^{3-}$ in 0.1 M HClO_4 (pH 1.5) on the ferrocene derivatized TA monolayer electrode. Electrode area is 0.12 cm^2 . Scan rate is 100 mV/s.



reversible processes, the thermodynamic parameter such as the redox formal potential, $E^{\circ'}$, can be calculated from the midpoint of the cathodic and anodic peak potentials:

$$E^{\circ'} = \frac{(E_{pc} + E_{pa})}{2} \quad (2-1)$$

The reversibility of the electrode reactions can be determined from the ΔE_p values in CV. For a diffusion controlled electron transfer process, the theoretical ΔE_p value for a reversible process is $0.059/n$ V at 25°C , where n is the number of electrons transferred per mole during the process. The ΔE_p value greater than $0.059/n$ V for a diffusion process is an indication of slow electrode kinetics (i.e. quasireversible or irreversible process).

For an adsorption controlled reversible process, the anodic peak is the mirror image of the cathodic peak reflected across the potential axis. Therefore, the peak separation ΔE_p is 0.0 V. The half-height of either the cathodic or anodic wave is $0.090/n$ V at 25°C .

Measurements of the peak current at different scan rate can be used to determine if the electrode reaction involves diffusion or adsorption. The presence of adsorption can be identified by using log-log plots of peak current versus scan rate ($\log i_p$ vs $\log v$). Consider a diffusion controlled process, the theoretical expression for the peak current, i_p , for a reversible process is⁷⁹

$$i_p = (2.69 \times 10^5) n^{\frac{3}{2}} A D_o^{\frac{1}{2}} v^{\frac{1}{2}} C_o^* \quad (2-2)$$

where n is the number of electrons, A is the electrode area in cm^2 , D_o is the diffusion

coefficient in cm^2/s , v is the scan rate in V/s and C_o^* is the bulk concentration of the electroactive species (mol/cm^3).

For an irreversible process, i_p , is given by⁷⁹

$$i_p = (2.99 \times 10^5) n (\alpha n_e)^{\frac{1}{2}} A D_o^{\frac{1}{2}} v^{\frac{1}{2}} C_o^* \quad (2-3)$$

where α is the transfer coefficient and n_e is the number of electrons involved in the rate determining step.

For the adsorption controlled process, the theoretical i_p value for a reversible process is

$$i_p = \frac{n^2 F^2 A v \Gamma_o}{4RT} \quad (2-4)$$

and for an irreversible process

$$i_p = \frac{n \alpha n_e F^2 A v \Gamma_o}{2.718 RT} \quad (2-5)$$

where F is the Faraday's constant (96484 C/equiv), R is the ideal gas constant ($8.314 \text{ J/K} \cdot \text{mol}$), Γ_o is the surface excess of the electroactive species in mol/cm^2 , and T is the temperature in K .

Equations 2-2 and 2-3 indicate that for a diffusion controlled process, $i_p \propto v^{1/2}$ regardless of reaction kinetics. From eq 2-4 and 2-5, it is clear that for an adsorption controlled process, $i_p \propto v$. Therefore, a plot of $\log i_p$ versus $\log v$ should yield a slope

value of 0.5 for a diffusion controlled process, and 1.0 for an adsorption controlled process. Slope values lying somewhere between 0.5 and 1.0 indicate that both diffusion and adsorption are involved in the electrode reaction.

The standard heterogeneous rate constant, k^0 , can be determined from the CV data. For a diffusion controlled process, k^0 , can be calculated from the Nicholson equation:¹³²

$$k^0 = \psi (\pi a D_{Red})^{1/2} (D_{Red}/D_{Ox})^{a/2} \quad (2-6)$$

where $a = nFv/RT$. Values of ψ were determined from the peak separation, ΔE_p , according to Nicholson's method. For adsorption controlled process, the Laviron equation was used:¹³³

$$\ln k^0 = \alpha \ln(1-\alpha) - (1-\alpha) \ln \alpha - \ln \frac{RT}{nFv} - \frac{nF(1-\alpha)\alpha}{RT} \Delta E_p \quad (2-7)$$

Assuming $\alpha = 0.5$, eq 2-7 is thus reduced to

$$\ln k^0 = - \ln \frac{RT}{nFv} - \frac{nF}{4RT} \Delta E_p \quad (2-8)$$

For a given scan rate v and the cathodic and anodic peak separation, ΔE_p , the rate constant k^0 can be obtained.

2.3.2.2 Cyclic voltammetry on the UMEs

Fundamental changes occur in the cyclic voltammograms at the UMEs. Mass transport at UMEs, which determines the shape of the voltammograms and the magnitude

of the faradaic current, will switch from the semi-infinite linear diffusion (planar diffusion) to hemispherical diffusion (radial diffusion) at typical subsecond time scales. Radial diffusion, as pointed out previously, is much more efficient than planar diffusion. Therefore, depletion of the electroactive species does not occur at the electrode, instead, a steady-state condition is obtained. This results in a sigmoidal shaped CV response at the UMEs while at the conventional size electrodes a peak shaped CV is observed due to the depletion.

The theoretical limiting current, i_L , for a microdisk-shaped electrode is given by^{80,81}

$$i_L = 4nFD \sqrt{C_o} r \quad (2-9)$$

where r is the radius of the disk electrode. Clearly, the limiting current i_L under radial diffusion conditions is independent of scan rate, v , indicating that in the diffusion layer there is no change in the electrolyte concentration with time.

The reversibility of the electrode reaction at the UMEs was examined by analyzing the current in the sigmoidal transition region as a function of potential.^{134,135} For a reversible system in the absence of reduced species in solution at the beginning of the experiment, the current-potential relationship should obey the following equation:

$$E = E_{1/2} + \frac{RT}{nF} \ln \frac{(i_L - i)}{i} \quad (2-10)$$

where E is the electrode potential (V), $E_{1/2}$ is the half-wave potential (V), R is the gas

constant ($8.314 \text{ J} \cdot \text{mol}^{-1} \cdot \text{K}^{-1}$), T is the temperature (K), n is the number of electrons, F is the Faraday constant ($96,485 \text{ C/equiv}$), and i_L is the limiting current (A). Rearranging eq 2-10, we obtain

$$\log \frac{(i_L - i)}{i} = \frac{nF}{2.303 RT} E - \frac{nF}{2.303 RT} E_{1/2} \quad (2-11)$$

Hence a plot of the logarithm of the normalized current function vs. potential should yield a slope whose reciprocal is equal to $59/n \text{ mV}$ at 25°C . Since eq 2-10 holds only for a reversible process, it sets the value of $59/n \text{ mV}$ in the plot of $\log (i_L - i)/i$ vs E as the criterion for the reaction reversibility. Deviations from $59/n \text{ mV}$ in such plots can be regarded as an indication of complications in the electron transfer reactions (e.g. quasireversible or irreversible behavior).

2.3.2.3 Chronocoulometry (CC)

Chronocoulometry was employed to determine the electrode area. CC involves stepping a potential from a value where the rate of the redox reaction is negligible to a potential value where the rate is diffusion controlled. The charge, Q which is accumulated, is monitored as a function of time t .⁷⁹

$$Q = \frac{2nFAD_o^{1/2}C_o^*t^{1/2}}{\pi^{1/2}} \quad (2-12)$$

A plot of Q vs. $t^{1/2}$ is linear. Given the bulk concentration of the species, C_o^* , and diffusion coefficient, D_o , the slope of this plot is useful for calculating electrode area A .

Throughout the experiments in this study, 1 mM $\text{Ru}(\text{NH}_3)_6^{3+}$ in 0.1 M phosphate at pH 7.4 was used to determine the electrode area. The diffusion coefficient of this probe is $5.5 \times 10^{-6} \text{ cm}^2/\text{s}$.¹³¹

2.3.3 Purification of Protein Cytochrome c

Horse heart cytochrome c (Type VI, 95 % purity, obtained from Sigma) was purified before use with the method described by Brautigan et al.¹³⁶ A cation exchange column with the dimensions of 1.5 i.d. cm x 30 cm packed with 10 cm high carboxyl methyl cellulose resin (CM-52, Whatman Biochemicals) was used. The column was conditioned by 70 mM phosphate buffer. Prior to applying the cytochrome c solution to the column, excess potassium ferricyanide was added to the cytochrome c solution to oxidize the cytochrome c in order to get a maximum yield of cytochrome c in the oxidized form. For a typical load of 50 mg of sample, a flow rate of 0.3 - 0.4 ml/min was used. A 70 mM phosphate buffer at pH 7.2 was used as an eluent. The eluent was collected by a linear fraction collector (LC 200, Buchler Corporation) monitored at 360 nm.

The major impurities in the commercially available cytochrome c are deamidated and polymeric forms of cytochrome c. Using the purification procedure described above, a chromatogram of 4 peaks was typically obtained, with 3 peaks for the deamidated forms and 1 for the native cytochrome c. The polymeric form of cytochrome c remained on the column and could be removed when the resin was regenerated in 0.5 M NaOH solution.

The purified cytochrome c was then concentrated by freeze drying (Labconco Freeze Dryer 8). Since the resulting samples had a high content of the phosphate salt from the eluent buffer, desalting of cytochrome c solution became necessary. Desalting was

conducted by ultracentrifugation using membranes with a molecular weight cutoff of 10,000 Daltons (Centricell 20, Polysciences, Inc.) at 4°C with a rotation speed of 2000 rpm. The samples on the membrane were rinsed with water and transferred to a 25-ml volumetric flask as the stock solution. The content of the phosphate in the stock solution was analyzed with 0.1 M ammonium molybdate in 5 M sulfuric acid. Using a calibration line, the content of phosphate in cytochrome c solution was found to be ca. 35 mM.

The concentration of cytochrome c solutions was determined spectroscopically by measuring the absorbance at 550 nm ($\epsilon=21,100$)¹³⁷ on a Cary UV-Vis spectrophotometer. Rhodamine b ($\lambda_{\text{max}} = 550$ nm, $\epsilon = 72,443$) was used as a standard in the absorbance calibration. The cytochrome c solution was kept at 4°C and was used within four weeks after purification.

CHAPTER 3

SELECTIVITY AND SENSITIVITY OF THE THIOCTIC ACID MONOLAYERS

In this Chapter, we describe the self-assembly of thioctic acid on a smooth gold electrode to form an organized packed monolayer with the carboxylic acid terminal in contact with solution controlling the response of the electrode. Electrochemical characterization, including capacitance measurements and cyclic voltammetry characterization in the determination of the quality of the monolayer packing and the effect of electrolyte properties on response will be discussed.

3.1 Capacitance Measurements and Monolayer Permeability

When a monolayer is assembled on the electrode, the surface double layer structure can be approximated by a simple two-capacitor system consisting of ideal compact monolayer and diffuse double layer capacitors, connected in series (Chapter 1, Section 1.4.2). The overall capacitance, C_{total} , is ⁷⁰

$$\frac{1}{C_{total}} = \frac{1}{C_{dl}} + \frac{1}{C_{ml}} \quad (3-1)$$

where C_{dl} is the double layer and C_{ml} is the monolayer capacitance in $\mu\text{F}/\text{cm}^2$. Each term in eq. 3-1 can be expressed explicitly (eq. 1-18 and 1-19). C_{total} can be measured from cyclic voltammetry. In this study, cyclic voltammetry was run from -0.2 to 0.2 V, and the

capacitance was calculated from the sum of the cathodic and anodic current divided by two times the scan rate and the electrode area ($C_{total} = i_c/2vA$).^{42,70}

At PZC on Au (ca. -0.07 ± 0.10 mV vs SCE⁹¹ where 0.00 V vs SCE was used in our experiments) an ionic strength of ca. 0.1 M results in $C_d = 72 \mu\text{F}/\text{cm}^2$ (eq. 1-19). Compared to the measured C_{total} , which is usually in the range of 1 to 10 $\mu\text{F}/\text{cm}^2$, C_d is about 7-70 times larger and thus becomes negligible. Thus,

$$C_{nl} \approx C_{total} \quad (3-2)$$

Using Helmholtz capacitor model:⁷⁹

$$C_{total} = \epsilon \epsilon_0 / d \quad (3-3)$$

where C is the capacitance per unit area, ϵ is the dielectric constant of the monolayer, ϵ_0 is permittivity of vacuum (8.85×10^{-14} F/cm), and d is the film thickness, we can calculate the dielectric constant of the monolayer when the film thickness is known and vice versa.

As discussed previously, extensive studies of self-assembled monolayers have revealed that *n*-alkylthiol monolayers on gold tilt ca. 27° from surface normal⁵⁷ and the optical ellipsometry and IR spectroscopy data indicate a correlation of 1.3 Å per CH_2 group.⁴⁷ Using this information, the thickness of some monolayers, such as the C_6SH monolayer, can thus be estimated to be ca. 8 Å including the Au-S bond. Such estimates are difficult for the TA monolayer, since the orientation and the molecular packing of TA in the monolayer are not known. However, Nuzzo and coworkers have found that a variation of the chain-terminating headgroup such as CH_3 and COOH may have little

effect on the structure of the film in the region of the hydrocarbon chains.⁶² Therefore, it is reasonable to assume that TA monolayers have similar molecular orientation as *n*-alkylthiol monolayers, though a variation in the alkyl chain tilt of ca. 10° would not affect the conclusions drawn here. Using the 27° tilt adopted for the *n*-alkylthiol monolayer, the calculation for the TA film, where TA has four CH₂ and one CH group, results in the same thickness. The dielectric constant, ϵ , for the monolayers thus can be calculated from eq. 3-3. Table 3.1 lists the results of the capacitance measurements for the TA monolayers in different electrolytes.

The results in Table 3.1 show that the measured capacitance of the TA film is in the range of 8.5-10.3 $\mu\text{C}/\text{cm}^2$. For comparison, the reported capacitance of ca. 3.7 $\mu\text{C}/\text{cm}^2$ for the HO(CH₂)₆SH monolayer⁴² is also listed in Table 3.1. The calculated dielectric constant ϵ (eq.3-3) for the TA monolayer in 0.1 M KCl is 8.3. This value of ϵ differs slightly in different electrolytes and at different pH. For HO(CH₂)₆SH monolayer, ϵ is calculated to be 3.3, compared to the dielectric constant of polyethylene ($\epsilon=2.3$)¹³⁸ and the dielectric constants for alkylthiol monolayers ($\epsilon=2.6$).⁴⁷

The dielectric constant is a measure of the resistive force of a medium against external electrical field. Water has a dielectric constant of 78, compared to the low ϵ values for a nonconductive organic film ($\epsilon=2.3$ for polyethylene).¹³⁸ The high value of ϵ measured for the TA monolayer must be a result of penetration of the monolayer by solvent and the electrolyte. This is not surprising in view of the TA molecular structure. The lack of a second alkyl chain in TA can lead to a more loose packing of the molecules at the Au surface.

Table 3.1 Results of capacitance measurements for the thioctic acid and $\text{HO}(\text{CH}_2)_6\text{SH}$ monolayer electrodes

electrode	electrolyte	C ($\mu\text{F}/\text{cm}^2$)	ϵ
Thioctic acid/Au	0.1 M KCl	9.2	8.3
	0.1 M KCl and 10 mM tris ^b	10	9
	0.1 M NaF	8.5	7.7
	0.1 M HClO_4 ^c	10.3	9.3
$\text{HO}(\text{CH}_2)_6\text{SH}/\text{Au}$ ^a	0.1 M KCl and 10 mM tris	3.7	3.3

^a From ref. 42. ^b pH 7.4. ^c pH 1.5.

The porosity of the TA monolayer is further supported by the capacitance measured in 0.1 M NaF. Porter et al. reported that the capacitance of methyl terminated alkylthiol monolayers is much smaller in solutions containing F^- than in Cl^- solutions.⁴⁷ It was argued that the large volume of the hydrated F^- hindered its transport. This is not observed (Table 3.1) for the TA monolayer, as expected for a porous film that can be penetrated by the large F^- ion.

In general, large ϵ values for the TA monolayers are obtained from the capacitance measurements, indicating that the film allows solvent and electrolyte to penetrate it. The implications of the high dielectric constant for the TA monolayer are significant, since the high dielectric constant values mean that less potential is dropped across the film and the whole monolayer functions like a "conductive" membrane.

3.2 Electrochemical Reactivity of Hydrophilic Probes on the TA Monolayer Electrodes

Electrochemical properties of the TA monolayer electrodes were investigated by cyclic voltammetry using $Fe(CN)_6^{3-}$ and $Ru(NH_3)_6^{3+}$ as probes. $Fe(CN)_6^{3-}$ and $Ru(NH_3)_6^{3+}$ were chosen as probes because they have opposite charge and reasonably fast kinetics on gold. Figure 3.1 shows the response of $Fe(CN)_6^{3-}$ on the TA monolayer electrodes as a function of the solution pH. The reversible response of $Fe(CN)_6^{3-}$ is only observed at pH 1.5. At pH 7.4 and 9.1, no response of $Fe(CN)_6^{3-}$ above the charging current is observed. Figure 3.2 shows the response of the cationic $Ru(NH_3)_6^{3+}$ as a function of solution pH. The response is essentially the same in neutral and basic solutions, but is significantly smaller at low pH.

Figure 3.1 Cyclic voltammetric response of $\text{Fe}(\text{CN})_6^{3-}$ on the TA monolayer electrode as a function of solution pH. Solution compositions: 0.1 M HClO_4 (pH 1.5), 0.1 M KCl and 10 mM tris (pH 7.4) and 0.1 M KCl and 10 mM borate (pH 9.1). Scan rate 100 mV/s. Electrode area 0.28 cm^2 .

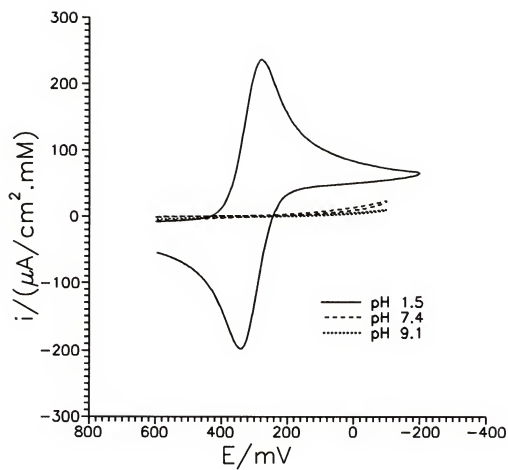
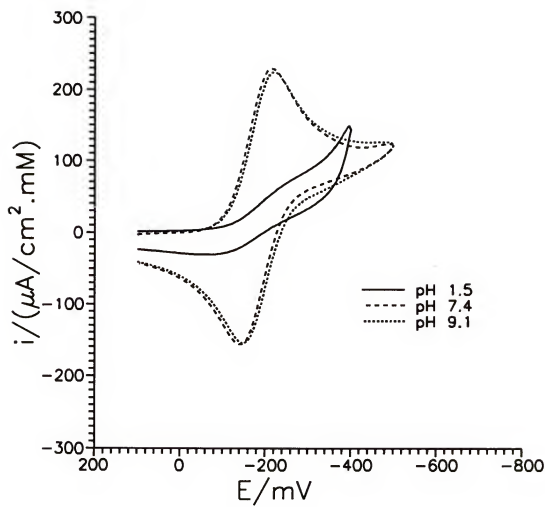


Figure 3.2 Cyclic voltammetric response of $\text{Ru}(\text{NH}_3)_6^{3+}$ on the TA monolayer electrode as a function of solution pH. Solution compositions: 0.1 M HClO_4 (pH 1.5), 0.1 M KCl and 10 mM tris (pH 7.4) and 0.1 M KCl and 10 mM borate (pH 9.1). Scan rate 100 mV/s. Electrode area 0.28 cm^2 .



The background corrected cathodic peak currents and the ΔE_p values for the probes were measured from the CV's at the TA monolayer electrodes and at the bare Au. Formal potential E° was measured as the average of E_{pc} and E_{pa} . The results are shown in Table 3.2. For $\text{Fe}(\text{CN})_6^{3-}$ at pH 1.5 and for $\text{Ru}(\text{NH}_3)_6^{3+}$ at pH 7.4 and 9.1, ΔE_p and i_{pc} values are essentially the same at the TA monolayer electrode and the bare Au electrode.

Comparison of the ΔE_p and the i_p values in Table 3.2 obtained from the CV data for the $\text{Fe}(\text{CN})_6^{3-}$ and the $\text{Ru}(\text{NH}_3)_6^{3+}$ at the TA monolayer electrode and the bare gold electrode reveals some interesting points. Since $\text{Fe}(\text{CN})_6^{3-}$ and $\text{Ru}(\text{NH}_3)_6^{3+}$ display essentially the same ΔE_p at the TA monolayer and the bare gold, the presence of the film must not noticeably affect kinetics of the probes. The fast kinetics of the $\text{Ru}(\text{NH}_3)_6^{3+}$ at the TA monolayer electrode are different from the slow kinetics reported by Chidsey and Loiacono at $\text{HO}_2\text{C}(\text{CH}_2)_{10}\text{SH}$ under similar solution conditions.⁴⁸ Combined with the experimental observation that the i_p and the ΔE_p values for $\text{Fe}(\text{CN})_6^{3-}$ (at pH 1.5) are also comparable to those observed on the bare Au electrodes, we conclude that fast kinetics can be obtained for these probes on the TA modified electrodes⁶⁹.

The selectivity of the TA modified electrode is clearly related to the solution pH and the probe charge. We ascribe the observed selectivity to the changes in the electrostatic environment created at the solution-film interface at different solution pH⁶⁹ due to the dissociation of the COOH ($\text{pK}_a=5$)¹³⁹ group of the TA at the electrode surface, even though the dissociation may only be partial. A recent quartz crystal microbalance (QCM) study¹⁴⁰ has shown that the dissociation of the COOH group of $\text{HS}(\text{CH}_2)_{15}\text{COOH}$ ($\text{pK}_a = 5$) on Au occurs at $\text{pH}\approx 6$, over a range as wide as 4 pH units, with the extent of

Table 3.2 Cyclic voltammetric results for $\text{Fe}(\text{CN})_6^{3-}$ and $\text{Ru}(\text{NH}_3)_6^{3+}$ on the bare Au and thioctic acid monolayer electrodes

probe ^a	electrode	electrolyte	pH	ΔE_p (mV)	E° ^b (V)	$i_{p,c}$ ^c ($\mu\text{A}/\text{cm}^2\cdot\text{mM}$)
$\text{Fe}(\text{CN})_6^{3-}$	bare Au	0.1 M HClO_4	1.5	65	0.33	237
	thioctic acid	0.1 M HClO_4	1.5	65 \pm 1	0.33	220 \pm 4
$\text{Ru}(\text{NH}_3)_6^{3+}$	bare Au	0.1 M HClO_4	1.5	66	-0.14	211
		0.1 M KCl and 10 mM tris	7.4	74 \pm 4	-0.18	230 \pm 8
		0.1 M KCl and 10 mM borate	9.1	78	-0.19	214
	thioctic acid	0.1 M HClO_4	1.5	d	d	d
		0.1 M KCl and 10 mM tris	7.4	75 \pm 2	-0.19	225 \pm 5
		0.1 M KCl and 10 mM borate	9.1	71	-0.19	224

^a Probe concentration is 1 mM. ^b Formal potential E° was calculated from $E^\circ = (E_{p,c} + E_{p,a})/2$ and was measured vs SCE. ^c Cathodic peak current normalized by the electrode area. ^d Poorly defined peaks could not be accurately measured.

the dissociation at pH 7.4 of 40 to 50% of the total surface population of the COOH groups. Assuming the same dissociation behavior for the TA film, almost half of the COOH surface groups of TA will be negatively charged at pH 7.4. The resulting charge of the TA film can significantly affect the surface potential, ϕ_s , and, therefore, the kinetics (selectivity) at the monolayer electrodes are affected by the non-zero surface potential through the Frumkin relationship:^{90,91}

$$k_{\text{ml}} = k_0 \exp [-z\phi_s/kT] \quad (3-4)$$

where k_{ml} is the apparent rate constant on the monolayer, z is the probe charge, k_0 (cm/s) is the standard heterogeneous rate constant, k is the Boltzmann's constant and T (K) is the absolute temperature. The anticipation of such behavior has been the initial motivation for the development of the "chemically modified"^{1,5} electrodes.

For $\text{Fe}(\text{CN})_6^{3-}$, when $\phi_s < 0$, the exponential term in eq.3-4 becomes negative, decreasing the apparent rate constant. It can be generalized based on eq 3-4 that the negatively charged probes will be selectively excluded from the negatively charged monolayers. On the other hand, the positively charged probes ($\text{Ru}(\text{NH}_3)_6^{3+}$) will be able to access the negatively charged surface when $\phi_s < 0$. A resulting increase in the heterogeneous rate constant is predicted by eq 3-4. It is not observed experimentally for $\text{Ru}(\text{NH}_3)_6^{3+}$ possibly because of the mass transport (diffusion) limitations of the response at the time scale of the experiment for this already fast probe. A fast response of $\text{Fe}(\text{CN})_6^{3-}$ on a positively charged alkylammonium terminated monolayer has been observed⁹³.

At pH 1.5 the surface COOH groups of the TA are neutral. Under such conditions the sign of ϕ_2 will depend only on the external applied potential, with respect to the potential of zero charge (PZC). When $E_{\text{ex}} > \text{PZC}$, $\phi_2 > 0$ and vice versa. At pH 1.5 both $\text{Fe}(\text{CN})_6^{3-}$ and $\text{Ru}(\text{NH}_3)_6^{3+}$ can be expected to display fast response since their reactions proceed at the optimum ϕ_2 ($\phi_2 > 0$ for $\text{Fe}(\text{CN})_6^{3-}$ and $\phi_2 < 0$ for $\text{Ru}(\text{NH}_3)_6^{3+}$). However, the expected behavior is not observed for $\text{Ru}(\text{NH}_3)_6^{3+}$. The response is in fact suppressed compared to the response at the bare surface. Originally the observed decrease in response in HClO_4 as the electrolyte was attributed to a high concentration of protons at the surface.⁶⁹ Additional experiments with ClO_4^- , however, have shown that the response of $\text{Ru}(\text{NH}_3)_6^{3+}$ at pH 1.5 is also affected by the formation of an insoluble salt with the ClO_4^- . The precipitate can block the monolayer surface, and can also reduce the bulk concentration of the $\text{Ru}(\text{NH}_3)_6^{3+}$, thus reducing the magnitude of the measured current.

To prevent the possibility of forming a precipitate with ClO_4^- , the response of the $\text{Ru}(\text{NH}_3)_6^{3+}$ was also studied in 0.1 M KCl and 0.1 M NaF solutions at low pH adjusted by 1 M HCl. Table 3.3 summarizes the result. In 0.1 M KCl at pH 1.0, ΔE_p increases compared to that at pH 7.4. After 3 scans, the value of ΔE_p increases by ca. 30 mV while in 0.1 M NaF the increase of ΔE_p is as large as ca. 50 mV. There was no steady state reached in three scans. Peak current i_p at low pH decreases by 13% in 0.1 KCl and 19 % in 0.1 NaF, clearly indicating some changes in the film structure at low pH that provoke slower response on the monolayer electrode. We ascribe the suppressed response of $\text{Ru}(\text{NH}_3)_6^{3+}$ at low pH to the preferential interaction between the hydrogen ions and the TA monolayer. The TA monolayer/solution interface may become positively charged,

Table 3.3 Cyclic voltammetric results of $\text{Ru}(\text{NH}_3)_6^{3+}$ on the TA monolayer electrode at low pH

electrolyte	pH	runs	ΔE_p (mV)	$i_{p,c}^c$ ($\mu\text{M}/\text{cm}^2 \cdot \text{mM}$)
0.1 M KCl and 10 mM tris	1.0 ^a	1	83	196±3
		2	97	
		3	104	
0.1 M NaF and 10 mM tris	1.5 ^b	1	113	113±2
		2	118	
		3	122	
0.1 M NaF and 10 mM tris	7.4 ^c		71±1	210±0

^a Solution pH was adjusted to 1.0 by 1 M HCl. ^b Solution pH was adjusted to 1.5 by 1 M HCl. ^c Average values of three runs

which can contribute to the slower kinetics of the $\text{Ru}(\text{NH}_3)_6^{3+}$.

It is worth noting that the charge developed here is due to surface interactions with the monolayer. Compared to the negative charge of the monolayer developed as a result of the dissociation of the carboxylic headgroups at higher pH, the charge density as a result of the interactions should be low. The selectivity toward the opposite charged probes is thus weak accordingly. The experimental observations are consistent with this model.

3.3 Electrolyte Effect on Film Structure and Reactivity

The effect of the electrolyte concentration and composition on the electrochemical response on the TA monolayer electrodes was investigated. The results are summarized in Table 3.4. From Table 3.4, $\text{Ru}(\text{NH}_3)_6^{3+}$ has the smallest ΔE_p in 0.5 M phosphate, compared to that in 0.05 M phosphate, indicating that the best kinetics of the $\text{Ru}(\text{NH}_3)_6^{3+}$ are obtained at high electrolyte concentrations on the TA monolayer electrode. The peak current of the $\text{Ru}(\text{NH}_3)_6^{3+}$, i_p , is higher in chloride than in phosphate electrolyte.

The effect of the electrolyte composition and concentration on the electrochemical response of the redox couples irreversibly attached to the self-assembled monolayers has received recent attention. Smith and White have recently proposed an electrostatic model to interpret the voltammetric behavior of the redox systems covalently attached to the film-coated electrodes.¹⁴¹ As is discussed in Section 1.4.3, the Gouy-Chapman-Stern (GCS) model of an impermeable compact layer of the double layer predicts that at high electrolyte concentration, the potential drop across the diffuse layer becomes smaller compared to at low electrolyte concentration. The potential that the electroactive species

Table 3.4 Cyclic voltammetric results of $\text{Ru}(\text{NH}_3)_6^{3+}$ and $\text{Fe}(\text{CN})_6^{3-}$ as a function of supporting electrolyte

probe	electrode	electrolyte	ΔE_p (mV)	$i_{p,c}$ ($\mu\text{A}/\text{cm}^2.\text{mM}$)
$\text{Ru}(\text{NH}_3)_6^{3+}$	thioctic acid	0.1 M KCl and 10 mM tris ^a	75 \pm 2	225 \pm 5
		0.05 M phosphate ^a	101 \pm 0	195 \pm 2
		0.5 M phosphate ^a	70 \pm 0	187 \pm 1
$\text{Fe}(\text{CN})_6^{3-}$	thioctic acid	0.5 M NaAc/CF ₃ COOH ^b	90 \pm 2	126 \pm 1
	bare Au	0.5 M NaAc/CF ₃ COOH ^b	69 \pm 8	210 \pm 4

^a pH 7.4. ^b pH 3.5

experiences at the monolayer surface is thus larger, leading to the fast kinetics of the $\text{Ru}(\text{NH}_3)_6^{3+}$.

However, the assumption of impermeability of the compact layer of the double layer in GCS model is not valid for the TA monolayer, where penetration of the monolayer by solvent and electrolyte has been evidenced by the high measured capacitance. The partitioning of electrolyte into the film will be more apparent at high electrolyte concentrations and will further contribute to higher C_{ml} values. In addition, at high electrolyte concentrations swelling of the hydrophilic headgroups can also occur,¹⁴² facilitating partitioning of ions into the film. Such effects have been observed in the studies of the ionic strength effects on the Langmuir-Blodgett monolayers where at a constant pressure, surface area/molecule increased with the electrolyte concentration, with more electrolyte penetration into the films.¹⁴²⁻¹⁴⁴ The experimentally observed faster kinetics of the $\text{Ru}(\text{NH}_3)_6^{3+}$ at high electrolyte concentrations are consistent with the expected increase in ϕ_2 with the increase in the electrolyte concentration.

From Table 3.4 a small difference in the magnitude of the peak current of $\text{Ru}(\text{NH}_3)_6^{3+}$ in Cl^- and phosphate is observed. This can be attributed to the different diffusion coefficients of $\text{Ru}(\text{NH}_3)_6^{3+}$ in different electrolytes ($7.5 \times 10^{-6} \text{ cm}^2/\text{s}$ in 0.1 M KCl ¹⁴⁵ and $5.5 \times 10^{-6} \text{ cm}^2/\text{s}$ in 0.1 M phosphate¹³¹).

Another electrolyte, fluoroacetate (CF_3COO^-), was used to test the effect of electrolyte structure on the TA film response. Table 3.4 includes the results for $\text{Fe}(\text{CN})_6^{3-}$ on the bare and the TA monolayer electrodes in 0.5 M $\text{CH}_3\text{COOH}/\text{CF}_3\text{COOH}$ at pH 3.5. On the bare electrode, $\Delta E_p = 69 \text{ mV}$ and $i_p = 210 \mu\text{A}/\text{cm}^2.\text{mM}$. The values are similar to

those obtained in Cl^- as the electrolyte. However, at the TA monolayer electrode, an increase in peak separation ΔE_p and a decrease in peak current i_p is observed compared to the response in Cl^- as the electrolyte. The results confirm that the choice of the electrolyte is important to the response observed at the TA monolayer electrodes. The results for the $\text{Fe}(\text{CN})_6^{3-}$ in 0.1 M HClO_4 are listed in Table 3.2 for comparison to the results for the $\text{Fe}(\text{CN})_6^{3-}$ in 0.5 M $\text{CH}_3\text{COOH}/\text{CF}_3\text{COOH}$ at pH 3.5. No significant changes in kinetics or currents for the $\text{Fe}(\text{CN})_6^{3-}$ on the bare and the TA monolayer electrode was observed in ClO_4^- , pointing out that the response of $\text{Fe}(\text{CN})_6^{3-}$ at low pH on the TA monolayer electrodes is not only dependent on pH which affects directly the carboxylic headgroups of the monolayer, but is also affected by the counterions in solution that can potentially alter the electrochemical response at the monolayer electrodes.

3.4 Effect of Probe Structure and Hydrophobicity on Reactivity at the TA Monolayers

The electrochemical response of hydrophobic molecules was also tested at the TA monolayer electrodes. Figure 3.3 shows the response of DA^{+1} ($\text{pK}_a=8.92$) and DOPAC^{-1} ($\text{pK}_a=4.22$) at pH 7.4 on the bare and the TA monolayer electrodes, and Table 3.5 summarizes the cyclic voltammetry results for DA on both the bare and the TA monolayer electrodes at different electrolyte concentrations. For positively charged DA, ΔE_p is 105 mV at the bare and 438 mV on the TA monolayer electrode in 0.1 M KCl. DOPAC^{-1} shows no faradaic response on the TA monolayer, indicating that the access of this probe to the TA monolayer surface is suppressed due to the negative probe charge.

Results in Table 3.5 show significantly slower kinetics and the low current of DA

Figure 3.3 Cyclic voltammograms of 0.5 mM DA and DOPAC in 0.1 M KCl and 10 mM tris (pH 7.4) on the bare gold and the TA monolayer electrodes. Scan rate 100 mV/s. Electrode area: 0.28 cm² for the bare, 0.21 cm² for the TA monolayer electrode

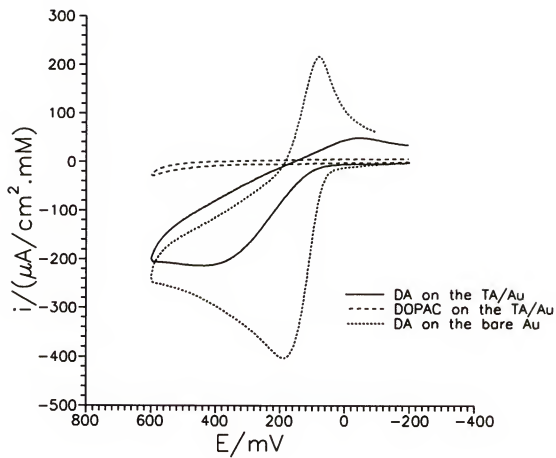
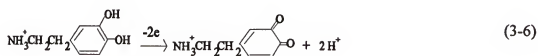


Table 3.5 Cyclic voltammetric results of DA and Q at pH 7.4

probe	electrode	electrolyte	ΔE_p (mV)	$i_{p,c}$ ($\mu A/cm^2 \cdot mM$)
DA	bare Au	0.1 M KCl and 10 mM tris	105 \pm 2	403 \pm 3
	thioctic acid	0.1 M KCl and 10 mM tris	438 \pm 25	213 \pm 9
		0.05 M phosphate	410 \pm 27	251 \pm 21
		0.5 M phosphate	526 \pm 12	183 \pm 15
Q	bare Au	0.1 M KCl and 10 mM tris	61	412
	thioctic acid	0.1 M KCl and 10 mM tris	570	232

on the TA monolayer than on the bare electrode. Slow kinetics of DA can be a result of unfavorable interactions of the probe with the film and the unfavorable molecular orientation of the probe at the monolayer, as well as from the possible complications in the electron transfer mechanism for the probe. The $2e$, $2H^+$ oxidation of DA, described by eq. 3-6,¹⁴⁶



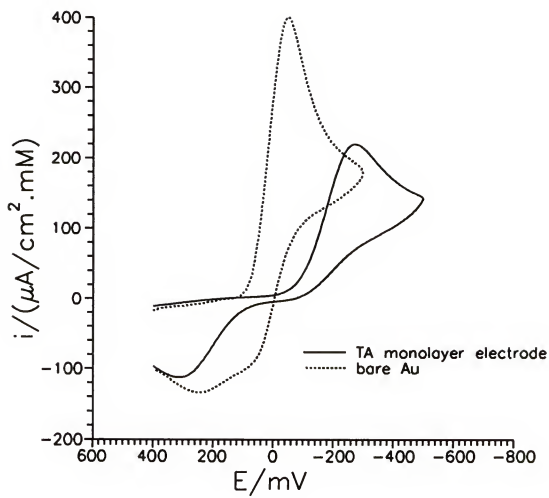
generates two protons. This may change the local pH at the monolayer surface, therefore, influencing the charge density as well as the surface interactions.

In contrast to $Ru(NH_3)_6^{3+}$, DA shows fastest kinetics at lowest ionic strength (Table 3.5). One possible explanation is that a high electrolyte concentration may "screen" the surface, making interactions between the surface and more hydrophobic DA terminal less efficient than for the hydrophilic $Ru(NH_3)_6^{3+}$.

In order to probe the hydrophobic contribution to the response of DA and DOPAC, benzoquinone (Q), a structural analog of the catecholamines which is neutral at pH 7, was investigated. Figure 3.4 and Table 3.5 summarize the results for Q. On the bare Au electrode at neutral pH, the ΔE_p between 30 to 60 mV was reported for Q. On the TA electrode at pH 7.4 the kinetics are much slower, with the $\Delta E_p = 570$ mV. The magnitude of the $i_{p,c}$ of Q is reduced by half compared to the i_p of Q on the bare Au electrode, indicating that the presence of the TA monolayer slows down the response of Q.

The response of Q on the TA monolayer electrode at pH 7.4 is similar to the slow

Figure 3.4 Cyclic voltammetric response of 0.5 mM benzoquinone (Q) in 0.1 M KCl and 10 mM tris (pH 7.4) on the bare gold and the TA monolayer electrode.

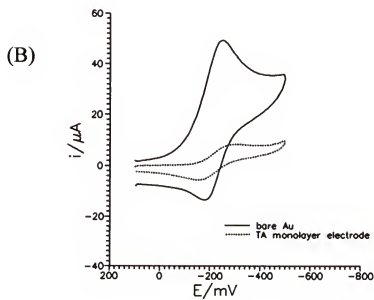
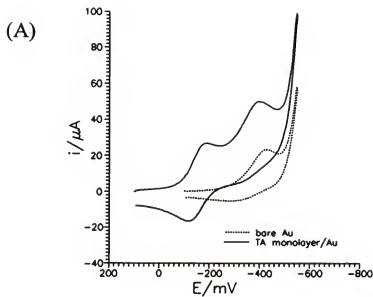


response of DA (Figure 3.3). The similar slow response of Q shows that DA charge does not significantly help it access the charged hydrophilic surface of the TA monolayer. Instead, the hydrophobic components in these probes appear to be more determinant for the observed slow kinetics, presumably due to the enlarged distance of the closest approach of the hydrophobic probes from the electrode as a result of the presence of a hydrophilic film. Further analysis will be presented in Chapter 4 where surface hydrophobicity is changed to reveal the relationship between the hydrophobicity of the probes and their response on the monolayer electrodes.

3.5 Effect of Redox Probe Size

The effect of the size of a hydrophilic probe on the electrochemical response at the TA monolayer was studied with $\text{Ru}(\text{EDTA})(\text{H}_2\text{O})^-$ as the probe. The hydrophilic $\text{Ru}(\text{EDTA})(\text{H}_2\text{O})^-$ has a relatively large radius ($d = 10 \text{ \AA}$)¹⁴⁷ and is known to be a simple, one electron, reversible system.¹⁴⁷ Figure 3.5A shows the response of $\text{Ru}(\text{EDTA})(\text{H}_2\text{O})^-$ in 0.1 M HClO_4 on both the bare and the TA monolayer electrode. On the bare electrode, two distinguishable redox processes are identified. The first process is reversible ($\Delta E_p = 68 \text{ mV}$ and $i_{p,c}/i_{p,a} = 1$), with $E^0 = (E_{p,c} + E_{p,a})/2 = -0.14 \text{ V}$. This process is identified as the reduction of $\text{Ru}^{\text{III}}(\text{HEDTA})(\text{H}_2\text{O})$ to $\text{Ru}^{\text{II}}(\text{HEDTA})(\text{H}_2\text{O})^-$. The solution used in this study was prepared from $\text{Ru}(\text{EDTA})(\text{H}_2\text{O})^-$, however, this molecule is known to be subject to protonation at low pH.¹⁴⁸ Therefore, the solution at pH 1.5 contains a mixture of $\text{Ru}^{\text{III}}(\text{HEDTA})(\text{H}_2\text{O})$ ($\text{pK}_a = 2.37$) and $\text{Ru}^{\text{III}}(\text{EDTA})(\text{H}_2\text{O})^-$ ($\text{pK}_a = 7.63$). The second process identified on the bare Au electrode is the $\text{Ru}^{\text{III}}(\text{EDTA})(\text{H}_2\text{O})^-$

Figure 3.5 (A) Voltammetric response of $0.5 \text{ mM Ru(EDTA)(H}_2\text{O)}^-$ in 0.1 M HClO_4 (pH 1.5) on the bare Au and the TA monolayer electrode.
(B) Voltammetric response of $\text{Ru(EDTA)(H}_2\text{O)}^-$ in $0.5 \text{ M NaAc/CF}_3\text{COOH}$ (pH 3.5) on the bare gold and the TA monolayer electrode. Scan rate 100 mV/s . Electrode area: 0.28 cm^2 for the bare, 0.20 cm^2 for the TA monolayer electrode.



$/\text{Ru}^{\text{III}}(\text{EDTA})(\text{H}_2\text{O})^{2-}$ couple. The presence of this couple at low pH may be due to the slow kinetics of the $\text{Ru}^{\text{III}}(\text{EDTA})(\text{H}_2\text{O})^-$ protonation. The absence of the anodic peak is due to the follow-up chemical reaction in which the ClO_4^- oxidizes the electrochemical reduction product $\text{Ru}^{\text{III}}(\text{EDTA})(\text{H}_2\text{O})^{2-}$.¹⁴⁸

On the TA monolayer electrode, the first redox process is not observed while the second continues to show only a cathodic peak. The suppression of the first redox process may be resulted from the unfavorable interaction between the monolayer and the probe. At low pH, the TA monolayer can be positively charged due to preferential partitioning of hydronium ions into the headgroup region, while protonation of $\text{Ru}^{\text{III}}(\text{EDTA})(\text{H}_2\text{O})^-$ may increase the surface positive charge density, leading to repulsion effect at the TA monolayer surface. The peak potential of the second process shows only a small negative shift (25 mV) vs that on the bare Au electrode, suggesting that the presence of the TA monolayer does not significantly affect the response of the large, hydrophilic redox probes such as $\text{Ru}(\text{EDTA})(\text{H}_2\text{O})^-$ in 0.1 M HClO_4 .

In order to assure that the solution investigated contains only one redox species, $\text{Ru}(\text{EDTA})(\text{H}_2\text{O})^-$ was also electrochemically studied in 0.5 M $\text{NaAc}/\text{CF}_3\text{COOH}$ electrolyte at pH 3.5. Figure 3.5B shows the results. On the bare electrode, a reversible, one electron response was observed with the $\Delta E_p = 71$ mV. On the TA monolayer, peak separation increases significantly to 157 mV while the peak current i_p decreases by 75% compared to the peak current at the bare electrode. Such a dramatic decrease in peak current and probe response can be ascribed to a combined effect of the electrolyte, the TA monolayer structure and possibly the probe structure change at low pH, since the probe

size does not influence the response significantly at low pH, as described earlier. From previous discussion, the response of Fe(CN)_6^{3-} decreases in 0.5 M NaAc/CF₃COOH. The larger ΔE_p and the smaller i_p observed for the $\text{Ru(EDTA)(H}_2\text{O)}^-$ on the TA monolayer compared to the Fe(CN)_6^{3-} indicates that the probe structure may be an additional factor in the response at the monolayers.

3.6 Film Stability and Probe Retention

Film stability was examined by applying overpotential to the monolayers and inspecting the extent to which the film selectivity and sensitivity was maintained. The TA monolayer is damaged when the potential exceeds the limits allowing large oxidation or reduction currents at positive and negative potentials respectively. Application of an overpotential may result in monolayer collapse, due to partial desorption of the TA molecules at overpotential. The damage is accompanied by the appearance of a characteristic reduction peak of the gold oxide, which may break the Au-thiolate bond between the TA and the electrode and further contribute to the TA desorption. The potential window of stability of the monolayer depends on the type of the electrolyte, the solution pH and the monolayer structure. For example at pH 1.5 the anodic background current begins to increase at approximately 0.7 V and the cathodic at -0.3 V. The anodic limit is ca. 0.3 V more positive at higher pH. The cathodic limit is approximately 0.5 V more negative in neutral solutions. In the potential window of 0.6 to -0.3 V the background currents do not exceed 3 $\mu\text{A}/\text{cm}^2$. The TA electrode response and the background current at the TA electrodes do not change as long as the TA electrode is

used in this potential window.

Retention of the probes on the monolayers was also examined. When the TA monolayer originally used at pH 7.4 in $\text{Ru}(\text{NH}_3)_6^{3+}$ was transferred to 0.1 M KCl no probe retention was detected.

Cyclic voltammetric experiments were performed at different scan rates (v) to test probe adsorption on the monolayers. The slopes of the $\log i_p$ vs $\log v$ plots obtained for the $\text{Ru}(\text{NH}_3)_6^{3+}$ on the TA monolayer were close to 0.5 and were independent of the electrolyte used in the measurements, indicating that diffusion controlled the electrochemical response. The values of the slope of the $\log i_p$ vs $\log v$ plots for DA were smaller than 0.5 indicating some degree of surface passivation in DA reaction consistent with the observed slow voltammetric behavior of this probe on the monolayers.

3.7 Effect of Substrate Quality

Substrate quality is an important factor in fabricating quality monolayers. The effect of substrate quality was examined by cyclic voltammetry using the selectivity of the monolayer toward $\text{Fe}(\text{CN})_6^{3-}$ as the measure of film quality, and the response on the monolayers prepared on the Au vacuum deposited on the silicon wafers was compared to on the conventional glass microscope slides. The cyclic voltammetry results show that the monolayers of TA formed on a glass slide did not show permselectivity. $\text{Fe}(\text{CN})_6^{3-}$ was not completely excluded at pH 7.4 while it was on the TA monolayer formed on the silicon wafer. Clearly the inhomogeneity and the roughness of the substrate can result in a poorly defined film. The capacitance measurements support this observation. The capacitance

measured on the TA monolayer assembled on a glass substrate was indistinguishable from that of the bare electrode.

Scanning tunneling microscope (STM) has been used by several authors^{149,150} to characterize the Au films deposited on different substrates. The electrochemical results presented here differ from the previous observations about substrate analysis which were based on the STM results¹⁴⁹. Since the STM is most effective in the determination of the surface roughness at a nanometer scale, the structural information from the relatively small area STM scans may not always be characteristic of the whole sample. On the other hand, the electrochemical behavior of the redox probes on thin monolayers is a very sensitive measure of the average properties of the substrates. In this study, the glass slides and the silicon wafers were pretreated in the exactly the same way before the monolayers were assembled on these substrates. Therefore, the observed electrochemically determined selectivity differences of the $\text{Fe}(\text{CN})_6^{3-}$ probe on the films formed on the two substrates must result from the differences in the two substrates which cause the films to form differently. The observed differences on the electrochemically measured selectivity of $\text{Fe}(\text{CN})_6^{3-}$ on the films assembled are most likely due to the differences in the substrate roughness and may explain the various, and somewhat controversial reports of the electrochemical responses of the self-assembled monolayers found in the literature.

3.8 Conclusions

In this Chapter, the electrochemical characteristics of the TA monolayer electrode are presented. The results indicate that the selectivity is maintained by the carboxylic acid

terminal group at the TA monolayer electrode, based on the electrostatic interactions between the probe and the surface, which can be modulated by changing the solution pH. The hydrophilic TA surface can display a high electrochemical sensitivity, since the high reactivity of the electroactive probes on this monolayer can be maintained as a result of a short distance of the closest approach to the electrode surface for the probes. A low potential drop across the short alkyl chain monolayers terminating in a hydrophilic COOH head group, caused by the penetration of the film by the solvent (water) and the electrolyte, contributes to the fast electrochemical response. Solution composition, including the electrolyte concentration, have an important impact on the electrochemical response at the short monolayers. For example, at high electrolyte concentrations film swelling can increase resulting in even lower potential drop across the film and faster probe kinetics.

Probe structure and hydrophobicity was found to be an important factor in determining the response on the monolayer electrodes. We have demonstrated that the hydrophobic catechol and quinone probes are slow on the hydrophilic TA monolayers, even when the probes carry a charge opposite to that of the monolayer surface. Consequently, the short hydrophilic monolayers have an additional degree of selectivity towards hydrophilic probes.

CHAPTER 4

CHARACTERIZATION OF MONOLAYERS OF DIFFERENT HYDROPHOBICITY

In this Chapter, we describe the electrochemical characterization of the monolayers of different hydrophobicity obtained by coadsorption of different ratios of TA and C₆SH. The aim of this study is to explore the response of biological molecules at the monolayers, and the correlation between probe kinetics, probe structure and probe hydrophobicity on the surface where the hydrophobicity of the self-assembled monolayer can be altered.

4.1 Investigation of Permeability of Multicomponent Monolayers by Capacitance Measurements

Capacitance measurements were used to evaluate the properties of the mixed monolayers. Table 4.1 lists the results of film capacitance for the monolayers, and the values of the dielectric constant of the film calculated using eq. 3-3.

The results in Table 4.1 show that the TA monolayer has the largest capacitance. Capacitance decreases for 1:1 and 1:100 TA/C₆SH mixed monolayers, while the pure C₆SH monolayer has the smallest capacitance. The dielectric constant ϵ for the C₆SH monolayer is calculated to be 2.4. This value agrees well with the dielectric constant of polyethylene ($\epsilon=2.3$)¹³⁸ and the dielectric constant for the long alkyl chain thiol monolayers ($\epsilon=2.6$)⁴⁷, indicating similarity of the C₆SH monolayer structure to that of the compact films of the long chain alkylthiols. With the increase of the TA fraction in the

Table 4.1 Results of capacitance measurements of the monolayers with multicomponents

electrode	electrolyte	C ($\mu\text{F}/\text{cm}^2$)	ϵ
thioctic acid (TA)	0.1 M KCl	9.2	8.3
	0.1 M KCl and 10 mM tris	10.0	9.0
1:1 TA/C ₆ SH	0.1 M KCl	5.2	4.7
1:100 TA/C ₆ SH	0.1 M KCl	3.0	2.7
hexanethiol (C ₆ SH)	0.1 M KCl	2.7	2.4

Scan rate is 5.12 V/s

monolayers, the measured dielectric constant of the monolayers increases. The highest dielectric constant is obtained for pure TA monolayer. As discussed in Chapter 3, the dielectric constant can be used as a measure to reflect the ability of a medium against the externally applied electrical field. The high value of ϵ measured for the TA monolayer indicates the high extent of solvent and possibly ion penetration this monolayer allows. As a consequence, the film resistance is small and the potential drop across the film is small.

On the other hand, small values of ϵ in the mixed monolayers indicate that the potential drop can be expected to be much larger for the C_6SH than for the TA monolayer. The decrease in the dielectric constant of the mixed monolayers also indicates changes in film structure. Compared to the TA monolayer, the C_6SH monolayer must be more compact. The mixed monolayers have intermediate porosity, which is determined by the ratio of the TA to the C_6SH in the film.

4.2 Effect of Increasing Hydrophobicity on the Response of Hydrophilic Probes

Cyclic voltammetric investigation of the mixed monolayers was conducted using $Fe(CN)_6^{3-}$ and $Ru(NH_3)_6^{3+}$ as the electroactive probes. As the C_6SH is coassembled into the TA monolayers, the CV response of both probes starts to change. Figure 4.1 illustrates the response of the $Ru(NH_3)_6^{3+}$ at pH 7.4 on the different monolayer electrodes. On the 1:1 monolayer, $Ru(NH_3)_6^{3+}$ displays relatively fast kinetics, comparable to those on the TA film. On the 1:100 TA/ C_6SH and on the C_6SH monolayers, the response of $Ru(NH_3)_6^{3+}$ becomes indistinguishable from the background current.

Figure 4.2 shows that the response of $Fe(CN)_6^{3-}$ at pH 1.5 also deteriorates when

Figure 4.1 Cyclic voltammograms of 1 mM $\text{Ru}(\text{NH}_3)_6^{3+}$ in 0.1 M KCl and 10 mM tris (pH 7.4) on the different monolayer electrodes. Scan rate 100 mV/s.

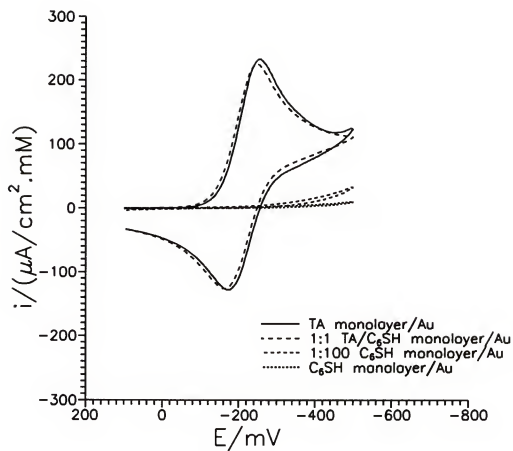
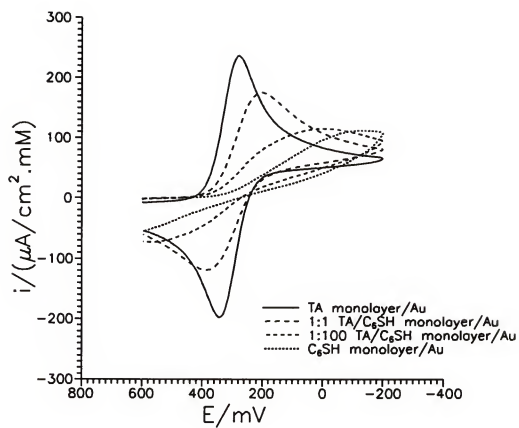


Figure 4.2 Cyclic voltammograms of 1 mM $\text{Fe}(\text{CN})_6^{3-}$ in 0.1 M HClO_4 (pH 1.5) on the different monolayer electrodes. Scan rate 100 mV/s.



C₆SH is coassembled with TA. On the 1:1 monolayer kinetics are slower as indicated by the larger ΔE_p , and the Fe(CN)₆³⁻ peak current is smaller than on the TA film. On the 1:100 TA/C₆SH and on the C₆SH monolayers, ΔE_p of Fe(CN)₆³⁻ increases further while i_p decreases.

The slow kinetics of both hydrophilic probes found on the mixed monolayers are consistent with the expected change of the monolayer capacitance. The capacitance measurements show that the capacitance of the films decreases with the increase in the hexanethiol fraction in the monolayer. Using the model proposed for the electrical double layer on the TA monolayer electrode, the surface potential of the monolayer ϕ_2 can be expressed as:⁹¹

$$\phi_2 = E_{\alpha} \frac{C_{ml}}{C_{ml} + C_d} \quad (4-1)$$

According to eq. 4-1, if C_{ml} is small, a larger fraction of the applied potential E_{α} is dropped across the monolayer. Therefore, larger potential is needed to drive the electrochemical reaction than on the TA monolayer. This will lead to slower kinetics of the probe on the monolayer at the potentials where kinetics are fast on the TA monolayer, and consequently to a decrease in current at these potentials.

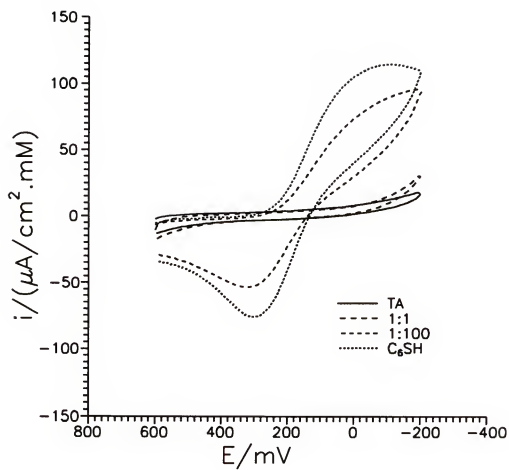
On the 1:1 TA/C₆SH monolayer at the pH, where the response of each probe is at a maximum on the TA monolayer (7.4 for Ru(NH₃)₆³⁺ and 1.5 for Fe(CN)₆³⁻), Ru(NH₃)₆³⁺ (Fig. 4.1) displays much faster kinetics than the Fe(CN)₆³⁻ (Fig. 4.2). The charge density at the monolayer solution interface can play an important role in the observed response. The negative charge of the TA headgroups can be expected to contribute to the faster

reduction of the $\text{Ru}(\text{NH}_3)_6^{3+}$ as predicted by eq. 3-4. More importantly, the negative surface charge density can make up for some of the potential drop at the monolayer caused by the lower capacitance of the mixed monolayer (eq. 4-1). At pH 1.5, where the TA/ C_6SH electrode surface is neutral because of the suppressed dissociation of the TA, the potential drop across the monolayer will be controlled by the low capacitance of the mixed monolayer. Therefore, the kinetics of the $\text{Fe}(\text{CN})_6^{3-}$ at pH 1.5 are slower than of the $\text{Ru}(\text{NH}_3)_6^{3+}$ at pH 7.4.

At the more hydrophobic monolayers of 1:100 TA/ C_6SH and of the C_6SH under the same solution pH conditions as were used to obtain the maximum response on the 1:1 monolayers, the kinetics of the two probes differ considerably. However, the same trend of a continuing decrease in the electrochemical kinetics of the hydrophilic probes with increase in film hydrophobicity is observed, which can be related to the further decrease in the film capacitance.

The effect of surface hydrophobicity on response is further highlighted by the experiments with $\text{Fe}(\text{CN})_6^{3-}$ conducted at pH 7.4. At this pH, $\text{Fe}(\text{CN})_6^{3-}$ is completely excluded from the TA film due to the electrostatic repulsion by the negatively charged surface (Fig. 3.1). However in 0.1 M KCl, the response improves when the C_6SH is coassembled with TA, with the best response observed on the C_6SH monolayer electrode (Fig. 4.3). With the coadsorption of C_6SH , the number of the COO^- groups on the monolayer decreases, making the electrostatic effects at the film insignificant. On the C_6SH monolayer the ΔE_p of $\text{Fe}(\text{CN})_6^{3-}$ at pH 7.4 in 0.1 M KCl (380 mV) is in fact smaller than at pH 1.5 in 0.1 M HClO_4 ($\Delta E_p = 700$ mV), indicating the effect of the electrolyte on

Figure 4.3 Cyclic voltammograms of 1 mM $\text{Fe}(\text{CN})_6^{3-}$ in 0.1 M KCl and 10 mM tris (pH 7.4) on the different monolayer electrodes. Scan rate 100 mV/s.

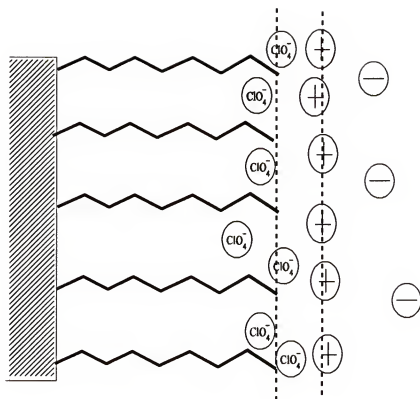


the response at the C_6SH monolayers.

Figure 4.4 illustrates a schematic model proposed to explain the different response of the $Fe(CN)_6^{3-}$ on the C_6SH monolayer electrode as a function of the electrolyte composition. The electrolyte partitioning into the monolayer can occur at the monolayer/solution interface, and the distribution of ions along the monolayer/solution interface depends on the ability of the species to partition into the hydrophobic C_6SH monolayer. In $HClO_4$, the partitioning of ClO_4^- is favored because of the hydrophobicity of ClO_4^- . As a result, the interface may acquire a net negative charge. In KCl solutions, on the other hand, neither ion is likely to partition into the monolayer because of their hydrophobicity, and closer access of the $Fe(CN)_6^{3-}$ to the C_6SH film surface may be provided. In general, the response of the $Fe(CN)_6^{3-}$ is slow on the C_6SH monolayer due to the increase in film resistance. However, the $Fe(CN)_6^{3-}$ response is slower in 0.1 M $HClO_4$ because of the additional expulsion from the monolayer which may be induced by ClO_4^- .

Comparing the responses in Figure 4.1 and 4.3, we notice that the kinetics of the $Ru(NH_3)_6^{3+}$ and the $Fe(CN)_6^{3-}$ at pH 7.4 in 0.1 M KCl on the C_6SH monolayer electrode are significantly different. Similar observations have been previously reported and no satisfying explanation has been given in the literature. In order to obtain a better explanation for the observed differences in the rates of electron transfer of the two hydrophilic probes, the self-exchange rates, the surface charge, the potential window, and the PZC of the monolayers were analyzed. However, we did not find any correlation between these parameters and the electrochemical results. The simplest explanation is that the high charge density of the $Ru(NH_3)_6^{3+}$ (higher than the $Fe(CN)_6^{3-}$) prevents its access

Figure 4.4 A schematic illustration of the double layer structure and the charge distribution at the C_6SH monolayer/solution interface in HClO_4 as the electrolyte.



to the hydrophobic surface. Creager et al. observed that on the monolayers containing (Fc) C_6SH (Fc=ferrocene) and n-alkylthiol, the formal potential of Fc shifted to a more positive value, and the peaks became broader, as the alkanethiol coadsorbate chain length increased¹⁵¹. This was used as evidence that the energy difference, caused by the changes in the hydrophobic vs hydrophilic microenvironment, influenced the response. Similar experiments may be able to differentiate the microenvironmental contribution to the kinetics of the $Ru(NH)_6^{3+}$ and the $Fe(CN)_6^{3-}$ on the C_6SH monolayers.

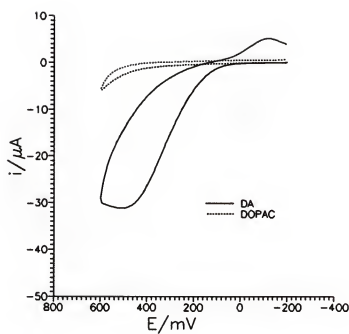
4.3 Reactivity of Hydrophobic Probes on the Hydrophobic Monolayers

One of the interesting features of the mixed monolayers is that the surface hydrophobicity can be altered easily. This property makes the mixed monolayers the best candidate for the studies of the redox molecules containing hydrophobic domains. Biological molecules often exhibit complicated electrochemical behavior, largely due to the different properties of these domains. Using the monolayers of mixed hydrophobicity, the effect of the hydrophobicity on the electrochemical response of the molecules may be investigated more closely.

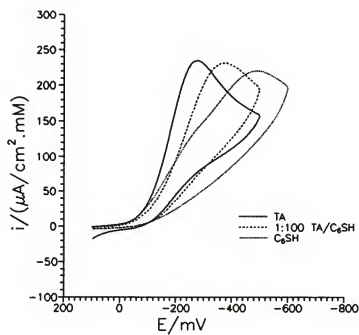
Figure 4.5A shows the response of DA (+1) and DOPAC (-1) at pH 7.4 on the 1:1 TA/ C_6SH monolayer electrodes. Compared to the response on the TA monolayer (Figure 3.3), the ΔE_p of DA increases with the coassembly of C_6SH into the TA monolayers. On the 1:100 TA/ C_6SH and the C_6SH monolayers, DA response becomes indistinguishable from the background current. DOPAC shows no response at this pH at any of the monolayers, indicating that the access of this probe to the monolayers studied here is

Figure 4.5 (A) Cyclic voltammograms of 0.5 mM DA and 0.5 mM DOPAC in 0.1 M KCl and 10 mM tris (pH 7.4) on the 1:1 TA/C₆SH monolayer electrodes. Scan rate 100 mV/s. Electrode area 0.24 cm².
(B) Cyclic voltammetric response of 0.5 mM benzoquinone (Q) in 0.1 M KCl and 10 mM tris on the different monolayer electrode. Scan rate 100 mV/s.

(A)



(B)



strongly suppressed. The response of DA disappears on the most hydrophobic monolayers, as does the response of the hydrophilic $\text{Ru}(\text{NH}_3)_6^{3+}$ (Figure 4.1).

The peak separation ΔE_p for DA at the 1:1 TA/ C_6SH electrodes is 540 mV, which is significantly larger than at the bare (105 mV) and at the TA monolayer electrodes (438 mV). Peak current, i_p , of DA at the 1:1 TA/ C_6SH electrode decreases almost by half compared to that on the bare electrode, and is comparable to that on the TA monolayer electrode. These results are different from those for $\text{Ru}(\text{NH}_3)_6^{3+}$ (Figure 4.1) where no significant differences in the ΔE_p and the i_p were observed on the TA and the 1:1 TA/ C_6SH monolayers.

As discussed in Chapter 3, slow kinetics of DA can be ascribed to the unfavorable interactions of the probe with the film and the unfavorable molecular orientation of the probe at the monolayer, as well as to the possible complications in the electron transfer mechanism for the probe. The $2e, 2H^+$ oxidation of DA may, for example, change the local pH, affecting the surface charge density. With the coadsorption of C_6SH , the monolayers become more compact and the passivation at the monolayer surface prevails.

The results obtained here for DA and DOPAC differ from the results reported recently for DA detection on the self-assembled monolayers with the COOH headgroups.¹⁵² The authors reported improved kinetics of DA on the $\text{HS}(\text{CH}_2)_2\text{COOH}$ monolayers, compared to the kinetics which were measured at the bare Au electrode³⁵. In our work DA oxidation is always more reversible, and occurs at less positive potentials on the bare Au than on the monolayer electrodes (Figures 3.3 and 4.5), including the TA monolayer. In addition, the authors observed the response of DA on the C_6SH monolayer

which was not observed in our study. This may be a result of a less compact film on the rough glass substrate used in their study.

Structural analog of DA and DOPAC, benzoquinone (Q), was investigated to reveal the effect of the positively charged terminal in DA on response. Figure 4.5B shows the cathodic response of Q as a function of surface hydrophobicity. With the incorporation of the C_6SH into the monolayer, the E_{pc} of Q becomes more negative. The magnitude of the peak current, i_{pc} , is reduced by half compared to the i_{pc} on the bare Au electrode (Figure 3.3). However, the peak current does not show a significant difference on the different monolayers, whether hydrophilic or hydrophobic.

As discussed in Chapter 3, the response of Q on the TA electrode at pH 7.4 is similar to the slow response of DA (Figure 3.3), pointing out that DA charge does not significantly help it access the charged hydrophilic surface of the TA monolayer. However, on the more hydrophobic 1:100 TA/ C_6SH and the C_6SH monolayers, uncharged Q continues to show response while the charged DA does not. This may reflect a combination of factors including probe neutrality and its more hydrophobic structure, as well as the reduction pathway of Q.

The poor response of DA and Q on the TA monolayer compared to the good kinetics of $Ru(NH_3)_6^{3+}$ highlights the differences in the response of hydrophobic vs hydrophilic probes on the hydrophilic TA monolayers, although factors other than hydrophobicity may also be important to the response (such as the reaction pathways). In previous work Miller and coworkers found that the reduction of $Fe(CN)_6^{3-}$ was 20 times faster on an -OH than on the CH_3 terminated C15 monolayers.¹⁵³ Our results with the

hydrophilic probes identify similar effect of the monolayer hydrophobicity on the probe response. However, we also observed that on our *short* TA/C₆SH monolayers the increase in surface hydrophobicity of the mixed monolayers does not improve the response of the hydrophobic probes tested here. Miller and coworkers found that on the films where the carbon chain length was >10 the hydrophobic Fe(bpy)(CN)₄⁻ responded much faster on the CH₃ than on the -OH terminated film.

4.4 Effect of Electrolyte Concentration and Composition on Response with Changes in Film hydrophobicity

The effect of electrolyte composition and concentration on the electrochemical response of both the hydrophilic and hydrophobic probes at the mixed monolayers (1:1 TA/C₆SH) was investigated using Ru(NH₃)₆³⁺ and DA as probes. The results are presented in Table 4.2. On the 1:1 TA/C₆SH monolayer electrode, Ru(NH₃)₆³⁺ has the smallest ΔE_p value in 0.5 M phosphate, and the smallest ΔE_p for DA is found in 0.05 M phosphate, similar to the results obtained on the TA monolayer electrodes (Table 3.4). Compared to the response on the TA monolayer, a small decrease in kinetics was observed on the 1:1 TA/C₆SH monolayer electrode as a result of the increased film resistance of the mixed monolayers, as previously discussed.

4.5 Stability of the Mixed Monolayer Electrodes

The stability of the mixed monolayers was examined by the methods described in Chapter 3. We have found that the TA electrodes are stable between -800 mV and +1000

Table 4.2 Cyclic voltammetric results of $\text{Ru}(\text{NH}_3)_6^{3+}$ and DA as a function of electrolyte concentration on the 1:1 TA/C6SH monolayer electrodes

probe	electrolyte ^a	ΔE_p (mV)	i_{pc} ($\mu\text{A}/\text{cm}^2.\text{mM}$)
$\text{Ru}(\text{NH}_3)_6^{3+}$	0.1 M KCl and 10 mM tris	80±10	210±5
	0.05 M phosphate	104±1	176±4
	0.5 M phosphate	77±1	169±1
DA	0.1 M KCl and 10 mM tris	540±20	232±14
	0.05 M phosphate	458±19	278±22
	0.5 M phosphate	625±50	208±15

^a pH 7.4.

mV vs SCE at neutral pH and pointed out that the potential window for a stable electrochemical response of the monolayers depends on the type of the electrolyte, and the solution pH. The stability windows for the mixed monolayers are the same as for the TA monolayer. In some cases the stability window can be even larger on the mixed monolayers due to the large resistance of the mixed film that can suppress the electrochemical reactions which can destroy the films. For instance, at very low pH, evolution of hydrogen at negative potential limit may destroy the monolayers. In 0.1 M HClO_4 hydrogen evolution occurs at ca. -550 mV on the TA film compared to ca. -400 mV vs SCE on the bare Au. On the C_6SH monolayer, even at ca. -800 mV, there is no sign that hydrogen is being generated.

An important issue is the thermodynamic stability of the mixed monolayers. Mixed monolayers with long alkyl chains ($n \geq 10$) are stable and behave reproducibly based on the contact angle measurement results.^{43,66,78} However, the stability of the short alkyl chain monolayers such as were used in this study has not been reported. In this study, Au electrodes stored in 1:1 TA/ C_6SH solution for 3 months have monolayers with significantly slower kinetics for the $\text{Ru}(\text{NH}_3)_6^{3+}$ than the monolayers prepared through much shorter contact with this solution, but the $\text{Ru}(\text{NH}_3)_6^{3+}$ current, although much smaller, can still be measured.

Theoretically, the alkyl thiols may eventually replace the carboxylic thiols from the monolayer since the pure alkylthiol monolayers are thermodynamically more stable in the ethanol solutions. If this were to happen during the 3 months of contact with the 1:1 TA/ C_6SH solution the TA should be largely replaced by the C_6SH , and the monolayer

should display a similar electrochemical behavior to the 1:100 TA/C₆SH or even the pure C₆SH films. However, this was not observed. The different electrochemical response of the Ru(NH₃)₆³⁺, does not reflect in our view, fast structural changes in the 1:1 films. This prompted us to conclude that the mixed monolayers are relatively stable thermodynamically.

4.6 Conclusions

The monolayers prepared by self-assembly and coassembly of the short alkyl chain thioctic acid and the hexanethiol display unique properties. By mixing the two compounds in a controlled ratio, surfaces with a different degree of hydrophobicity can be obtained. The kinetics of the electroactive species on the hydrophobic surfaces, however, decrease predominantly as a result of the increase in potential drop across the monolayer film.

The increase in the monolayer hydrophobicity results in the slower kinetics for the hydrophilic probes. At the same time, the increased monolayer hydrophobicity does not improve the response of the hydrophobic catechols and quinone probes. For a fast response of such hydrophobic probes an ideal surface may need to be hydrophobic, but with a low potential drop, a surface which has not yet been successfully built. As an alternative choice, high film porosity should be pursued whenever possible. In many cases, such an objective can only be accomplished by making ultrathin films.

CHAPTER 5 CHARACTERIZATION OF MONOLAYER ULTRAMICROELECTRODES

5.1 Background

Ultramicroelectrodes (UME) have been a subject of considerable research for many years and continue to receive attention⁸¹. Due to the tiny physical size and the resulting small electrode/solution interfacial capacitance UMEs have found applications as electrochemical sensors in microenvironments such as the brain tissue^{124, 154}, extracellular spaces¹⁵⁵⁻¹⁵⁷, and in fast scan cyclic voltammetry¹⁵⁸⁻¹⁶⁰.

In order to obtain the desired sensitivity and selectivity, UMEs are often modified with polymers. The polymer-based chemically modified UMEs suffer drawbacks such as poorly defined surface morphology²⁰. Therefore, the effect of structure of the modified layer on the electrode response is often difficult to determine. It is highly desirable to have a more ordered environment at the surface, to investigate the correlation between the properties of the modified layer and the resulting electrochemical response.

In this Chapter, we describe a new strategy for obtaining ultrathin membranes, for modifying UMEs, in which molecular architecture and, therefore, film order is under the experimental control. The method used to prepare the membranes exploits molecular self-assembly of thioctic acid.

The key characteristics of the TA monolayer have been described in the previous chapters. The short five carbon long alkyl chain, together with the hydrophilic carboxylic

terminal, assemble into an ultrathin film which produces diffusion-controlled response of the electrodes. In addition, the self-assembly technique allows a convenient adjustment of the film properties, such as the charge density at the film/solution interface. Since such parameters are involved in determining the response of the film electrodes, they can be controlled to fit the measurement requirements.

The electrochemical investigation of fast redox reactions of osmium complexes, covalently attached to thin monolayers on Pt microelectrodes, has been reported by Faulkner and coworkers.¹⁶¹ However, the modification of UMEs with ultrathin, relatively well ordered monolayers aiming at analytical applications has not yet been explored. This is likely due to the difficulties in obtaining a high quality, micrometer dimensions substrate on which molecular organization can be controlled. Substrate quality has been shown to influence the monolayer quality on macroelectrodes, and the monolayer properties⁷⁰.

The problem of the monolayer order becomes more significant on the UMEs. As the electrode size becomes smaller, at subsecond timescales, the semi-infinite planar diffusion is replaced by hemispherical diffusion. Therefore, mass transport to an UME becomes very effective^{80,81}. As a result, diffusion-controlled processes observed on large electrodes can become a subject to kinetic limitations. Since order/structure of the monolayer ultimately determines film properties, film order can have a significant impact on the electron transfer kinetics at the electrode, and thus on the selectivity and sensitivity of the resulting electrodes.

In this Chapter we describe a strategy which allows formation of self-assembled monolayers of TA on the Au fiber UMEs. Electrochemical measurements reveal that the

strategy developed to prepare the monolayers produces films which exhibit excellent selectivity, pointing to a reasonable order of the films. The response of fast redox couples, $\text{Fe}(\text{CN})_6^{3-/4-}$ and $\text{Ru}(\text{NH}_3)_6^{3+/2+}$ as a function of the electrolyte composition and the solution pH, was investigated to characterize the monolayers.

The new UMEs were tested in amperometric pH sensing. Measurement of pH with UMEs can provide insight into interfacial phenomena, such as pH-dependent phase transition of monolayers on electrodes, and may also allow convenient measurement of headgroup pK_a . In addition, micrometer pH sensors will allow pH measurements in microenvironments. Such measurements are essential to the understanding of biological processes such as regulation of proton dependent enzymes, and ion uptake upon pH change¹⁶².

Wrighton and coworkers have developed an amperometric pH sensor, by immobilizing a ferrocenyl thiol and a quinone thiol on a microelectrode array, using self-assembly. The quinone half-wave potential, $E_{1/2}$, is pH-sensitive and the changes in $E_{1/2}$ were used to measure pH while the ferrocene center, which has an $E_{1/2}$ that is pH-insensitive, was used as a reference¹⁶³.

The TA UME described in this Chapter provides an alternative approach to pH sensing where the changes in surface charge density with pH lead to the measured changes in the current of an electroactive probe. Application of the $\text{Fe}(\text{CN})_6^{3-}$ as a probe in pH sensing at TA UMEs is described.

5.2 Preparation and Characterization of Ordered Monolayers on Au Fiber Electrodes

Figure 5.1 summarizes the response of $\text{Fe}(\text{CN})_6^{3-}$ on the bare and the TA modified UMEs in 0.1 M KCl (pH 7.4). Fig. 5.1 (a) shows the sigmoidal steady state response of the $\text{Fe}(\text{CN})_6^{3-}$ on the bare electrode while Figs. 5.1 (b) and (c) show the response on the TA monolayer electrodes prepared by two different methods.

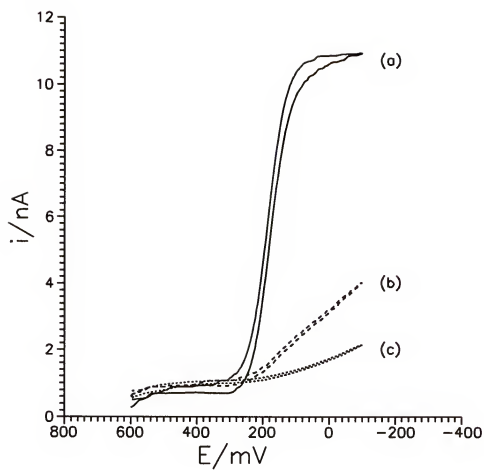
Results in Fig. 5.1 (b) were obtained on an Au electrode that was processed by mechanical polishing with alumina slurry while the results in Fig. 5.1 (c) were obtained on an electrode that was additionally etched in dilute aqua regia for 5 min before assembly of the TA.

As the results in Fig. 5.1 show, $\text{Fe}(\text{CN})_6^{3-}$ response is greatly suppressed on both modified surfaces. Dissociation of the carboxylic terminal groups of the TA at pH 7.4 can produce negative charged groups at the surface,^{20,21} suppressing the response of the negatively charged $\text{Fe}(\text{CN})_6^{3-}$. However, as is clear from the comparison of Figs. 5.1 (b) and (c), the extent to which the current is suppressed depends on the Au surface treatment. Compared to the response on the bare polished Au electrode, $\text{Fe}(\text{CN})_6^{3-}$ current at 0.00 V on the TA electrodes decreases by ca. 94% on the monolayers prepared on the acid etched Au and by ca. 78 % on the mechanically polished Au surface.

As was previously reported, substrate quality has a significant impact on the response of self-assembled monolayer electrodes prepared on macroelectrode substrates. Therefore, voltammetric results can be used as a guide to film quality.

A significant decrease of the $\text{Fe}(\text{CN})_6^{3-}$ current shown in Fig. 5.1, reflects poor access of the $\text{Fe}(\text{CN})_6^{3-}$ to the monolayers prepared on the acid etched surfaces which

Figure 5.1 Cyclic voltammograms of 5 mM Fe(CN)_6^{3-} in 0.1 M KCl and 10 mM tris (pH 7.4) on (a) bare UME; (b) TA monolayer electrode formed on mechanically polished Au; (c) TA monolayer electrode formed on aqua regia etched Au. Scan rate is 25 mV/s. Electrode diameter is 12.7 μm .



likely reflects the quality of this monolayer. Presumably, a microscopically smoother substrate is formed by etching. Similar effect of etching on substrate quality was observed by Creager and coworkers on large polycrystalline plate electrodes¹⁶⁴. The authors took the inability of a monolayer of $C_{12}H_{25}SH$ to block electron transfer of (hydroxymethyl)ferrocene in solution, and a tendency of the monolayer toward exchange of bound thiol for free thiol ($FeCONH(CH_2)_{10}SH$, Fe =ferrocene) in solution, as evidence for a large number of surface defects. They found that polycrystalline plate electrode substrates that were chemically etched with aqua regia ($HCl:HNO_3:H_2O$ 3:1:6) yielded monolayers with significantly fewer defects than monolayers prepared on mica. The STM results further revealed that while the etched electrodes were macroscopically rough (with grains as wide as 100 μm), they were certainly very smooth on a microscopic scale.¹⁶⁴

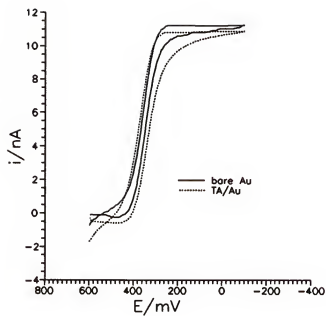
In short, the results indicate that polished polycrystalline Au fiber may have necessary quality to form selective TA monolayers which can suppress $Fe(CN)_6^{3-}$ response by ca. 78 % compared to the response of the bare Au electrode. However, the apparent substrate quality, and the resulting monolayer selectivity, can be significantly enhanced by acid etching of the Au electrode where the signal can be suppressed by ca. 94 % compared to that of the bare Au electrode. As a result, all experiments reported here were conducted on acid etched Au substrates unless otherwise specified.

5.3 Selectivity And Sensitivity of the Thioctic Acid Monolayer Ultramicroelectrodes

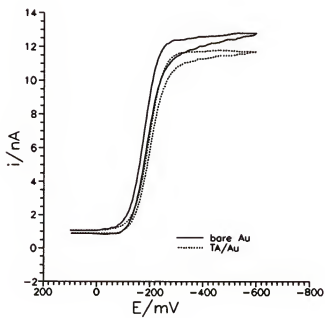
The response of the $Fe(CN)_6^{3-}$ on the TA monolayer UMEs was also studied as a function of the solution pH. Figure 5.2 (a) shows the response at pH 1.5. In contrast to

Figure 5.2 (A) Cyclic voltammograms of 5 mM $\text{Fe}(\text{CN})_6^{3-}$ in 0.1 M HClO_4 (pH 1.5) on bare (solid line) and TA monolayer electrodes (dash line). (B) Cyclic voltammograms of 5 mM $\text{Ru}(\text{NH}_3)_6^{3+}$ in 0.1 M KCl and 10 mM tris (pH 7.4) on bare (solid line) and TA monolayer electrodes (dash line). Scan rate is 25 mV/s. Electrode diameter is 12.7 μm .

(A)



(B)



the response at pH 7.4 (Fig. 5.1(c)), the response of the $\text{Fe}(\text{CN})_6^{3-}$ at pH 1.5 is well defined. Fig. 5.2 (b) shows the cyclic voltammograms of the $\text{Ru}(\text{NH}_3)_6^{3+}$ at pH 7.4 where a well defined sigmoidal response is also obtained.

The electrochemical reversibility^{134,135} of the two probes was also investigated on the monolayer electrodes at the time scales of the experiments. Fig. 5.3 illustrates the plots of $\log((i_L - i)/i)$ vs. E for the $\text{Fe}(\text{CN})_6^{3-}$ and the $\text{Ru}(\text{NH}_3)_6^{3+}$ and the results are summarized in Table 5.1. The results in Table 5.1 show that the reciprocals of the slopes are all close to 59 mV, indicating that fast response of the two probes was obtained except in F^- as the electrolyte. Table 5.1 also shows that half-wave potential, $E_{1/2}$, for $\text{Ru}(\text{NH}_3)_6^{3+}$, is ca. -0.18 V vs SCE while for the $\text{Fe}(\text{CN})_6^{3-/4-}$ couple the $E_{1/2}$ is ca. 0.36 V vs SCE. The latter $E_{1/2}$ obtained at pH 1.5 is significantly more positive than at pH 7.4 ($E_{1/2} = 0.18$ V vs SCE obtained at the bare electrode). The positive shift is due to the expected protonation of $\text{Fe}(\text{CN})_6^{3-}$,¹⁶⁵ which shifts the potential anodically.

Under steady state conditions limiting current at the UME is time independent since the rate of diffusion is faster than the rate of depletion by electrolysis. Theoretical values of i_L for a microdisk electrode can be obtained from:

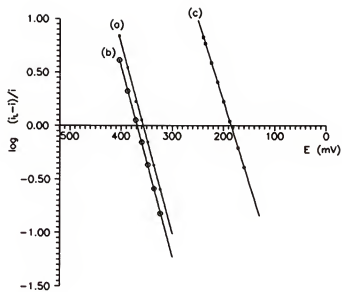
$$i_L = 4nFrD_0c^* \quad (5-1)$$

where r is the radius of the electrode (cm), D_0 is the diffusion coefficient (cm^2/s) and c^* is the bulk concentration of the electroactive species (mole/cm^3). Table 5.2 summarizes the results of the steady state current obtained for the two probes and compares them to the calculated values.

The results in Table 5.2 show that the values of the measured limiting currents at

Figure 5.3 (A) Plot of $\log ((i_L-i)/i)$ verses E for the reduction of 5 mM Fe(CN)_6^{3-} in (a) 0.1 M HClO_4 (pH 1.5) on the bare Au UME; (b) 0.1 M KCl and 10 mM tris (pH 7.4) on the bare Au and (c) 0.1 M KCl and 10 mM tris (pH 7.4) on the TA UME. (B) Plot of $\log ((i_L-i)/i)$ verses E for the reduction of $\text{Ru(NH}_3)_6^{3+}$ in 0.1 M KCl and 10 mM tris (pH 7.4) on (a) bare Au UME and (b) TA UME.

(A)



(B)

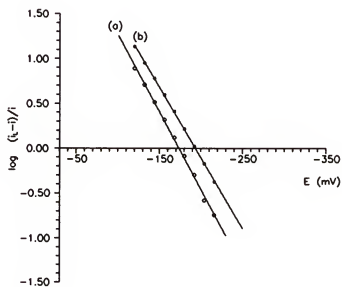


Table 5.1. Half-wave potentials and Nernstian slopes for $\text{Fe}(\text{CN})_6^{3-}$ and $\text{Ru}(\text{NH}_3)_6^{3+}$ in different electrolytes

probe ^a	electrode ^b	electrolyte	pH	$E_{1/2}$ (V vs. SCE)	reciprocal of the slope
$\text{Fe}(\text{CN})_6^{3-}$	bare Au	0.1 M HClO_4	1.5	0.36	56
	bare Au	0.1 M KCl and 10 mM tris	7.4	0.18	62
	TA	0.1 M HClO_4	1.5	0.37	56
$\text{Ru}(\text{NH}_3)_6^{3+}$	bare Au	0.1 M KCl and 10 mM tris	7.4	-0.18	58
	bare Au	0.1 M phosphate	7.4	-0.22	59
	bare Au	0.1 M NaF and 10 mM tris	7.4	-0.19	56
	bare Au	0.1 M NaF and 10 mM tris	9.6	-0.18	55
	TA	0.1 M KCl and 10 mM tris	7.4	-0.19	63
	TA	0.1 M phosphate	7.4	-0.23	63
	TA	0.1 M NaF and 10 mM tris	7.4	-0.20	84
	TA	0.1 M NaF and 10 mM tris	9.6	-0.19	55
	TA passivated in F^-	0.1 M KCl and 10 mM tris	7.4	-0.20	69

^a scan rate is 25 mV/s, concentration of probe is 5 mM. ^b electrode diameter is 12.7 μm .

Table 5.2. Voltammetric results for 5 mM $\text{Fe}(\text{CN})_6^{3-}$ and $\text{Ru}(\text{NH}_3)_6^{3+}$ on the TA and bare Au microelectrodes

probe	electrolyte	pH	$i_{\text{calc}}^{\text{a}}$ (nA)	i_{ml} (nA)	i_{bare} (nA)	$i_{\text{ml}}/i_{\text{bare}}$ (%)
$\text{Fe}(\text{CN})_6^{3-}$	0.1 M HClO_4	1.5	9.3	10.6±0.1	11.0±0.3	96
	0.1 M KCl and 10 mM tris	7.4	9.3	-	10.4±0.1	-
$\text{Ru}(\text{NH}_3)_6^{3+}$	0.1 M KCl and 10 mM tris	1.0	9.3	-	9.6±0.4	-
	0.1 M KCl and 10 mM tris	7.4	9.3	10.3±0.1	10.8±0.1	95
	0.1 M phosphate	7.4	6.8	7.8±0.2	9.5±0.1	82
	0.1 M NaF and 10 mM tris	7.4	-	0.5	10.5	5
	0.1 M NaF and 10 mM tris	9.6	-	9.8	11.0	89

^a calculated from eq. 1 using $\text{Fe}(\text{CN})_6^{3-}$ diffusion coefficient in 0.1 M KCl ($D_0 = 7.6 \times 10^{-6} \text{ cm}^2/\text{s}$), $\text{Ru}(\text{NH}_3)_6^{3+}$ in 0.1 M KCl ($D_0 = 7.6 \times 10^{-6} \text{ cm}^2/\text{s}$) and $\text{Ru}(\text{NH}_3)_6^{3+}$ in 0.1 M phosphate ($D_0 = 5.5 \times 10^{-6} \text{ cm}^2/\text{s}$). Theoretical current for $\text{Ru}(\text{NH}_3)_6^{3+}$ in F^- was not calculated due to lack of diffusion coefficient data.

the bare and the monolayer electrodes agree well for the $\text{Fe}(\text{CN})_6^{3-}$ at pH 1.5 and for the $\text{Ru}(\text{NH}_3)_6^{3+}$ at pH 7.4 in Cl^- electrolytes. However, the measured values are systematically larger than the values calculated from eq. 5-1 by an average of ca. 13%. This is likely due to the deviation from eq. 5-1 which assumes a microdisk model for the electrode geometry. In addition, since eq. 5-1 predicts that current is proportional to the electrode radius rather than area a small polishing angle may result in an elliptical surface which could produce larger currents.

A sensitive response of the $\text{Ru}(\text{NH}_3)_6^{3+}$ at pH 7.4 (Figure 5.2) compared to the suppressed response of $\text{Fe}(\text{CN})_6^{3-}$ at this pH (Figure 5.1) confirms the pH induced selectivity of the monolayer electrodes and points, as previously described, to the electrostatic interactions as the reason for the pH induced monolayer selectivity⁷⁰.

A modified double layer model (see Chapter 1) has been proposed to depict the surface of the monolayer where the potential at the outer Helmholtz plane (OHP)⁷⁰, ϕ_2 , can have a non-zero value due to the presence of the negatively charged carboxylate. The kinetics of the electrochemical reaction under these conditions are corrected for the Frumkin diffuse layer effect, as described in eq. 3-4.^{90,91}

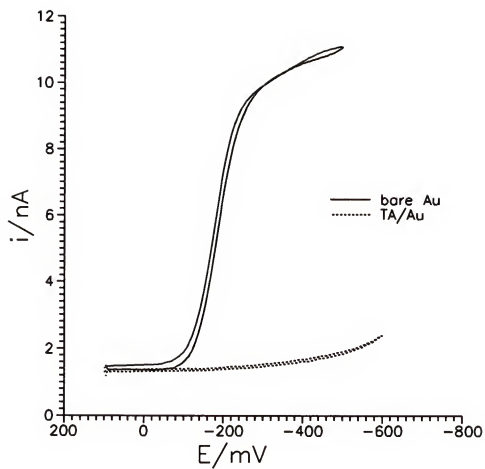
Based on eq. 3-4, the response of the anionic $\text{Fe}(\text{CN})_6^{3-}$ ($z = -3$) can be expected to be suppressed when the surface is negatively charged ($\phi_2 < 0$) at pH 7.4. On the other hand, eq. 3-4 predicts that the kinetics of the cationic $\text{Ru}(\text{NH}_3)_6^{3+}$ ($z = +3$) can be expected to be enhanced. Since the $\text{Ru}(\text{NH}_3)_6^{3+}$ kinetics are inherently fast ($k_0 = 1.22 \text{ cm/s}$)¹⁶⁰, the observed response is under diffusion control, and the enhancement is not observed at the low scan rates used here.

Fast response observed for the $\text{Fe}(\text{CN})_6^{3-}$ at pH 1.5 (Table 5-1) points to the ability of the $\text{Fe}(\text{CN})_6^{3-}$ to access closely the electrically neutral TA surface. The response of the $\text{Ru}(\text{NH}_3)_6^{3+}$ at pH 1.0 is shown in Fig 5.4 and displays no faradaic current. At high concentrations of the H_3O^+ , the positively charged $\text{Ru}(\text{NH}_3)_6^{3+}$ does not effectively access the monolayer surface. Under the same conditions, $\text{Fe}(\text{CN})_6^{3-}$ response however, is favored. Here, the possibility that the fast kinetics of the $\text{Fe}(\text{CN})_6^{3-}$ (Figure 2) may result from an inner-sphere proton-bridged mechanism can not be excluded. For example, different rate constants of $\text{Fe}(\text{CN})_6^{3-}$ have been measured on Pt electrodes in the presence of K^+ , where the role of K^+ as a bridge atom between $\text{Fe}(\text{CN})_6^{3-}$ and the electrode that facilitated ET was anticipated^{166,167}. Protonation of $\text{Fe}(\text{CN})_6^{3-}$ occurs in acidic solutions¹⁶⁵ and a bridge may be envisioned if hydrogen ion partitions into the film. In addition to fast kinetics at pH 1.5 in 0.1 M HClO_4 , fast response of $\text{Fe}(\text{CN})_6^{3-}$ at pH 1.0 in 0.1 M KCl/HCl electrolyte was also observed confirming the importance of pH to the response. $\text{Ru}(\text{NH}_3)_6^{3+}$ response was not studied in HClO_4 because of a formation of an insoluble salt between ClO_4^- and the $\text{Ru}(\text{NH}_3)_6^{3+}$.

5.4 Effect of Electrolyte and Solution pH on Response

Electrolyte concentration has an effect on the monolayer structure through the Donnan effect and can consequently influence the electrochemical response of the monolayer electrodes²¹. Conclusive investigation of the electrolyte effect in acidic electrolytes is difficult because of the possible hydrogen ion partitioning into the TA film. Therefore, electrolyte effects were studied at pH 7.4 with the $\text{Ru}(\text{NH}_3)_6^{3+}$ as the

Figure 5.4 Response of 5 mM $\text{Ru}(\text{NH}_3)_6^{3+}$ in 0.1 M KCl (pH 1.0) on the bare (solid line) and the TA monolayer microelectrodes (dash line). Scan rate is 25 mV/s.



electroactive probe. Cyclic voltammograms for $\text{Ru}(\text{NH}_3)_6^{3+}$ in 0.1 M KCl/10 mM tris are shown in Fig. 5.2 (b) while Figs. 5.5 (a) and (b) show the response in 0.1 M phosphate and in 0.1 M NaF, respectively. The results are summarized in Table 5.2.

Compared to the response in Cl^- the response of the $\text{Ru}(\text{NH}_3)_6^{3+}$ changes dramatically in phosphate and F^- electrolytes. The ratios of the steady state currents on the monolayers to the steady state current at the bare electrode ($i_{\text{ss}}/i_{\text{bare}}$) are summarized in Table 5.2.

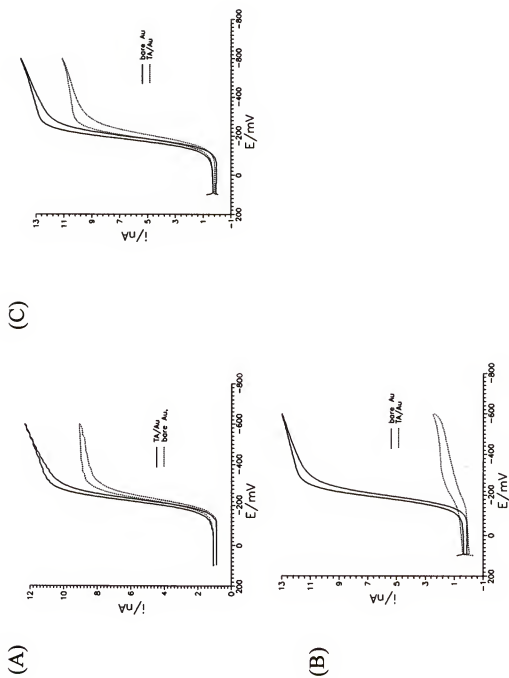
In phosphate, the magnitude of the $\text{Ru}(\text{NH}_3)_6^{3+}$ steady state current decreases by ca. 18 % compared to the response at the bare electrode, while in 0.1 M NaF the current decreases even further, and is only slightly higher than the charging current (Fig. 5.5 (b)). The response of the $\text{Ru}(\text{NH}_3)_6^{3+}$ in 0.1 M sodium phosphate is indistinguishable from that in potassium phosphate indicating that the observed i_{L} current decrease is anion dependent.

The reversibility of the $\text{Ru}(\text{NH}_3)_6^{3+}$ reaction at pH 7.4 was determined from the slopes of the $\log((i_{\text{L}}-i)/i)$ vs. E plots (Table 5.1). In phosphate buffer, the kinetics of $\text{Ru}(\text{NH}_3)_6^{3+}$ remain fast compared to the response in Cl^- . In F^- , while the steady state current decreases by 95% the log slope increases indicating effects of kinetics on the larger slope. The kinetic effects in F^- may be due to structural changes at the monolayer due to, for example, interactions of F^- with the TA headgroups such as hydrogen bonding, which could change film fluidity.

This model of F^- /film interactions is further supported by the experiments conducted at a higher pH (pH 9.6) summarized in Fig. 5.5 (c) and Table 5.1. At pH 9.6

Figure 5.5

Response of 5 mM $\text{Ru}(\text{NH}_3)_6^{3+}$ on bare (solid line) and the TA monolayer microelectrodes (dash line). (A) in 0.1 M phosphate (pH 7.4). (B) in 0.1 M NaF and 10 mM tris (pH 7.4). (C) in 0.1 M NaF (pH 9.6)



the response of the $\text{Ru}(\text{NH}_3)_6^{3+}$ in F^- is only suppressed by ca. 10 % and becomes more reversible (Table 5.1), consistent with the different interactions between the $\text{Ru}(\text{NH}_3)_6^{3+}$ and the film at the higher pH, i.e., different effect of F^- on $\text{Ru}(\text{NH}_3)_6^{3+}$ response at this pH.

After initial measurements in F^- which produced the markedly suppressed response of the $\text{Ru}(\text{NH}_3)_6^{3+}$ (pH 7.4), the response of the $\text{Ru}(\text{NH}_3)_6^{3+}$ can be partially reestablished at the same pH in Cl^- (the steady state current reaches 3 nA compared to 10.3 nA on the freshly made TA monolayer), and the kinetics become again reasonably fast (Table 5.1). However, this switching effect is not observed in phosphate. It is possible that Cl^- can replace F^- in the monolayer reestablishing in part the fluidity of the monolayer due to the larger hydrophilicity of Cl^- .

5.5 Amperometric pH Sensing with the TA UME Using $\text{Fe}(\text{CN})_6^{3-}$ as the Mediator.

The response of the $\text{Fe}(\text{CN})_6^{3-}$ on the TA UME depends on the charge density of the carboxylate head groups at the monolayer surface which is controlled by the solution pH. At sufficiently high pH, the response of the $\text{Fe}(\text{CN})_6^{3-}$ is suppressed when the COOH groups are fully dissociated, but as the pH is lowered the response of the $\text{Fe}(\text{CN})_6^{3-}$ is fully restored. Therefore, the magnitude of the $\text{Fe}(\text{CN})_6^{3-}$ current is a function of the solution pH and may be used to reveal the interfacial properties of the film such as the acid dissociation constant of the head groups. Solution pH should have a most significant effect on the $\text{Fe}(\text{CN})_6^{3-}$ current near the pK_a of the thioctic acid. As a result, the measurement of the $\text{Fe}(\text{CN})_6^{3-}$ current as a function of the solution pH should allow the determination of the pK_a of the surface bound thioctic acid.

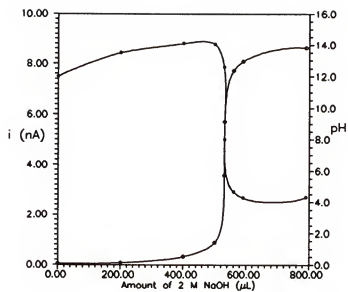
Figure 5.6 (a) (closed circles) shows the result of a pH titration monitored at the TA UME with the $\text{Fe}(\text{CN})_6^{3-}$ as the amperometric indicator. The solution pH was simultaneously monitored with a conventional glass electrode and the results are also shown in the figure (open circles). Figure 5.6 (b) is the first derivative of the titration curve obtained in the amperometric titration. The pK_a determined for the surface bound TA from the amperometric data is ca. 7.0, which is significantly higher than that for the thioctic acid in solution ($\text{pK}_a = 5.0$)¹³⁹. The shift in the pK_a for the surface bound TA may be due to the surface interactions between the COOH groups such as the nearest-neighbor electrostatic interactions, and the hydrogen-bonding stabilization of the acid form which will both contribute to the higher pK_a values of the TA at the surface. The dissociation of the surface COOH groups occurs over ca. 6-7 pH units.

Ward and coworkers used quartz crystal microbalance (QCM) to investigate the properties of the carboxylic terminated self-assembled monolayers at the monolayer-water interface¹⁴⁰. They reported that the pK_a of $\text{HS}(\text{CH}_2)_{15}\text{COOH}$ monolayer was ca. 8.0 and that the transition region was approximately 4 pH units. Compared to the solution pK_a , which is typically between 4-5, surface bound carboxylic acid also showed higher pK_a values. Similar behavior was observed by Whitesides and coworkers for the carboxylic terminated thiol monolayers using contact angle measurements.⁴⁴

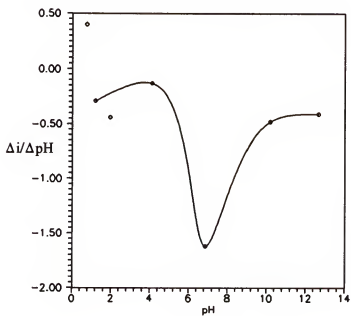
Amperometric pH sensing described in this study may provide a complementary route for measuring the pK_a 's of the surface groups at monolayers. Ward et al. observed that the QCM frequency did not change when the experiments were performed with monolayers prepared from $\text{HSCH}_2\text{CH}_2\text{COOH}$, indicating that QCM measurements may be

Figure 5.6 (A) Titration curve of 0.1 M HClO_4 by 2 M KOH. \circ results obtained by potentiometric monitoring. \bullet results by amperometric method using 5 mM $\text{Fe}(\text{CN})_6^{3-}$ as the mediator. The electrode diameter is 12.7 μm , scan rate is 25 mV/s. (B) First derivative of the amperometric titration curve.

(A)



(B)



insensitive at monolayers of small thickness¹⁴⁰.

Considering the electrode area and assuming ca. 1×10^{-10} mol/cm² as the monolayer surface coverage by the COO⁻ groups, ca. 1.27×10^{-16} moles of H⁺ are required to protonate this monolayer fully if the buffer effect is ignored. This value is equivalent to ca. 7.6×10^7 H⁺ ions, which shows that in the present design TA UMEs (ca. 10 μ m radius) are capable of sensing extremely small quantities of protons indicating that this approach may find use in measurements at cellular level. For example, for cultured cells such as fibroblasts, pumping rates of 10^8 protons per second are often obtained in steady state¹⁶⁸. Considering a 10 second pumping duration and a 20 mM buffer concentration, the pH 1 μ m away from the cell surface drops by 0.20 pH unit. The sensitivity of the TA UME design using 5 mM Fe(CN)₆³⁻ as the probe is found to be 800 pA/pH unit. A 0.20 pH unit change corresponds to 160 pA current, which can be easily detected by modern electrochemical devices. The algebra presented here shows strongly the perspective of the TA UME design in pH sensing at single cell level, provided that the presence of the Fe(CN)₆³⁻ in the medium does not change the cellular activity significantly.

5.6 Conclusions

With the strategy developed in this work for obtaining quality Au fiber substrates for self-assembly, molecular fabrication of well-organized self-assembled monolayers of thioctic acid has been accomplished at electrodes of the micrometer dimensions. High selectivity and electrochemical sensitivity of the TA UMEs is comparable to that on the TA monolayers formed on gold vacuum deposited on silicon wafers. The TA UMEs

provide a new interface for the investigation of electrochemical processes at ultrathin membranes. Since mass transport to the electrodes of the micrometer dimensions can be made effective, kinetic influences on the electrochemical response at the monolayer electrodes, which can be overshadowed at large electrodes due to slow transport, can be investigated more readily. Much more information relating to the surface interactions can thus be revealed compared to the experiments conducted at modified macroelectrodes.

Another interesting point is that by using electroactive mediators surface properties such as its acid/base properties, can be explored. This is particularly significant to the understanding of the structural and chemical changes during modification of the layers. The method could be used along with other techniques such as QCM to provide complementary information about surface properties of the surface bound materials. By employing redox species as mediators, structural changes on the monolayers induced by the solution pH can be transformed to current changes of the redox species, which allows amperometric pH sensing on the monolayers such as the TA monolayer electrode.

The TA UMEs, as ultrathin hydrophilic films with carboxylic headgroups, are anticipated to be useful in sensor design. Willner and coworkers have recently reported enzyme electrodes prepared by covalent immobilization of enzymes onto cystamine assembled on Au electrodes.¹⁶⁹ Related strategies with TA monolayer electrodes to tackle enzyme response will be discussed in the next Chapter.

CHAPTER 6

DIRECT ELECTROCHEMISTRY OF CYTOCHROME C ON THE MONOLAYER ELECTRODES AND *IN SITU* CHEMICAL DERIVATIZATION OF THE ULTRATHIN FILMS

In this chapter, the TA monolayer electrode is used in the electrochemical characterization of a redox protein, cytochrome c, to reveal the potential applications of the TA monolayer in the design of biosensors. First, direct electrochemistry of cytochrome c on the TA monolayers is investigated to illustrate the importance of the monolayer surface in promoting reversible electron transfer of a protein at the electrode. Focus will be placed on the ability of the TA monolayer to provide a favorable, interfacial interactions between the monolayer and the protein. A model including electrostatic interactions between the carboxylic headgroup of the monolayer and the amino acid residues of the protein, which lead to an appropriate molecular orientation of the protein at the interface is proposed to explain the reversible electrochemical behavior of cytochrome c.

Second, a strategy of redox mediation on the TA monolayers is developed for promoting the performance of the TA monolayer electrode towards biologically important molecules. The enhanced performance of the TA monolayers towards the molecules with large reduction or oxidation potential is proposed to be achieved through electrical relaying on the TA monolayer as a result of facilitated electron transfer between the electrode and the analyte. The results and the problems associated with the *in situ* chemical derivatization of the TA monolayers are discussed.

6.1 Background of Direct Electrochemistry of Cytochrome c

Direct electrochemistry of proteins has attracted chemists' attention for many years because of its important impact on both fundamental and applications research.¹⁷⁰

Electrochemical response of proteins can provide important information about thermodynamic and kinetic properties of proteins. In addition, a great deal of dynamic operation of macromolecules at the interfaces such as interfacial specificity, compatibility, and denaturation of proteins may be disclosed.¹⁷⁰ This has far-reaching implications, particular in the fields of macromolecular recognition, electron-transfer mechanisms and biosensor design.¹²⁸

The scope of the direct electrochemistry of proteins is well represented by the extensive studies of a small redox protein cytochrome c.¹²⁸ Cytochrome c is an electron transfer carrier and plays an important role in the oxidative phosphorylation of ADP to form ATP.¹²⁷ Figure 6.1 illustrates the electron transfer chain for the oxidation of NADH and FADH₂ in which the necessary free energy to generate ATP is provided. The potential difference between NADH and oxidizer O₂ is so huge ($E^{\circ}_{\text{NADH}} = -0.315 \text{ V}$ and $E^{\circ}_{\text{O}_2} = 0.815 \text{ V vs. SHE}$) that a direct oxidation of NADH must be an irreversible process.¹²⁷ Therefore, a series of protein complexes and coenzymes, including cytochrome c, function as electron carriers to break down the overall process into several subprocesses where in each step the potential difference is small and the process is reversible.

The structure and the properties of cytochrome c have been studied extensively. The heme (Fe porphyrin) group resides in a protein pocket with the heme edge exposed at

Figure 6.1 The oxidative phosphorylation electron transport chain¹²⁷

the protein surface.¹²⁸ The molecular weight of cytochrome c is approx. 12500 with dimensions of 25x25x38 Å. The net charge (horse heart cytochrome c) is +9 at pH 7 due to the excess of lysines on the surface which are distributed in the vicinity of the exposed heme edge.¹²⁸ Upon receiving an electron, the native form of cytochrome c (Fe(III)) is reduced to cytochrome c (Fe(II)).

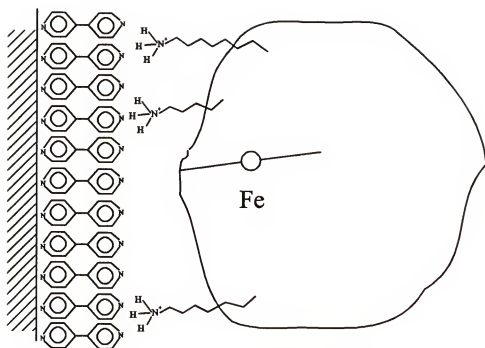
Direct electrochemistry of cytochrome c must overcome several problems. The protein redox center is largely buried in a protein molecular pocket with a small edge of the heme group exposed to the surface. As a result, the electron transfer activity is considerably suppressed. However, evidence of fast electron transfer of the protein with its physiological partner such as cytochrome c peroxidase (CcP) indicates that the "buriedness" is not prohibitive for electron transfer.⁸⁶ Instead, orientation of the two molecules, under the influence of various intermolecular interactions including electrostatic results in the hemes at the closest approach distance and appears to be the prerequisite for fast electron transfer. Compared to the 3-D interactions between cytochrome c and CcP, an electrode surface, usually a plane, serves as a poor redox partner. Another problem is irreversible adsorption and denaturation of the protein on the electrode surface. The tendency of proteins to adsorb at surfaces is extensive. Denaturation of proteins occurs as a result of the change in the balance of forces which normally favor the native conformation.¹⁷¹ At an electrode surface, a protein molecule is subject to many disruptive influences: large electric field generated across the double layer may cause protein distortion. Part of the protein surface is in contact with the electrode, and normal ionic and hydration shell may be broken, and the unfolding and reburying of

the hydrophobic interior of the protein may occur.¹⁷¹

It is therefore clear that suitable modification or functionalization of the electrode surfaces is a must to allow stable and reversible direct electrochemistry. In 1977, Yeh and Kuwana¹⁷² studied cytochrome c and first showed that a quasi-reversible cyclic voltammetric response could be obtained at a tin-doped indium oxide electrode. At about the same time Eddowes and Hill¹⁷³ demonstrated reversible cyclic voltammetry of cytochrome c at a gold electrode onto which a monolayer of the promoter 4,4'-bipyridyl was adsorbed from the same solution. Peak separations of cytochrome c were close to 60 mV and the faradaic currents changed linearly with (scan rate)^{1/2}. The half-wave potential, $E_{1/2} = 260$ mV vs. NHE, is identical to that obtained by potentiometric methods, and the response is stable, showing no marked attenuation with time.¹⁷⁴

Introduction of 4,4'-bipyridyl onto the electrode surface is significant for the investigation of the reversible voltammetry of cytochrome c. Since then, many other compounds including bis(4-pyridyl)disulfide¹⁷⁵, 4-mercaptapurine¹⁷⁶, thiodiethanoic acid¹⁷⁷, cysteine¹⁷⁸, and thioglucose¹⁷⁹ have been reported to be useful as promoters. It was proposed that 4,4'-bipyridyl allowed electron transfer to occur directly by providing functionalities at the electrode surface with which the protein could interact specifically and reversibly and, therefore, donate or accept electrons rapidly.^{170, 174} 4,4'-Bipyridyl was found to adsorb on gold in an end-on fashion; i.e., one pyridyl nitrogen coordinates to the gold surface, leaving the remaining nitrogen directed into the solution. Figure 6.2 shows a proposed schematic of the electrode-protein complex for the idealized limiting case of a planar surface. The nitrogen in solution was proposed to interact with lysines ($-NH_3^+$)

Figure 6.2 A schematic of the interactions of cytochrome c on the Au electrode modified by adsorption of 4,4'-bipyridyl. Note the hydrogen bonding between the N of the 4,4'-bipyridyl and the NH_3^+ amino acid residue on the protein surface.¹⁷⁰



cytochrome c

surrounding the exposed heme edge of cytochrome c. Hill and coworkers⁷³ further proposed that the hydrogen bonding between these lysines and the pyridyl nitrogens at the modified electrode surface stabilized a transient protein-electrode complex oriented so as to allow rapid electron transfer to and from the heme group. This proposal was supported by the observation that the electrochemical activity disappeared as the pH was lowered from 7 to 4. Presumably, the protonation of the pyridyl nitrogen leads to a loss of the hydrogen-bond acceptor capability. The interactions of the promoter on the surface and the protein are best considered to be dynamic. Protein may not remain in the same place during the lifetime of an electrode-protein complex, rather lateral diffusion across the surface may be possible.¹⁷⁰

In contrast to introducing surface functionalities by maintaining certain concentration of the promoter in solution, some electrodes, especially carbon electrodes, including glassy carbon (GC) and pyrolytic graphite (PG) can provide a naturally functionalized surface with stable oxide groups. Hill and coworkers¹⁸⁰⁻¹⁸³ examined the voltammetric response of cytochrome c at various faces and preparations of PG. Based on the orientation of the conjugated hexagonal rings of carbon atoms arranged in planes, PG's are classified as basal plane, where the planes are parallel to the solution interface, and edge plane where the planes are perpendicular to the solution interface. The cytochrome c response is very different on these two surfaces. On a polished PG electrode with the edge plane exposed, a near-reversible cyclic voltammogram was obtained. Peak currents were proportional to (scan rate)^{1/2}, demonstrating a diffusion-controlled process. By contrast, the response at the freshly cleaved PG electrode with exposed basal plane was weak,

showing only a pair of faint sigmoidal-like waves.¹⁸⁰

Again, the formation of the surface functionalities results in a different response of cytochrome c at the PG electrode with edge plane exposed (PGE) and the PG with the basal plane exposed (PGB). XPS analysis (ESCA) showed that the polished PGE was rich in surface oxides while the cleaved PGB contained only a very small number of oxides.^{182, 183} Polishing across the basal layers apparently creates a rich layer of C-O functionalities including carboxylates, alcohols, ketones and quinones¹⁸⁴ that function as natural promoter to orientate the protein as to allow fast electron transfer.

A strategy of stabilizing the protein response at the carbon electrode surface was developed by Marino and Brajter-Toth.¹⁸⁵ In this strategy, a molecular assembly of bile surfactant was constructed at the carbon electrodes by adding surfactants in solution during electroanalysis of cytochrome c to provide a continuously renewable surface. In addition, the surface was designed in such a way that electron transfer through this surfactant layer was not significantly hindered. The surfactant assembly at the electrode also prevents strong protein-graphite interactions, eliminating the irreversible adsorption and the permanent changes in the protein structure.

However, drawbacks exist in these methods. On the electrode coated with oxides, only quasi-reversible voltammetry of cytochrome c was obtained.^{181, 182} Preparation of the electrode surface becomes a critical factor for achieving well-defined behavior.¹⁸³ For methods involving bipyridyl promoters or surfactants, a significant level of the promoter or surfactant in solution must be maintained in order to achieve the monolayer coverage required for well-defined cyclic voltammetry.

In this chapter, we describe a new strategy for the direct electrochemistry of cytochrome c. Well characterized self-assembled monolayers of thioctic acid are formed on the Au surface to provide the electrode with the carboxylic functionality. The bond of the TA to Au is strong, therefore, the problem of maintaining high concentration of a free promoter in solution can be eliminated. Moreover, the thickness of the TA monolayer is fixed at the monomolecular level, ca. 8 Å, and the electron transfer rate through the film is expected not be hindered significantly at this short distance.

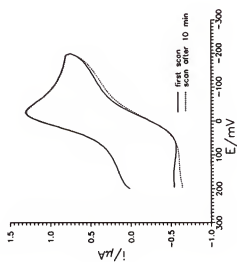
6.2 Characterization of Cytochrome c on the TA Monolayer Electrodes

Figure 6.3 shows the cyclic voltammetric response of cytochrome c (46 μM in 35 mM phosphate electrolyte) on the TA monolayer Au electrode at the scan rate of 25 mV/s at pH 7.4. The peak separation of the forward (reduction) and the reverse (oxidation) peaks, ΔE_p , was found to be 60 mV, indicating a fully reversible, one-electron transfer process. The formal potential, E^0 , calculated from the midpoint between the cathodic and the anodic peaks, was 0.01 V vs. SCE. This value agrees very well with the redox potential of cytochrome c at the physiological pH (0.01 V vs SCE) determined by potentiometric methods,¹²⁸ showing that the observed response of cytochrome c originated from the native form of cytochrome c. The peak current, i_p , is $3.8 \pm 0.2 \mu\text{A}/\text{cm}^2$, which is larger than the theoretical peak current $2.5 \mu\text{A}/\text{cm}^2$ calculated from eq. 2-2 using diffusion coefficient $D_0 = 1.1 \times 10^{-6} \text{ cm}^2/\text{s}$ ¹⁷⁴ and the electrode area $A = 0.27 \text{ cm}^2$, suggesting that some surface interactions are contributing to the cytochrome c current at the TA monolayer electrode.

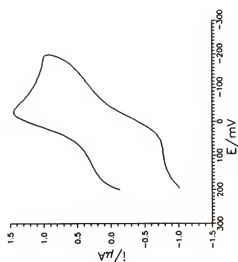
Figure 6.3

(A) Cyclic voltammetric response of 46 μM cytochrome c in 35 mM phosphate at pH 7.4 on the a freshly prepared TA monolayer electrode. (B) Cyclic voltammogram of 46 μM cytochrome c in 35 mM phosphate at pH 7.4 on a TA monolayer electrode redipped in the 0.1 % TA ethanol solution for 10 min. See text for detail. Scan rate is 25 mV/s. The electrode area is 0.27 cm^2 . (C) A plot of $\log i_p$ vs $\log v$ in 46 μM cytochrome c in 35 mM phosphate at pH 7.4. Scan rate range: 10–100 mV/s. The slope of the line is 0.66.

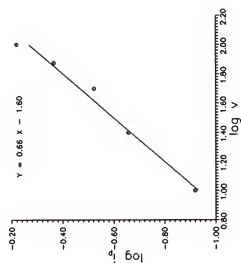
(A)



(B)



(C)



Cyclic voltammetric response of cytochrome c on the TA monolayer electrode is stable and reproducible at the scan rate of 25 mV/s (Figure 6.3A). No significant change in response was observed after 10 min (3 cycles). However, a decrease in the peak current magnitude and an increase in the peak potential separation was observed when the electrode was continuously scanned between 200 mV and -200 mV for 5 min at 25 mV/s scan rate. Immersing the electrode back for 10 min in the 0.1 % TA/ethanol solution from which the monolayer was assembled reestablished the reversible behavior of cytochrome c (Figure 6.3B). The background current in Figure 6.3B is slightly different from that in Figure 6.3A, indicating that there might be some minor structural difference in the two films.

In order to obtain an insight into the possible adsorption of cytochrome c on the monolayer and in order to understand its role in the resulting current response of cytochrome c on the TA monolayer electrode, cyclic voltammetry at different scan rates was employed. Figure 6.3C shows a plot of $\log i_p$ vs \log scan rate v for 46 μM cytochrome c in 35 mM phosphate at pH 7.4. A linear relationship for the current in the scan rate range between 10 mV/s to 100 mV/s was observed. The slope, which is 0.5 for the diffusion controlled process (eq. 2-2) and 1.0 for the adsorption controlled process (eq. 2-4), was found to be 0.66, confirming that there is some adsorption of cytochrome c on the TA monolayer electrode in 35 mM phosphate buffer. This result is consistent with the peak current measurements shown above.

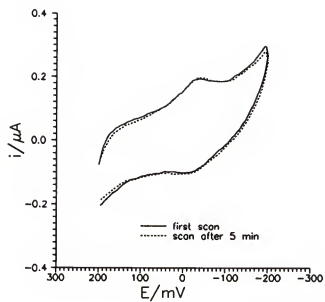
In order to further investigate the behavior of cytochrome c, the electrode used previously in cytochrome c solution was subsequently transferred to a buffer solution

which did not contain free cytochrome c. Figure 6.4A shows the cyclic voltammograms of cytochrome c in 10 mM phosphate buffer (pH 7.4) at scan rate of 10 mV/s. Symmetric voltammetric response was obtained with the peak potential separation $\Delta E_p = 0$ mV. A plot of $\log i_p$ vs $\log v$ gives a slope of 1.05, which clearly points to an adsorption process involved. The response is stable and reproducible in 10 mM phosphate (Figure 6.4A), indicating that the adsorption of cytochrome c on the TA monolayer is irreversible in this solution.

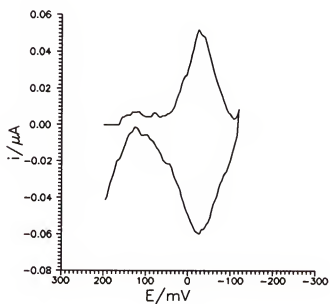
The well-defined cyclic voltammetric response of cytochrome c on the TA monolayer electrodes reflects the ability of cytochrome c to interact favorably with the TA monolayer. Poulos and coworkers¹⁸⁶ reported the detailed molecular organization between cytochrome c and its biological partner cytochrome c peroxidase (CcP) and explained the enzyme-substrate interaction in terms of charge matching, spatial fitting and hydrogen bonding. It is shown that a ring of lysines, which are positively charged at physiological pH, extends away from the surface of cytochrome c to form salt bridges with a group of complimentary negatively charged carboxylate groups of aspartate residues in CcP. The electrostatic interaction draws the two molecules together so that the two heme groups lie in parallel, thus facilitate electron transfer. The TA monolayer bears resemblance to CcP with respect to its ability to bind cytochrome c. The negative charge of the TA monolayers develops as a result of the dissociation of the carboxylic headgroup at pH 7.4 which can interact with the positively charged lysine residues on the protein surface. Such interactions are essential to the reversible response of cytochrome c since the lysine groups reside around the edge of the heme group so that the interactions result

Figure 6.4 (A) Cyclic voltammetric response of adsorbed cytochrome c (from 46 μM cytochrome solution in 35 mM phosphate) on the TA monolayer electrode in 10 mM phosphate (pH 7.4). The electrode area is 0.27 cm^2 .
(B) Background subtracted CV for (A).

(A)



(B)



in a favorable orientation of the cytochrome c molecule at the monolayer with the heme group exposed toward the electrode. Therefore, the electron transfer distance can be minimized.

Different from the weak adsorption of cytochrome c on the promoters such as 4,4'-bipyridyl, cytochrome c adsorption on the TA monolayer is irreversible. Therefore, the electron transfer mechanism involving fast adsorption/desorption of the protein at the electrode surface proposed for the bipyridyl promoter systems is no longer valid on the TA monolayer electrode. However, since the diffusion influenced voltammetry is observed on the TA monolayer despite the irreversible protein adsorption, it clearly suggests that the electrons are transferred between the electrode and the protein molecules in bulk solution. Presumably, such transfer proceeds indirectly through a layer of adsorbed protein via rapid rotation and consequent translocation of the redox center, or through mediation of a relay system of the hemes in adsorbed cytochrome c, as suggested by Armstrong for oxide coated electrodes.¹²⁸ The self-exchange rate constant for cytochrome c is relatively fast (ca. $1.2 \times 10^3 \text{ M}^{-1} \text{ s}^{-1}$),⁸⁶ this value can become significantly larger (ca. $10^8 \text{ M}^{-1} \text{ s}^{-1}$) when cytochrome c molecules are arranged in the heme-heme self-exchange pattern.⁸⁶ The mediation is anticipated for the electron transfer on the TA monolayer where the protein/surface interaction is dynamic.

It is worth noting that in order to observe a sharp and reversible voltammetric response of cytochrome c, the protein-TA electrode interactions must occur in such a manner that they are intimate enough to accomplish fast electron transfer. In the case of the irreversible protein adsorption, the native form of the protein must be preserved. The

ability of the TA monolayer to preserve the native form of cytochrome c is evidenced by the fact that the observed formal potential of cytochrome c is identical to that at physiological conditions. In a practical point of view, the modification of the TA monolayer on the electrode surface prevents protein denaturation, and the problems of electrode fouling due to the irreversible adsorption of the denatured proteins can be eliminated.

For comparison, the voltammetric response of cytochrome c on the bare Au electrodes was studied as well. In this work, two gold substrates were polycrystalline gold rod electrodes sealed in Teflon, and a gold film electrode prepared by vacuum deposition of gold on silicon wafers. Prior to use, the rod electrode was polished on a polishing cloth using 0.1 μm gamma alumina slurry, sonicated in deionized water, and scanned between -100 mV and 1200 mV in 1 M H_2SO_4 for 5 min to remove surface impurities, as described by Oesch and Janata.¹⁸⁷ Vacuum deposited gold electrode was cleaned in a piranha solution and rinsed extensively with a large volume of deionized water before use.

On a rod electrode, cytochrome c does not show a voltammetric response, as reported by Hill and coworkers under similar conditions,^{173, 174} pointing to a possible fast passivation of the electrode by possible irreversible adsorption of cytochrome c or the solution impurities. However, on a vacuum deposited Au electrode, voltammetric response of cytochrome c (46 μM) was observed in 35 mM phosphate at pH 7.4. Figure 6.5 shows the results for cytochrome c at different scans. Table 6.1 summarizes the results on both the TA monolayer electrodes and the vacuum deposited Au electrodes.

From Table 6.1, the cathodic and anodic peak separation, ΔE_p , is 265 mV on the

Figure 6.5 Voltammetric response of 46 μM cytochrome c in 35 mM phosphate at pH 7.4 on a bare Au electrode vacuum deposited on a silicon wafer. Scan rate is 25 mV/s. The electrode area is 0.21 cm^2 . Solid line (-): response for the first run. Dash line (- - -): for the second run (5 min later). Dotted line (...): for the third run (10 min later). During the three runs, the electrode stayed in the cytochrome c solution.

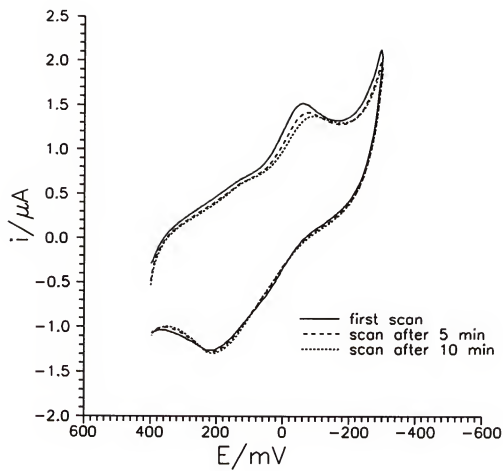


Table 6.1 Cyclic voltammetric results of cytochrome c

Electrode	ΔE_p (mV)	$E_{p,c}$ (mV vs. SCE)	i_p^a ($\mu\text{A}/\text{cm}^2$)
TA monolayer/Au	60	-22	3.8 ± 0.2
restored TA/Au	61	-23	3.9
bare Au, first run ^b	265	-55	2.3
bare Au, second run ^b	285	-75	2.1
bare Au, third run ^b	305	-95	1.8

^a The concentration of cytochrome c is 46 μM in 35 mM phosphate solution at pH 7.4, the scan rate is 25 mV/s. The theoretical peak current, i_p , is 2.5 $\mu\text{A}/\text{cm}^2$ using $D_0 = 1.1 \times 10^{-6} \text{ cm}^2/\text{s}$. ^c vacuum deposited Au electrode

bare electrode in the first cycle, indicating that an irreversible electrochemical response was obtained compared to the reversible behavior observed on the monolayer electrode. Cathodic peak current, i_p , is $2.3 \mu\text{A}/\text{cm}^2$, which is much smaller than that at the monolayer electrode. The response observed on the bare electrode depends on the scan numbers. For the third scan, the current declines by ca. 20% compared to that in the first scan, and the peak potential $E_{p,c}$ shifts ca. 40 mV cathodically.

The irreversible response of cytochrome c on the bare electrodes may reflect strong interactions between the protein and the bare Au electrode that may result in protein conformation change. Compared to the shut off response on the rod electrode, limited (irreversible) voltammetry of cytochrome c on the vacuum deposited Au electrode may be a result of high wettability of the vacuum deposited Au, which has been documented by several authors using contact angle experiments.⁴⁴⁻⁴⁶ Hawkrige and coworkers pointed out that the formation of a hydration layer of H_2O or OH on Au and Pt was responsible for the observed electrochemistry of cytochrome c.¹⁸⁸ However, since Au or Pt has low affinity for aqua-adsorbates as compared to the hydrophobic components of the proteins, the surface soon becomes coated with non-native forms of cytochrome c, and the native voltammetric response of the protein dies away.¹⁸⁸ Hawkrige and coworkers reported response of cytochrome c on the polycrystalline Au electrode which was not observed in our study. This may be ascribed to the different procedures used in pretreatment of the electrodes and solution/cell clearness. It is well documented that the electrochemical behavior of cytochrome c on the bare electrodes is strongly dependent on the electrode pretreatment procedure which may result in varied surface wettability.

6.3 Electrochemical Behavior of Surface Bound Cytochrome c

As indicated in Figure 6.4A, irreversible adsorption of cytochrome c occurs on the TA monolayer electrodes. Since the current in Figure 6.4A results solely from the adsorbed protein, it is therefore possible to calculate the surface coverage by integrating the area defined by the current. Figure 6.4B shows a background subtracted CV of the adsorbed cytochrome c. The current background used for subtraction is the response baseline. From Figure 6.4B, the surface coverage is calculated to be 1.51×10^{-11} mol/cm², which is equivalent to a theoretical monolayer coverage considering the area of a cytochrome c molecule as 25x38 Å. This value is also consistent with those obtained on the 16-mercaptohexadecanoic acid monolayer (1.7×10^{-11} mol/cm²)¹⁸⁹ and the tin oxide electrodes ($1.3\text{--}1.5 \times 10^{-11}$ mol/cm²)¹⁹⁰ under similar conditions (pH 7 and 10 mM phosphate). The total width at half height of cathodic wave is 91 mV, indicating characteristics of a reversible adsorption process.⁷⁹

The peak potential, which is also the formal potential, is -0.03 V vs. SCE. Compared to the value obtained from Figure 6.3 (0.01 V vs. SCE) for 46 μM cytochrome c in 35 mM phosphate at pH 7.4, the formal potential of cytochrome c undergoes a ca. 40 mV negative shift upon adsorption on the TA monolayer electrode. Similar negative shifts have been reported for cytochrome c binding to phosvitin (20-30 mV),¹⁹¹ cytochrome oxidase and reductase (35-40 mV),¹⁹² tin oxide (20-25 mV),¹⁹⁰ 16-mercapto-hexadecanoic acid monolayer (45 mV)¹⁸⁹ and mitochondrial membranes (50-60 mV).¹⁹³ In all of these cases, negative formal potential shifts ranging in magnitude from 20 to 50 mV were ascribed to that the oxidized form (ferricytochrome c) binding more strongly than the

reduced form (ferrocycytochrome c), pointing to a substantial electrostatic contribution to the binding. The membranous lipid systems exhibit larger negative shifts, probably reflecting additional nonelectrostatic binding components in the case of lipid membranes, i.e. hydrophobic interactions.¹⁹³

The electron transfer rate constant for adsorbed cytochrome c was studied. At the low scan rate (10 mV/s), the peak potential separation is 0 mV, indicating a reversible process where kinetic factors have no effect on the response. With the increase in scan rate, the time scale of the experiment is getting smaller and can become comparable to that of the electron transfer process. Therefore, kinetic influence on the response may be detected. The peak split starts to show up when the scan rate is increased to 50 mV/s, and is 51 mV when the scan rate is 100 mV/s. Using Laviron's equation (eq 2-7 and 2-8) and assuming $\alpha = 0.5$, the electron transfer rate constant is approximated to be 2.4 s^{-1} .

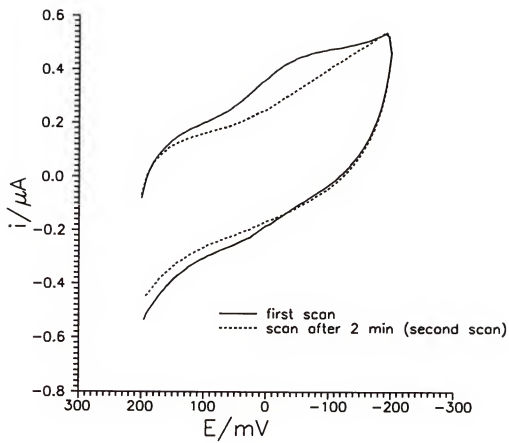
The rate constant (2.4 s^{-1}) obtained in this work is comparable to that obtained by Hill and coworkers (50 s^{-1}).¹⁷⁰ However, it differs from that reported by Bowden and coworkers¹⁸⁹ who have reported that a reversible voltammetry of diffusion-free cytochrome c was observed up to 200 mV/s scan rate on the 6-mercaptotaxanoic acid monolayer electrodes in pH 7, 10 mM phosphate. The different observation may stem from the different impact of the monolayer structure on response. In Bowden's study, a straight 6-mercaptotaxanoic acid molecule was used to form monolayers which may result in a more compact monolayer. Presumably, a compact monolayer may allow electron tunneling to take place through the film, while on a porous membrane ion partitioning occurs extensively and electron transfer may proceed in a different mechanism.

The effect of the solution properties on the response of cytochrome c on the TA monolayer electrode was investigated to further reveal the characteristics of the irreversible adsorption of cytochrome c on the monolayer. We focussed on the effect of the electrolyte concentration, because it is known to have a significant effect on the electrostatic interactions.^{128, 189,190} In addition, the electrolyte concentration can be experimentally controlled, and the measurement conditions can thus be optimized.

In our early effort where high electrolyte concentrations (~0.1-0.5 M phosphate) were used, no response of cytochrome c was observed on the TA monolayer electrode, though a well-defined voltammetry of cytochrome c has been established at this electrolyte concentration range in the presence of promoters.¹⁷³⁻¹⁷⁹ Apparently, the electrostatic interactions between the COOH group and cytochrome c are more sensitive to the influence of the electrolyte concentration than the interaction of 4,4'-bipyridyl with cytochrome c in 0.1 M NaClO₄ or 0.1 M NaCl supporting electrolyte at pH 7.¹⁷³⁻¹⁷⁹

Figure 6.6 shows the voltammetric results at the TA monolayer electrode with the adsorbed cytochrome c in a 0.1 M phosphate solution at pH 7.4. The experimental procedure and conditions are the same as those in Figure 6.4 except a 0.1 M phosphate solution is used. The response current of cytochrome c is much smaller in 0.1 M phosphate than in 10 mM phosphate. The integral of the adsorption current gives a surface coverage of 8.60×10^{-12} mol/cm² as compared to 1.51×10^{-11} mol/cm² in 10 mM phosphate, indicating that a great deal of the adsorbed cytochrome c is desorbed from the surface. In the second run, no cytochrome c response can be detected. Similar results have been reported by Bowden and coworkers that on the 16-mercaptohexadecanoic acid

Figure 6.6 Cyclic voltammetric response of adsorbed cytochrome c (from 46 μM cytochrome c solution in 35 mM phosphate) on the TA monolayer electrode in 0.1 M phosphate (pH 7.4). Scan rate is 25 mV/s.



monolayer.¹⁸⁹ Varying electrolyte concentration between 10 mM and 38 mM phosphate had no apparent effect on the cyclic voltammetry of the adsorbed cytochrome c, while a higher concentrated electrolyte (ca. 1 M) results in a complete desorption of the adsorbed cytochrome c layer; on a tin oxide electrode, use of the electrolyte concentration larger than 100 mM results in a substantial loss of the adsorbed cytochrome c.¹⁹⁰ The results obtained here confirm that the interactions of cytochrome c on the TA monolayer are predominantly electrostatic.

6.4 In Situ Chemical Derivatization of the TA Monolayers

Biosensors are devices employing biochemical molecular recognition properties as the basis for a selective bioanalysis. One of the most popular configurations of a biosensor is that of the amperometric enzyme electrode. A range of amperometric enzyme electrodes with non-physiological redox-active mediator molecules serving as electron donors and acceptors for redox enzymes have been reported.¹⁰⁴⁻¹¹⁶ For instance, in the case of detection of glucose using glucose oxidase, mediator such as ferrocene immobilized on the electrode surface is employed.^{117,118} The electrogenerated ferricinium ion acts as oxidant for the reduced glucose oxidase. Once the ferricinium ion has been reduced, it is reoxidized at the electrode surface by polarizing the electrode and allowing current to flow. Use of mediators in biosensors allows detection of biological analytes at the mild electrode potential that can electrochemically oxidize or reduce the mediator, therefore, an overpotential for direct electron transfer between the electrode and the enzyme can be avoided.

However, it has been known that the mediated response of the electrode is not only a function of the intrinsic reactivity of the mediator but also of the properties of the supporting materials such as the film permeability, in which the mediator is immobilized.¹⁰² On enzyme electrodes, the redox proteins are subject to various interactions from the matrix, including hydrophobic and electrostatic interactions. The effects of these interaction on response are difficult to evaluate since the sensor structure is usually complicated and the matrix morphology is often poorly defined.

We have focussed our interest on the development of a mediated biosensor with a well-defined interface structure in order to obtain a clear picture of the environment inside the biosensor matrix, including the orientation of the enzyme so as to explore the consequence of such an orientation on the electrochemical response, and ultimately, optimize the sensor performance. The TA monolayer electrodes, capable of providing a well-defined hydrophilic carboxylic interface and bearing desirable electrochemical characteristics such as high sensitivity and selectivity as discussed previously, appear to be a good candidate for such a design.

A strategy for designing a sensor by covalently linking ferrocene redox centers to the TA monolayers is illustrated in Figure 1.15. Since ferrocene moiety is hydrophobic, a ferrocene derivative (N-(2-aminoethyl)ferrocylacetamide) with an extended chain was synthesized as the immobilization precursor. Formation of an amide link between the amine end of the immobilization precursor and the carboxylic headgroup of the TA monolayer provides a separation of the ferrocene moiety from the hydrophilic carboxylic surface of the monolayer by ca. 5-6 Å. Therefore, the existing ordered structure of the TA

monolayer was expected to be preserved after immobilization of ferrocene on the monolayer (Chapter 1).

Before covalently immobilizing the Fc precursor onto the TA monolayer, electrochemical characterization of the free precursor in 0.1 M phosphate (pH 7.4) was conducted on the TA monolayer electrode. Figure 6.7A shows the voltammetric results. The peak separation, ΔE_p , is 62 mV, indicating a fast electrochemical process. The formal potential, calculated from the midpoints of the cathodic and the anodic peaks, is 0.20 V vs. SCE, compared to a formal potential of 0.24 V vs. SCE for a similar compound 2-aminoethylferrocene in 0.1 M phosphate.¹¹⁶ A plot of $\log i_p$ vs $\log v$ in the scan rate range of 75 - 500 mV/s (Figure 6.7B) reveals a slope of 0.61, indicating that both adsorption and diffusion contribute to the response of the Fc at the TA electrode surface.

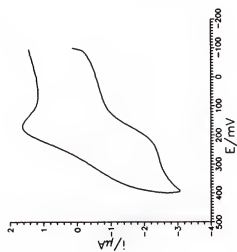
Covalent linking between the amine end of the immobilization precursor and the carboxylic headgroup of the TA monolayer was pursued by forming amide bond under the activation of DEC (1,3-(dimethylamino)propyl-3-ethylcarbodiimide hydrochloride), as described in the Experimental Section and in the scheme in Figure 1.15. Figure 6.7C shows the CV of ferrocene in 0.1 M HClO₄ at pH 1.5 after the covalent immobilization procedure was completed at the TA monolayer electrode. The current for the surface bound ferrocene is very small, indicating that the yield of the surface reaction must be extremely low.

DEC, or more generally a carbodiimide, is a very effective coupling reagent widely used in the synthesis of peptides due to its ability to activate the carboxylic acid group to form amide linkage between two amino acids under mild conditions (in aqueous solution

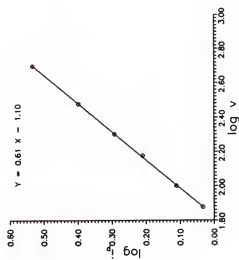
Figure 6.7

(A) Cyclic voltammogram of 0.5 mM N-(2-aminoethyl) ferrocylacetamide in 0.1 M phosphate at pH 7.4 on the TA monolayer electrode. Scan rate is 100 mV/s. The electrode area is 0.12 cm². (B) A plot of log i_p vs. log v in the scan rate range of 75 - 500 mV/s for 0.5 mM N-(2-aminoethyl) ferrocylacetamide on the TA monolayer electrode. (C) Cyclic voltammogram of the covalently bound ferrocene derivatized TA monolayer electrode in 0.1 M HClO₄ at pH 1.5. The electrode area is 0.18 cm².

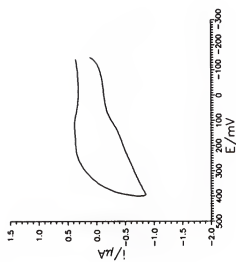
(A)



(B)



(C)



and at the room temperature).¹²² Modifications of the electrodes or enzymes via a DEC catalyzed process have been reported.^{115, 117} Osa and coworkers reported the covalent binding of 2-aminoethylferrocene in the polyacrylic acid film coated on a graphite electrode through carbodiimide.¹¹⁶ Heller and coworkers used carbodiimide to covalently bind ferrocylcarboxylic acid to lysine amines of glucose oxidase to introduce electrical relays onto the enzymes.¹¹⁷⁻¹¹⁹ Recently, Willner and coworkers immobilized, through DEC activation, a redox protein (malic enzyme) on a thin film of cysteamine, which was derivatized with carboxylic substituted quinone headgroup, on a gold foil electrode.¹⁶⁹ Compared to those applications of DEC to form covalent linkages on rough electrode surfaces such as polycrystalline Au and graphite, the TA monolayer has a significantly different properties. The TA monolayer bears relatively well-ordered structure so that the steric effects in the surface chemical reaction must be stronger. The activation of the carboxylic group by DEC, a key step to form the covalent bond with the immobilization precursor, may be less effective on the TA monolayer for two reasons: (1) access of the bulky carbodiimide to the surface carboxylic groups to form intermediate *o*-acylisourea (Figure 1.15) may be hindered; (2) nucleophilic substitution of the activated carbonyl by the amine from the precursor may be difficult due to the steric hinderance. Heller reported that binding of ferrocylcarboxylic acid to glucose oxidase could not be achieved unless 2 M urea was added to the solution to unfold the enzyme to eliminate the steric hindering effect on access of DEC to the protein.¹⁰¹ This observation is consistent with the results for the DEC activated immobilization of Fc compound on the TA monolayer. Thus, it can

be concluded that an *in situ* reaction on the well ordered monolayer such as the thioctic acid monolayer using DEC may be not effective.

6.5 Conclusions

Redox protein cytochrome c has been used as a probe to investigate the electrochemical behavior of large biological molecules on the TA monolayer. The fast, reversible response of cytochrome c observed in this study confirms the ability of the TA monolayer to provide suitable environment for the favorable interactions between the protein and the monolayer which result in the necessary molecular orientation of the protein as to allow fast electron transfer. The protein/TA monolayer interactions are predominantly electrostatic and subject to the influence of the electrolyte concentration. In contrast to the response of cytochrome c on the bare electrode, cytochrome c exhibits native redox properties such as physiological formal potential and fast electron transfer on the TA monolayer electrode.

Derivatization of the TA monolayers with fast redox aimed to achieve electrical communication between the biological analyte and the electrode coupled with ferrocene mediator was attempted. Preliminary results indicate that *in situ* chemical derivatization of the ordered TA monolayer is not effective, possibly due to the strong steric effects at the well-ordered monolayer. New approaches, focused primarily on *ex situ* synthesis, will be discussed in Chapter 7.

CHAPTER 7

SUMMARY AND FUTURE WORK

The objective of this research was to develop strategies for design and fabrication of molecular assemblies with well-defined structure in order to achieve controllable electrochemical properties on electrodes; to determine the effect of solution properties including pH, electrolyte composition and concentration on the assembly microstructure and consequently on the electrochemical response; and to elucidate factors related to species' structure, electrode dimensions and interface hydrophobicity in governing the response on the monolayers. The ability of the monolayer electrodes for providing favorable protein/interface interactions as to render direct electrochemistry of proteins is illustrated, and the perspective of the monolayer electrodes in the evolution of new biosensors is discussed.

Well-defined molecular assembly on the electrodes was obtained through self-assembly of thioctic acid monolayer on atomically smooth gold substrates. Macroscopic characterization of the self-assembled monolayers was achieved by capacitance measurements. Based on the molecular structure, the thickness of the TA film was estimated to be ca. 8 Å. The dielectric constant of the film was found to be higher than of a polyethylene membrane and also higher than of a long chain alkylthiol monolayer, indicating that penetration of solvent/ions into the films must occur. As a result, the TA monolayer displays high ionic permeability and functions like a conductive membrane.

High sensitivity was obtained on the TA monolayer as a result of the permeability. Chemical selectivity of the TA monolayer was achieved as a result of the electrostatic interactions between the interface and the probes. The dissociation of carboxylic headgroups produces negative charge on the TA monolayer that favors the response of positively charged molecules while suppressing the negatively charged ones.

Qualitative analysis of the effect of the electrolyte properties on the electrochemical behavior of the TA monolayer electrodes was achieved by measuring the voltammetric response of the redox probes as a function of the electrolyte concentration and composition. At higher electrolyte concentrations, potential drop across the diffuse layer decreases. Under the same conditions of high electrolyte concentration, penetration of the films by solvent and possibly the electrolyte occurs extensively. This further contributes to the decrease in film resistance, and the potential drop across the membrane is minimized, which results in fast kinetics of the probes.

A comparison of the voltammetric results of the electroactive species on the TA monolayers formed at different substrates suggests that the substrate quality is critical to the observed sensitivity and selectivity of the monolayer electrodes. At rough surfaces, the ability of the monolayer to expel species with opposite charge declines dramatically, presumably due to the disrupted monolayer structure on the rough substrates.

A strategy was developed for investigation of the biologically important molecules such as catecholamines and quinones on the monolayer electrodes. Varied surface hydrophobicity was obtained by conveniently incorporating different fractions of the hydrophobic hexanethiol into the TA monolayer. Capacitance measurements revealed that

film's capacitance declined when alkylthiols coadsorbed into the monolayer, pointing to an increase in the potential drop across the film. On the hydrophilic TA monolayer electrode, the electrochemical detection of positively charged dopamine was possible while the negatively charged DOPAC was excluded completely, indicating the selectivity of the monolayer electrode toward positively charged biological molecules was maintained. On the hydrophobic monolayer electrodes, the kinetics of all probes, no matter if hydrophilic or hydrophobic, became significantly slower as a result of the increase in film resistance. Compared to the diminishing response of dopamine on the hydrophobic monolayers, uncharged quinone continued to show a response on these films, reflecting a combined effect of probe neutrality, structure and possibly reaction pathway on response. The results clearly suggest that the TA monolayers with hydrophilic features should be the choice for the selective detection, though an ideal film for the latter should be one with a combined features of hydrophobicity and low potential drop, which has not yet been built.

Ultramicroelectrodes (UME) modified with the TA monolayer were characterized to reveal the selectivity and sensitivity of the TA monolayers on these electrodes with the micrometer dimensions. A strategy is described for obtaining a high quality substrate surface of micrometer dimensions on which high quality self-assembled monolayers, comparable in quality to those formed on vacuum deposited Au electrodes were obtained. Using this strategy, sensitivity and selectivity on the TA monolayer ultramicroelectrodes comparable to that obtained on the TA monolayers prepared on vacuum deposited Au on silicon wafers was observed. Control of the solution pH provides a capability to fine tune the surface charge density which consequently results in selectivity of the film, as observed

at large electrodes. However, the extent to which the pH changes affect the response, and the effect of the electrolyte composition on response, become more dramatic at UMEs. The electrochemical results of the redox probes on the TA UMEs were analyzed and used to demonstrate the ability of the UMEs for revealing structural information about the ultrathin film.

By taking the advantages of high current sensitivity and electrochemical selectivity as a function of the solution pH on the TA UME, amperometric pH sensing using Fe(CN)_6^{3-} as a probe was demonstrated in this work. With this method, the ionization constant of the thioctic acid in a monolayer was determined, and the results are comparable to the literature values.

The last part of this dissertation focuses on the ability of the TA monolayer electrodes in providing preferential interactions with large biological molecules, which could possibly lead to sensitive detection of these molecules. Direct electrochemistry of cytochrome c on the TA monolayer electrode obtained in this work clearly demonstrates that the TA monolayer is an ideal surface for the investigation of this protein. The carboxylic headgroup provides a negatively charged, hydrophilic interface which bears resemblance to that of its biological partner such as CcP. Therefore, the protein molecules can be oriented and the protein/interface electron transfer precursor may be stabilized on the monolayer. As a result, fast electron transfer between the protein and the electrode can be obtained. In addition, the results for cytochrome c support the conclusion that the use of the TA monolayer can prevent protein denaturation on the electrode, pointing to the perspective of the TA monolayers for biosensor design involving proteins.

The perspective of the TA monolayer electrodes for evolution of new biosensors is preliminarily explored. The strategy used here was to introduce fast redox centers, i.e. ferrocene onto the monolayer surface. Electron mediation is expected to take place at the interface to enhance the sensitivity of detection. However, as presented in Chapter 6, *in situ* chemical derivatization of an ordered monolayer is tremendously complicated, and the proposed immobilization has not been achieved in an expected scale. As a result, the immediate future work should be focused on developing more efficient route for immobilizing redox centers onto the monolayer. This may be pursued by developing more effective reactions on the monolayer surface to overcome the steric effect on surface immobilization. An alternative choice is to conduct the synthesis of the adsorbent with designed redox center before hand *ex situ*, and fabricate the monolayer assembly by means of coadsorption of the adsorbent and the thioctic acid. Since this method presents flexibility of changing surface coverage of the redox centers, the resulted monolayer can thus be optimized to obtain optimum mediation effects. In addition, redox centers can be attached to the TA monolayer by hydrocarbon chains of different length, therefore, the optimized effect for mediated response may be achieved for proteins with different size.

REFERENCE LIST

1. Murray, R.W. In *Electroanalytical Chemistry*, Bard, A.J., Ed.; Marcel Dekker: New York, 1984, Vol. 13, pp. 191-368
2. Murray, R.W.; Ewing, A.G.; Durst, R.A. *Anal. Chem.* **1987**, *59*, 379A
3. Murray, R.W. *Molecular Design of Electrode Surfaces, Techniques of Chemistry Series* Vol. 22; John Wiley & Sons: New York, 1992
4. Edmonds, T.E. *Chemical Sensors*; Blackie & Son: Glasgow, 1988
5. Lane, R.F.; Hubbard, A.T. *J. Phys. Chem.* **1973**, *77*, 1401
6. Moses, P.R.; Wier, L.; Murray, R.W. *Anal. Chem.* **1975**, *47*, 1882
7. Watkins, B.J.; Behling, J.R.; Kariv, E.; Miller, L.L. *J. Am. Chem. Soc.* **1975**, *97*, 3549
8. Blaedel, W.G.; Jenkins, R.A. *Anal. Chem.* **1975**, *47*, 1337
9. Facci, J.S. In *Techniques of Chemistry Series*, Vol. 22; John Wiley & Sons: New York, 1992, p 119
10. Rocklin, R.D.; Murray, R.W. *J. Electroanal. Chem.* **1979**, *100*, 271
11. Tse, D.C.-S.; Kuwana, T. *Anal. Chem.* **1978**, *50*, 1315
12. Collman, J.P.; Denisevich, P.; Konai, Y.; Morrocco, M.; Koval, C.; Anson, F.C. *J. Am. Chem. Soc.* **1980**, *102*, 6027
13. Kanazawa, K.K.; Diaz, A.F.; Geiss, R.H.; Gill, W.D.; Kuak, J.F.; Logan, J.A.; Robolt, J.F.; Street, G.B. *J. Chem. Soc. Chem. Comm.* **1979**, 854
14. Schneider, J.R.; Murray, R.W. *Anal. Chem.* **1982**, *54*, 1508
15. Lau, A.N.K.; Miller, L.L. *J. Am. Chem. Soc.* **1983**, *105*, 5271
16. Chao, S.; Robbins, J.L.; Wrighton, M.S. *J. Am. Chem. Soc.* **1983**, *105*, 181

17. Pickup, P.G.; Kutner, W.; Leidner, C.R.; Murray, R.W. *J. Am. Chem. Soc.* **1984**, *106*, 1991
18. Kittlesen, G.P.; White, H.S.; Wrighton, M.S. *J. Am. Chem. Soc.* **1985**, *107*, 7373
19. Rubinstein, I. *J. Electroanal. Chem.* **1985**, *195*, 431
20. Whitesides, G.R.; Mathias, J.P.; Seto, C.T.; *Science*, **1991**, *254*, 1312
21. White, H.S.; Leddy, J.; Bard, A.J. *J. Am. Chem. Soc.* **1982**, *104*, 4811
22. Martin, C.R.; Rubinstein, I.; Bard, A.J. *J. Am. Chem. Soc.* **1982**, *104*, 4817
23. Buttry, D.A.; Anson, F.C. *J. Am. Chem. Soc.* **1983**, *105*, 686
24. Samec, Z.; Trojanek, A.; Samcova, E. *J. Phys. Chem.* **1994**, *98*, 6352
25. Witkowski, A.; Brajter-Toth, A.F. *Anal. Chem.* **1992**, *64*, 635
26. Hsueh, C.C.; Brajter-Toth, A.F. *Anal. Chem.* **1994**, *66*, 2458
27. Lenhard, J.R.; Murray, R.W. *J. Electroanal. Chem.* **1977**, *78*, 195
28. Evans, J.F.; Kuwana, T. *Anal. Chem.* **1977**, *49*, 1632
29. Lennox, J.C.; Murray, R.W. *J. Electroanal. Chem.* **1977**, *78*, 395
30. Koval, C.A.; Anson, F.C. *Anal. Chem.* **1978**, *50*, 223
31. Yacynych, A.M.; Kuwana, T. *Anal. chem.* **1978**, *50*, 640
32. Elliott, C.M.; Murray, R.W. *Anal. Chem.* **1976**, *48*, 1247
33. Murray, R.W. *Acc. Chem. Res.* **1980**, *13*, 135
34. Ulman, A. *An Introduction to Ultrathin Organic Films From Langmuir-Blodgett to Self-Assembly*; Academic Press: San Diego, 1991
35. Zhang, X.; Bard, A.J. *J. Am. Chem. Soc.* **1989**, *111*, 8098
36. Bilewicz, R.; Majda, M. *J. Am. Chem. Soc.* **1991**, *113*, 5464
37. Bilewicz, R.; Majda, M. *Langmuir* **1991**, *7*, 2794

38. Nuzzo, R.G.; Allara, D.L. *J. Am. Chem. Soc.* **1983**, *105*, 4481
39. Nuzzo, R.G.; Zegarski, B.R.; Dubois, L.H. *J. Am. Chem. Soc.* **1987**, *109*, 733
40. Nuzzo, R.G.; Fusco, F.A.; Allara, D.L. *J. Am. Chem. Soc.* **1987**, *109*, 2358
41. Dubois, L.H.; Zegarski, B.R.; Nuzzo, R.G. *J. Am. Chem. Soc.* , **1990**, *112*, 570
42. Miller, C.; Cuendet, P.; Gratzel, M. *J. Phys. Chem.* **1991**, *95*, 877
43. Troughton, E.B.; Bain, C.D.; Whitesides, G.M.; Nuzzo, R.G.; Allara, D.L.; Porter, M.D. *Langmuir*, **1988**, *4*, 365
44. Bain, C.D.; Whitesides, G.M. *Langmuir* **1989**, *5*, 1370
45. Bain, C.D.; Troughton, E.B.; Tao, Y.T.; Evall, J.; Whitesides, G.M.; Nuzzo, R.G. *J. Am. Chem. Soc.* **1989**, *111*, 321
46. Whitesides, G.M.; Laibinis, P.E. *Langmuir*, **1990**, *6*, 87
47. Porter, M.D.; Bright, T.B.; Allara, D.L.; Chidsey, C.E.O. *J. Am. Chem. Soc.* **1987**, *109*, 3559
48. Chidsey, C.E.O.; Loiacano, D.N. *Langmuir*, **1990**, *6*, 682
49. Chidsey, C.E.O.; Bertozzi, C.R.; Putvinski, T.M.; Muijsce, A.M. *J. Am. Chem. Soc.* **1990**, *112*, 4301
50. Finklea, H.O.; Avery, S.; Lynch, M.; Furttsch, T. *Langmuir*, **1987**, *3*, 409
51. Sun, L.; Johnson, B.; Wade, T.; Crooks, R.M. *J. Phys. Chem.* **1990**, *94*, 8869
52. Bryant, M.A.; Pemberton, J.E. *J. Am. Chem. Soc.* **1991**, *113*, 8284
53. Allara, D.L.; Nuzzo, R.G. *Langmuir*, **1985**, *1*, 45
54. Bain, C.D.; Whitesides, G.M. *Angew. Chem. Int. Ed. Engl.* **1989**, *28*, 506
55. Folkers, J.P.; Zerkowski, J.A.; Laibinis, P.F.; Seto, C.T.; Whitesides, G.M. In *Supramolecular Architecture: Synthetic Control in Thin Films and Solids*; ACS: Washington, D.C., 1993, Vol. 499, pp. 10-23

56. Bard, A.J.; Abruna, H.D.; Chidsey, C.E.; Faulkner, L.R.; Feldberg, S.W.; Itaya, K.; Majda, M.; Melroy, O.; Murray, R.W.; Porter, M.C.; Soriaga, M.P.; White, H.S. *J. Phys. Chem.* **1993**, *97*, 7147
57. Dubois, L.; Nuzzo, R.G. *Ann. Rev. Phys. Chem.* **1992**, *43*, 437
58. Strong, L.; Whitesides, G.M. *Langmuir*, **1988**, *4*, 546
59. Bain, C.D.; Biebuyck, H.A.; Whitesides, G.M. *Langmuir*, **1989**, *5*, 723
60. Biebuyck, H.A.; Whitesides, G.M. *Langmuir*, **1993**, *9*, 1766
61. Hagenhoff, B.; Benninghoven, A.; Spinke, J.; Liley, M.; Knoll, W. *Langmuir*, **1993**, *9*, 1622
62. Nuzzo, R.G.; Dubois, L.H.; Allara, D.L. *J. Am. Chem. Soc.* **1990**, *112*, 558
63. Häußling, L.; Michel, B.; Ringsdorf, H.; Rohrer, H. *Angew. Chem. Int. Ed. Eng.* **1992**, *30*, 569
64. Johnson, R.E.; Dettre, R.H. *J. Colloid Sci.* **1965**, *20*, 173
65. Neumann, A.W.; Good, R.J. In *Surface and Colloid Science*, Good, R.J., Stromberg, R.R., Eds.; Plenum: New York, 1979, Vol. 11, pp 31-91
66. Bain, C.D.; Evall, J.; Whitesides, G.M. *J. Am. Chem. Soc.* **1989**, *111*, 7155
67. Wolfenden, R. *Science*, **1983**, *222*, 1087
68. Schmidt, U.; Grafen, P.; Goedde, H.W. *Angew. Chem. Int. Ed. Eng.* **1965**, *4*, 846
69. Cheng, Q.; Brajter-Toth, A.F. *Anal. Chem.* **1992**, *64*, 1998
70. Cheng, Q.; Brajter-Toth, A.F. submitted to *Anal. Chem.*
71. Marino, A.; Brajter-Toth, A.F. *Anal. Chem.* **1993**, *65*, 370
72. Jaramillo, A.; Marino, A.; Brajter-Toth, A.F. *Anal. Chem.* **1993**, *65*, 3441
73. Eddowes, M.J.; Hill, H.A.O. In *Electrochemical and Spectrochemical Studies of Biological Redox Components*, ACS Adv. Chem. Ser.; Kadish, K.M., Ed.; ACS: Washington, D.C., 1982, Vol. 201, p173

74. Armstrong, F.A.; Hill, H.A.O.; Walton, N.J. *Quart. Rev. Biophys.* **1986**, *18*, 261
75. Brash, J.L.; Horbett, T.A., Ed., *Proteins at Interfaces*, ACS Adv. Chem. Ser.; ACS: Washington, D.C., 1987
76. Moore, G.R.; Pettigrew, G.W. *Cytochromes C*; Springer: New York, 1987
77. Bain, C.D.; Whitesides, G.M. *J. Am. Chem. Soc.* **1988**, *110*, 3665
78. Laibinis, P.E.; Nuzzo, R.G.; Whitesides, G.M. *J. Phys. Chem.* **1992**, *96*, 5097
79. Bard, A.J.; Faulkner, L.R. *Electrochemical Methods: Fundamentals and Applications*; John Wiley & Sons: New York, 1980
80. Wightman, R.M.; Wipf, D.O. In *Electroanalytical Chemistry*; Bard, A.J., Ed.; Marcell Dekker: New York, 1989, Vol. 15, p267
81. Heinze, J. *Angew. Chem. Int. Ed. Engl.* **1993**, *32*, 1268
82. Freund, M.S. Ph.D. Dissertation, University of Florida, 1992
83. Weaver, M.J. In *Electrode Kinetics: Reactions*; Compton, R.D. Ed.; Elsevier: Amsterdam, 1987, Vol. 27, p 1
84. Winkler, J.R.; Gray, H.B. *Chem. Rev.* **1992**, *92*, 369
85. Heller, A. *Acc. Chem. Res.* **1990**, *23*, 128
86. Marcus, R.A.; Sutin, N. *Biochim. Biophys. Acta* **1985**, *811*, 265
87. Delahay, P. *Double Layer and Electrode Kinetics*; Wiley-Interscience: New York, 1965
88. Rowe, G.K.; Creager, S.E. *J. Phys. Chem.* **1994**, *98*, 5500
89. Caivo, E.J. In *Electrode Kinetics: Reactions*, Bamford, C.H.; Compton, R.G.; Elsevier, Amsterdam, 1986, Vol. 26, p 1
90. Creager, S.E.; Weber, K. *Langmuir*, **1993**, *9*, 844
91. Becka, A.M.; Miller, C.J. *J. Phys. Chem.* **1993**, *97*, 6233
92. Creager, S.E.; Rowe, G.K. *Langmuir*, **1993**, *9*, 2330

93. Doblhofer, K.; Figura, J.; Fuhrhop, J. *Langmuir*, **1992**, *8*, 1811
94. Gaines, G.L. *Insoluble Monolayers at Liquid-Gas Interfaces*, Interscience, New York, 1966
95. Wring, S.A.; Hart, J.P. *Analyst*, **1992**, *117*, 1215
96. Hill, H.A.O.; Sanghara, G.S. *Biosensors: A Practical Approach*, IRL Press, Oxford, 1990
97. Mascini, M.; Palleschi, G. *Selective Electrode Rev.* **1989**, *11*, 191
98. Schiltz, J. *Sci. Amer.* **1991**, 64
99. Andrieux, C.P.; Dumas-Bouchiat, J.M.; Saveant, J.M. *J. Electroanal. Chem.* **1982**, *131*, 1
100. Anson, F.C.; Ohsaka, T.; Saveant, J.M. *J. Am. Chem. Soc.* **1983**, *105*, 4883
101. Heller, A. *J. Phys. Chem.* **1992**, *96*, 3579
102. Andrieux, C.P.; Saveant, J.M. In *Molecular Design of Electrode Surfaces*, Ed. by R.W. Murray, *Techniques of Chemistry Series*, John Wiley & Sons: New York, 1992, Vol. 22, p207
103. Zakeeruddin, S.M.; Fraser, D.M.; Nazeeruddin, M.K.; Gratzel, M. *J. Electroanal. Chem.* **1992**, *337*, 253
104. Frew, J.E.; Hill, H.A.O. *Anal. Chem.* **1987**, *59*, 933A
105. Case, A.E.G.; Davis, G.; Francis, G.D.; Hill, H.A.O. *J. Electroanal. Chem.* **1985**, *190*, 117
106. Bradley, J.; Kidd, A.J.; Anderson, P.A.; Dear, A.M.; Ashly, R.E.; Turner, A.P.F. *Analyst*, **1989**, *114*, 375
107. Hilditch, P.I.; Green, M.J. *Analyst*, **1991**, *116*, 1217
108. Degani, Y.; Heller, A. *J. Am. Chem. Soc.* **1988**, *110*, 2615
109. Frew, J.E.; Green, M.J. *Anal. Proc.* **1988**, *25*, 276

110. Hale, P.D.; Inagaki, T.; Lee, H.S.; Karan, H.I.; Okamoto, Y.; Skotheim, T.A. *Anal. Chim. Acta* **1990**, *228*, 31
111. Mascini, M.; Moscone, D.; Palleschi, G. *Anal. Chim. Acta* **1984**, *157*, 45
112. Mascini, M.; Mazzei, F. *Anal. Chim. Acta* **1987**, *192*, 9
113. Matsue, T.; Kato, T.; Akiba, U.; Osa, T. *Chem. Lett.* **1986**, 843
114. Matsue, T.; Suda, M.; Uchida, I.; Kato, T.; Akiba, U.; Osa, T. *J. Electroanal. Chem.* **1987**, *234*, 163
115. Case, A.E.G.; Francis, D.G.; Hill, H.A.O.; Aston, W.J.; Higgins, I.J.; Plotkin, E.V.; Scott, L.D.L.; Turner, A.P.F. *Anal. Chem.* **1984**, *56*, 667
116. Kashiwagi, Y.; Osa, T. *Chem. Lett.* **1993**, 677
117. Degani, Y.; Heller, A. *J. Phys. Chem.* **1987**, *91*, 1285
118. Schuhmann, W.; Ohara, T.J.; Schmidt, H.L.; Heller, A. *J. Am. Chem. Soc.* **1991**, *113*, 1394
119. Maidan, R.; Heller, A. *J. Am. Chem. Soc.* **1991**, *113*, 9003
120. Badia, A.; Carlini, R.; Fernandez, A.; Battaglini, F.; Mikkelsen, S.R.; English, A.M. *J. Am. Chem. Soc.* **1993**, *115*, 7053
121. Bourdillon, C.; Majda, M. *J. Am. Chem. Soc.* **1990**, *112*, 795
122. Parker, L.; Tristram, S.; Herz, J.M.; Russell, C.; Borders, C.L. *FEBS. Lett.*, **1979**, *108*, 243
123. Solomons, T.W. *Organic Chemistry*, John Wiley & Sons, New York, 1980
124. Wightman, R.M.; May, L.J.; Michael, A.C. *Anal. Chem.* **1988**, *60*, 769A
125. Patai, S. *The Chemistry of Quinonoid Compounds*; John Wiley & Sons: New York, 1974
126. Hawley, M.D.; Tatawawadi, S.V.; Piekarski, S.; Adams, R.N. *J. Am. Chem. Soc.* **1967**, *89*, 447
127. Voet, D.; Voet, J.G. *Biochemistry*, John Wiley & Sons: New York, 1990

128. Armstrong, F.A. In *Structure and Bonding*; Springer-Verlag: Berlin, 1990, Vol. 72.
129. Baar, R.B. Ph.D. Thesis, California Institute of Technology, 1985
130. Huang, H.J.; He, P.; Faulkner, L.R. *Anal. Chem.* **1986**, *58*, 2889
131. Baur, J.E.; Wightman, R.M. *J. Electroanal. Chem.* **1991**, *305*, 73
132. Nicholson, R.S. *Anal. Chem.* **1965**, *37*, 1351
133. Laviron, E. *J. Electroanal. Chem.* **1979**, *101*, 19
134. Howell, J.O.; Wightman, R.M. *Anal. Chem.* **1984**, *56*, 524
135. Pena, M.J.; Fleischmann, M.; Garrard, N. *J. Electroanal. Chem.* **1987**, *220*, 31
136. Brautigan, D.L.; Ferguson-Miller, S.; Margoliash, E. *Methods Enzymol.* **1978**, *53*, 131
137. Van Gelder, B.F.; Slater, E.C. *Biochim. Biophys. Acta* **1962**, *58*, 593
138. Lanza, V.L.; Herrman, D.B. *J. Polym. Sci.* **1958**, *28*, 622
139. Wagner, A.F.; Folkers, K. *Vitamins and Coenzymes*; Interscience, New York, 1964
140. Wang, J.; Frostman, L.M.; Ward, M.D. *J. Phys. Chem.* **1992**, *96*, 5224
141. Smith, C.P.; White, H.S. *Anal. Chem.* **1992**, *64*, 2398
142. Ghaicha, L.; Leblanc, R.M.; Chattopadhyay, A.K. *Langmuir*, **1993**, *9*, 288
143. Chattopadhyay, A.K.; Ghaicha, L.; Oh, S.G.; Shah, D.O. *J. Phys. Chem.* **1992**, *96*, 6509
144. Ghaicha, L.; Chattopadhyay, A.K.; Tajmir-Raihi, H.A. *Langmuir*, **1991**, *7*, 2007
145. Bard, A.J.; Crayston, J.A.; Kittleson, G.P.; Shea, T.V.; Wrighton, M.S. *Anal. Chem.* **1986**, *58*, 2321
146. Ishimitsu, T.; Hirose, S.; Sakurai, H. *Talanta*, **1977**, *24*, 555

147. Gonzalez, S.; Anson, F.A. *J. Electroanal. Chem.* **1981**, *129*, 243
148. Shimizu, K.; Matsubara, T.; Sato, G.P. *Bull. Chem. Soc. Jpn.* **1974**, *47*, 1651
149. Vancea, J.; Reiss, G.; Schneider, F.; Bauer, K.; Hoffmann, H. *Surface Sci.* **1989**, *218*, 108
150. Widrig, C.A.; Chung, C.; Porter, M.D. *J. Electroanal. Chem.* **1991**, *310*, 335
151. Creager, S.E.; Rowe, G.K. *Anal. Chim. Acta* **1991**, *246*, 233
152. Malem, F.; Mandker, D. *Anal. Chem.* **1993**, *65*, 37
153. Becka, A.M.; Miller, C.J. *J. Phys. Chem.* **1992**, *96*, 2657
154. Adams, R.N. *Prog. Neurobiol.* **1990**, *35*, 297
155. Grunewald, R.A. *Brain Res. Rev.* **1993**, *18*, 123
156. Cammack, J.; Ghasemzadeh, B.; Adams, R.N. *Brain Res.* **1991**, *565*, 17
157. Pierce, R.C.; Miller, D.W.; Reising, D.B.; Rebec, G.V. *Brain Res.* **1992**, *597*, 138
158. Andreux, C.P.; Hapiot, P.; Saveant, J.-M. *Chem. Rev.* **1990**, *90*, 723
159. Wipf, D.O.; Michael, A.C.; Wightman, R.M. *J. Electroanal. Chem.* **1989**, *269*, 15
160. Hsueh, C.C.; Brajter-Toth, A.F. *Anal. Chem.* **1993**, *65*, 1570
161. Forster, R.J.; Faulkner, L.R. *J. Am. Chem. Soc.* **1994**, *116*, 5453
162. Carpppo, R.; Coppola, S.; Fromter, E. *Pflugers Archiv.* **1994**, *429*, 193
163. Hickman, J.J.; Ofer, D.; Laibinis, P.E.; Whitesides, G.M.; Wrighton, M.R. *Science*, **1991**, *252*, 688
164. Creager, S.E.; Hockett, L.A.; Rowe, G.K. *Langmuir*, **1992**, *8*, 854
165. Hanania, G.I.H.; Irvine, D.H.; Eaton, W.A.; George, P. *J. Phys. Chem.* **1967**, *71*, 2022
166. Sohr, R.; Muller, L. *Electrochim. Acta* **1975**, *20*, 451

167. McCreery, R.L. in *Electroanalytical Chemistry*; Bard, A.J., Ed.; Marcell Dekker: New York, 1991, Vol. 17
168. McConnell, H.M.; Owicki, J.C.; Parce, J.W.; Miller, D.L.; Baxter, H.G.; Wada, H.G.; Pitchford, S. *Science*, **1992**, 257, 1906
169. Willner, I.; Riklin, A. *Anal. Chem.* **1994**, 66, 1535
170. Armstrong, F.A.; Hill, H.A.O.; Walton, N.J. *Acc. Chem. Res.* **1988**, 21, 407
171. Scheller, F.; Janchen, M.; Prumke, H.J. *Biopolymers* 1975, 14, 1553
172. Yeh, P.; Kuwana, T. *Chem. Lett.* **1977**, 1145
173. Eddowes, M.J.; Hill, H.A.O. *J. Chem. Soc., Chem. Commun.* **1977**, 3154
174. Eddowes, M.J.; Hill, H.A.O. *J. Am. Chem. Soc.* **1979**, 101, 7113
175. Taniguchi, I.; Toyosawa, K.; Yamaguchi, H.; Yasukouchi, K. *J. Chem. Soc. Chem. Commun.* **1982**, 1032
176. Tanoguchi, I.; Higo, N.; Umekita, K.; Yosukouchi, K. *J. Electroanal. Chem.* **1986**, 206, 341
177. Allen, P.M.; Hill, H.A.O.; Walton, N.J. *J. Electroanal. Chem.* **1984**, 178, 69
178. DiGleria, K.; Hill, H.A.O.; Lowe, V.J.; Page, D.J. *J. Electroanal. Chem.* **1986**, 213, 333
179. Hill, H.A.O.; Lawrance, G.A. *J. Electroanal. Chem.* **1989**, 270, 309
180. Armstrong, F.A.; Hill, H.A.O.; Oliver, B.N. *J. Chem. Soc., Chem. Commun.* **1984**, 976
181. Armstrong, F.A.; Driscoll, P.C.; Hill, H.A.O. *FEBS Lett.* **1985**, 190, 242
182. Armstrong, F.A.; Cox, P.A.; Hill, H.A.O.; Lowe, V.J.; Oliver, B.N. *J. Electroanal. Chem.* **1987**, 217, 331
183. Armstrong, F.A.; Hill, H.A.O.; Oliver, B.N.; Walton, N.J. *J. Am. Chem. Soc.* **1984**, 106, 921

184. Kamau, G.N.; Willis, W.S.; Rusling, J.F. *Anal. Chem.* **1985**, *57*, 545
185. Marino, A.; Brajter-Toth, A.F. submitted to *Anal. Chem.*
186. Poulos, T.L.; Freer, S.T.; Alden, R.A.; Edwards, S.L.; Skogland, U.; Takio, K.; Eriksson, B.; Xuong, N.; Yonetani, T.; Kraut, J. *J. Biol. Chem.* **1980**, *255*, 575
187. Oesch, U.; Janata, J. *Electrochim. Acta* **1983**, *28*, 1237
188. Bowden, E.F.; Hawkrige, F.M.; Blount, H.N. *J. Electroanal. Chem.* **1984**, *161*, 355
189. Song, S.; Clark, R.A.; Bowden, E.F.; Tarlov, M.J. *J. Phys. Chem.* **1993**, *97*, 6564
190. Willit, J.L.; Bowden, E.F. *J. Phys. Chem.* **1990**, *94*, 8241
191. Peterson, L.C.; Cox, R.P. *Biochem. J.* **1980**, *192*, 687
192. Vanderkooi, J.; Erecinska, M. *Arch. Biochem. Biophys.* **1974**, *162*, 383
193. Vanderkooi, J.; Erecinska, M.; Chance, B. *Arch. Biochem. Biophys.* **1973**, *154*, 531


BIOGRAPHICAL SKETCH

Quan Cheng was born on October 26, 1964, in Xuzhou, Jiangsu, P.R. China, where he attended primary school and high school. He entered Nanjing University in 1982, choosing chemistry as his major. While an undergraduate student, he started to get involved in scientific research, under the supervision of Mr. Shimin Zhu. After obtaining a B.S. degree in 1986, he continued to stay at Nanjing University working with Prof. Xinquan Xin in the field of solid state inorganic chemistry. He obtained an M.S. degree in inorganic chemistry in 1989.

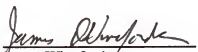
After briefly working as a university lecturer, he came to the University of Florida in 1990, working with Dr. Anna Brajter-Toth to study electrochemistry. He completed his Ph.D. research in April, 1995, and will begin postdoctoral training at the University of California at Berkeley.

In 1989, Quan Cheng married Lan Huang in Nanjing. Their daughter, Rebecca, was born on February 20, 1993, in Gainesville, Florida.

I certify that I have read this study and that in my opinion it conforms to acceptable standards for scholarly presentation and is fully adequate, in scope and quality, as a dissertation for the degree of Doctor of Philosophy.


Anna Brajer-Toth
Associate Professor of Chemistry


I certify that I have read this study and that in my opinion it conforms to acceptable standards for scholarly presentation and is fully adequate, in scope and quality, as a dissertation for the degree of Doctor of Philosophy.


James Winefordner
Graduate Research Professor of Chemistry


I certify that I have read this study and that in my opinion it conforms to acceptable standards for scholarly presentation and is fully adequate, in scope and quality, as a dissertation for the degree of Doctor of Philosophy.


William Jones
Distinguished Service Professor
of Chemistry

I certify that I have read this study and that in my opinion it conforms to acceptable standards for scholarly presentation and is fully adequate, in scope and quality, as a dissertation for the degree of Doctor of Philosophy.


Robert Kennedy
Assistant Professor of Chemistry

I certify that I have read this study and that in my opinion it conforms to acceptable standards for scholarly presentation and is fully adequate, in scope and quality, as a dissertation for the degree of Doctor of Philosophy.


Paul Holloway
Professor of Materials Science
and Engineering

This dissertation was submitted to the Graduate Faculty of the Department of Chemistry in the College of Liberal Arts and Sciences and to the Graduate School and was accepted as partial fulfillment of the requirements for the degree of Doctor of Philosophy.

May 1995

Dean, Graduate School